Creep Introduction

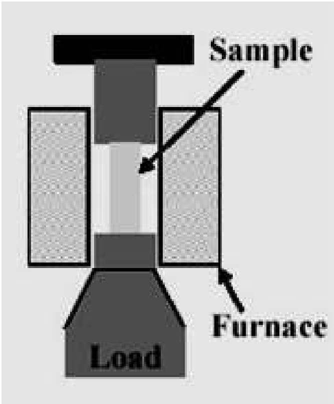

G.H. Farrahi

ASM Handbook & Dieter & Smith

Introduction

- CREEP is the slow deformation of a material under a stress that results in a permanent change in shape. Generally, creep pertains to rates of deformation less than *1.0%/min;* faster rates are usually associated with mechanical working (processes such as forging and rolling).

Introduction

- Although creep can occur at any temperature, only at temperatures exceeding about 0.4 of the melting point of the material are the full range of effects visible.

General behavior during creep

Stage	Temperature	Characteristic
First (primary)	...... $T > 0.4\ T_M$ or $T \leq 0.4\ T_M$	$\dot{\epsilon}$ decreases as t and ϵ increase
Secondary (steady state)	... $T \geq 0.4\ T_M$	$\dot{\epsilon}$ is constant ($\dot{\epsilon}_{ss}$)
Third (tertiary)	.... $T \geq 0.4\ T_M$	$\dot{\epsilon}$ increases as t and ϵ increase

3

Introduction

- A schematic representation of creep in both temperature regimes is shown in Fig. I. At time=0 the load is applied. Once loaded, the material initially deforms at a very rapid rate, but as time proceeds, the rate of deformation progressively decreases.

Fig. 1 Low-temperature and high-temperature creep of a material under a constant engineering stress

A and B denote the elastic strain on loading; C denotes transition from primary (first-stage) to steady-state (second-stage) creep; D denotes transition from steady-state to tertiary (third-stage) creep.

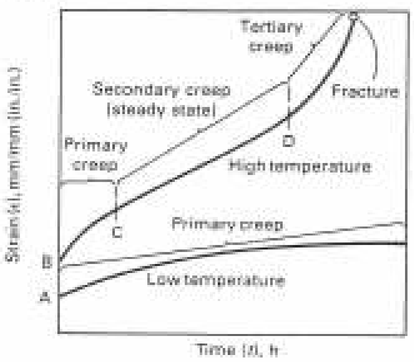

Introduction

- At high temperatures however, the regime of constantly decreasing strain rate (primary or first-stage creep) leads to conditions where the rate of deformation becomes independent of time and strain. When this occurs, creep is in its second stage or steady-state regime. eventually the strain rate begins to accelerate with time, and the material enters tertiary or third-stage creep. Deformation then proceeds at an ever-faster rate until the material can no longer support the applied stress and fracture occurs.

Creep Curves

Fig. 1 Variation of creep and creep rate with time

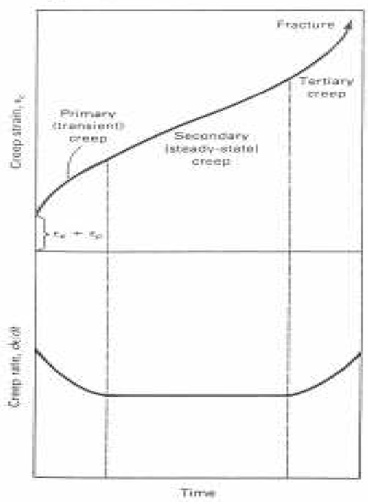

Introduction

Creep

Primary (or transient) creep
Continuously decreasing creep rate
Material experiencing strain hardening

Secondary (or steady state) creep
Constant creep rate
Long duration
Strain hardening and recovery being balanced
Steady-state creep rate: the slope of the secondary portion of the creep curve

Tertiary creep
Also termed rupture
Reduction in cross-section through necking, internal void formation near precipitates

7

Introduction

Creep

Creep is very structure sensitive

Microstructure
Prior working and heat treatment

Grain size – boundaries are sites for dislocation generation
Solute atoms – dislocation pinning

8

Introduction

Creep

Influence of stress and temperature:

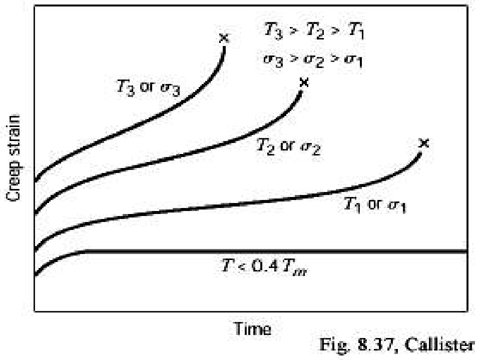

Fig. 8.37, Callister

9

Introduction

- **Microstructure.** During creep. significant micro structural changes occur on all levels. On the atomic scale, dislocations are created and forced to move through the material. This leads to work hardening as the dislocation density increases and the dislocations encounter barriers to their motion. At low temperatures, an ever-diminishing creep rate results. The combined action of hardening and recovery processes during primary creep can lead to the formation of a stable distribution of sub grains or loose three-dimensional dislocation networks in some materials, or an approximately uniform dislocation distribution without sub grains in other materials. These stable dislocation configurations are maintained and are characteristic of second stage creep.
- Figure 9 is an example of a stress/temperature-dependent microstructure.

10

خزش

- نرخ مینیمم خزش ($\dot{\varepsilon}_{II}$) minimum creep rate مهمترین پارامتر طراحی ناشی از منحنی خزش است . با دو استاندارد این پارامتر مورد استفاده قرار می گیرد:

(1) تنشی که نرخ خزش 0.0001% درساعت ویا 1% در10000 h
(2) تنشی که نرخ خزش0.00001% در ساعت و یا 1% در h 100000 (حدود 11.5 سال) ایجادکند.

- معیاراول معمولا نیاز یک آلیاژ موتور جت است و معیار دوم برای توربین های بخارو یا مشابه آن بکار می رود.
- از آنحاییکه انجام این آزمایشات وقت زیادی می گیرد بنابراین روشهایی باید یافت شوند که از نتایج آزمایشات کوتاه مدت بتوان اطلاعات عمر طولانی را برون یابی کرد.

11

معیارهای طراحی در خزش

- استحکام خزش مواد (ازدید مهندسی) معمولا با یک یا هردو پارامتر $\dot{\varepsilon}_{II}$و t_f (زمان تا شکست یا عمر) مشخص می شود. $\dot{\varepsilon}_{II}$ و t_f بطور معکوس با یکدیگر رابطه دارند.
- اگر یک قطعه قرار است برای یک مدت زمان کوتاه در درجه حرارت بالا کار کند (مثل قطعات موتور یک موشک یک با ر پرتاب) تغییر شکل خزش می تواند قابل تحمل باشد اما شکست نه. در این مورد، t_f متغیر مناسب طراحی است.
- برای قطعاتیکه برای کار در درجه حرارت بالا برای چند صد ساعت (مثل پره های توربین موتور جت) یا در بعضی موارد برای چندین سال (مثل لوله های بویلر) طراحی می شوند ، انسجام سازه ای در یک کرنش دائمی کم لازم است و $\dot{\varepsilon}_{II}$ یک پارامتر تر جیحی طراحی می شود.

12

Theory of Creep Deformation

- **Temperature Dependence of Steady-State Creep**

Although creep is known to be a thermally activated process, it is less generally understood that the measured activation energy varies significantly with temperature at low temperatures and becomes independent of temperature only above approximately $0.6T_M$ Figure 3 illustrates the activation energy for creep in pure aluminum as a function of temperature (Ref 3).

Above $0.6T_M$ the activation energy for creep deformation is independent of temperature and is equal to the activation energy for self-diffusion. For many pure metals, an excellent correlation exists between the activation energy for self diffusion and the activation energy for creep at high temperatures (Ref 3). Such a correlation is shown in Fig. 4.

13

Theory of Creep Deformation

- **The Dorn Equation**

In the temperature/stress regime in which power-law stress dependence exists and in which dislocation climb determines the temperature dependence of creep, the temperature/stress dependence of steady-state creep may be expressed by the Dorn equation (Ref 6):

$$\dot{\varepsilon}_s = A D_L \frac{Gb}{kT} \left(\frac{\sigma}{G}\right)^n$$

where A and n are constants; b is the burgers vector, representative of the discontinuity in the crystal caused by the dislocation; D_L is the self-diffusion coefficient; k is Boltzman' s constant; T is the absolute temperature; σ is the applied stress; and G is the shear modulus.

14

Theory of Creep Deformation

- **Dislocation Creep Mechanisms**

Creep has been considered to result from the competing processes of work hardening and thermal recovery. The Bailey-Orowan equation defines this concept mathematically:

$$d\sigma = \left(\frac{d\sigma}{d\epsilon}\right)d\epsilon + \left(\frac{d\sigma}{dt}\right)dt$$

where $d\sigma$ represents the change in flow stress, $d\sigma/d\varepsilon$ represents the hardening that results from an increment of plastic strain $d\varepsilon$, and $d\sigma/dt$ represents the softening due to recovery in a time increment dt.

15

نمایش تجربی رفتار خزش

- ج) تابع درجه حرارت : متداولترین تابع درجه حرارت عبارت است از :

$$f_{\text{۳}}(T) = \exp\left\{\frac{-\Delta H}{RT}\right\}$$

- که ΔH انرژی فعال سازی، R ثابت بولتزمن و T در جه حرارت مطلق است.
- از آنجاییکه در طراحی همانگونه که گفته شد مرحله دوم (نرخ مینیمم کرنش که در مدت زمان طولانی ثابت می ماند) مطرح می شود، مرحله سوم ندیده گرفته می شود و مرحله اول نیز با یک کرنش ثابت جایگزین می شود : بنابراین

$$\in_c = \in_0 + \left(\frac{d\varepsilon}{dt}\right)t \qquad (5)$$

که نرخ خزش مرحله دوم است و این نرخ مینیمم خزش بصورت تجربی عبارت است از

16

نمایش تجربی رفتار خزش

$d\varepsilon / dt = \dot{\varepsilon}_c = \dot{\varepsilon}_{II}$ نرخ خزش مرحله دوم است و این نرخ مینیمم خزش بصورت تجربی عبارت است از

$$\dot{\in}_c = B\,\sigma^N \qquad (6)$$

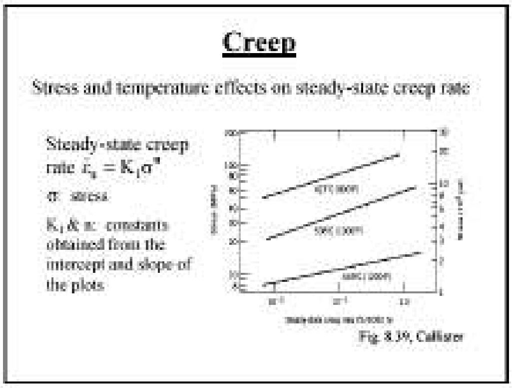

17

نمایش تجربی رفتار خزش

تاثیر درجه حرارت و تنش نیز با فرمول زیر نشان داده می شود.

$$\dot{\varepsilon}_{c,II} = B\sigma^n \exp\left(\frac{-\Delta H}{RT}\right) \qquad (7)$$

که B ثابت ماده و ΔH انرژی فعال سازی خزش است

18

Larsen Miller Parameter

- ***Larsen Miller parameter*** is used to represent creep-stress rupture data.

  P(Larsen-Miller) = T[log t_r + C]

  T = temperature(K), tr = stress-rupture time h

  C = Constant (order of 20)

Also, P(Larsen-Miller) = [T(^{0}C) + 273(20+log t_r)

or P(Larsen-Miller) = [T(^{0}F) + 460(20+log t_r)

- At a given stress level, the log time to stress rupture plus constant multiplied by temperature remains constant for a given material.

19

7-25

Larsen Miller Parameter

If two variables of time to rupture, temperature and stress are known, 3rd paramete that fits L.M. parameter can be determined.

Example:

For alloy CM, at 207 MPa,
LM parameter is 27.8 x 10^3 K
Then if temperature is known,
time to rupture can be found.

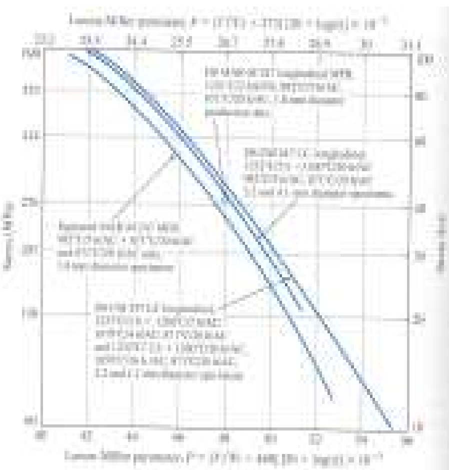

Figure 6.36

7-26

(After "Metals Handbook," vol.1, 10th ed., ASM International, 1990, p.998.)

Experiment

- **Creep Experiments;** The creep behavior of a material is generally determined by uniaxial loading of test specimens heated to temperature in some environment. Creep-rupture experiments measure the deformation as a function of time to failure. If strain-time behavior is measured, but the test is stopped before failure, this is termed an interrupted creep experiment. Finally, if an inadequate strain-measuring system or no attempt to determine length is employed, and the test is run to fracture, a stress-rupture experiment results.

- **Direction of Loading;** Most creep-rupture tests of metallic materials are conducted in uniaxial tension. Although this method is suitable for ductile metals. compressive testing is more appropriate for brittle, flaw sensitive materials. In compression, cracks perpendicular to the applied stress do not propagate as they would in tension; thus, a better measure of the inherent plastic properties of a brittle material can be obtained.

21

Experiment

- **Test specimens;** for uniaxial tensile creep-rupture tests are the same as those used in short-term tensile tests. *Solid* round bars with threaded or tapered grip ends or thin sheet specimens with pin and clevis grip ends (Ref 3) are typical. However, many other types and sizes of specimens have been used successfully where the choice of geometry was dictated by the available materials.

- **Environment;** The optimum conditions for a creep-rupture test are those in which the specimen is influenced only by the applied stress and temperature. This rarely occurs. particularly at elevated temperatures, and these conditions do not exist for real structures and equipment operating under creep conditions. For example, turbine blades are continuously exposed to hot, reactive gases that cause corrosion and oxidation.

22

Experiment

- **Strain Measurement.** Care must be taken to ensure that the measured deformation occurs only in the gage section. Thus, measurements based on the relative motion of parts of the gripping system above and below the test specimen are generally inaccurate, because the site of deformation is unknown. Extensometry systems are currently available that attach directly to the specimen (shoulders, special ridges machined on the reduced section, or the gage section itself) and transmit the relative mo-tion of the top and bottom of the gage section via tubes and rods to a sensing device such as a linear variable differential transformer (LVDT). Figure 3 illustrates such a system. These systems are quite accurate and stable over long periods of time.

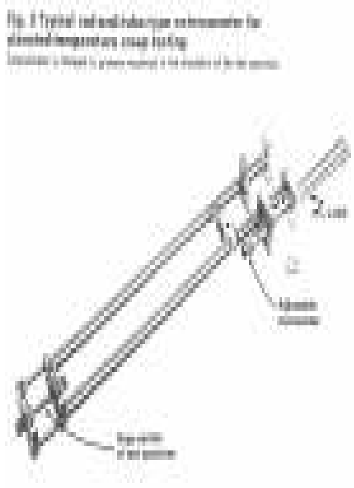

23

Experiment

- **Data Presentations;** Generally, all creep- and stress-rupture related data are analyzed in terms of three variables: time, stress, and temperature. **The time-to-rupture** *(t_r)* from either isothermal stress-rupture or creep-rupture testing is presented as a function of stress as:

$$t_r = K_1 \exp(a\sigma) \qquad \text{(Eq 1)}$$

and

$$t_r = K_2\sigma^m \qquad \text{(Eq 2)}$$

- where K_1, K_2, and a are constants. and m is the stress exponent for rupture. An example of time-to-rupture results and the use of these equations to describe the data at several tem-peratures are shown in Fig. 4(a) and (b). Generally. In both cases, the data lie on straight lines, and coefficients of determination (R^2) for the linear regression fits of the data have high values.

24

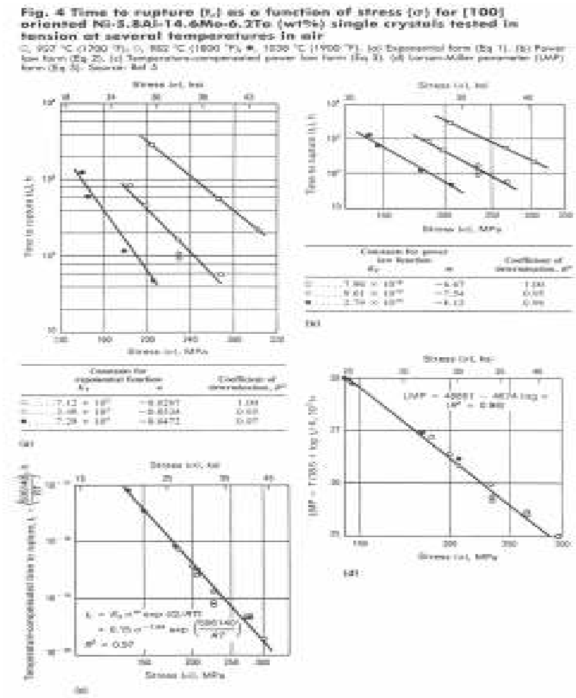

25

Experiment

- When temperature effects as well as stress effects on time-to-rupture are to be consid-ered, one common presentation is:

$$t_r = K_3 \sigma^{m} \exp\left(\frac{Q_r}{RT}\right) \qquad \text{(Eq 3)}$$

- where K_3 is a constant; Q_r is the activation energy for rupture; R is the universal gas con-stant (8.314 *kJlmol . K);* and T is the absolute temperature in Kelvin. Figure 4(c) describes time-to-rupture data for several temperatures as a single line. The Larson-Miller parameter (LMP) (Ref 6) represents another approach using a single curve to represent data gath-ered under a variety of conditions. where:

$$\text{LMP} = T(C + \log t_r) \qquad \text{(Eq 4)}$$

and

where C, K_4. and K_5 are constants

$$\text{LMP} = K_4 \log \sigma + K_5 \qquad \text{(Eq 5)}$$

26

Experiment

- **Creep curves** generated by either creep rupture or interrupted creep testing are usu-ally presented as strain versus time or log strain versus log time. Examples of both forms are given in Fig. 5.

Fig. 5 Creep curves for [100] oriented NASAIR 100 (Ni-5.5Al-8.5Cr-0.7Mo-3Ta-1Ti-10W (wt%)) single crystals tested in tension to rupture at 1 000 °C (1830 OF) in air
(a) Strain versus time. (b) Log strain versus log time. Source, Ref 7

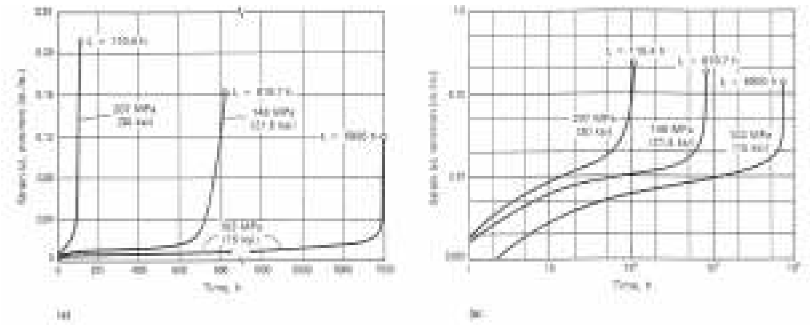

Experiment

- **Steady-State Creep Rate.** The most important creep parameter in terms of theo-retical analysis is the steady-state creep rate. Its dependence on stress is generally expressed as:

$$\dot{\epsilon}_{ss} = K_6\sigma^n \qquad \text{(Eq 6)}$$

and for temperature and stress:

$$\dot{\epsilon}_{ss} = K_7\sigma^n \exp\left(\frac{Q_c}{RT}\right) \qquad \text{(Eq 7)}$$

- where *K6* and *K7* are constants, n is the stress exponent for creep, and Q_c is the activation energy for creep.

- Examples of steady-state creep rates as functions of stress and temperature are shown in Fig. 6, along with the results of linear regression fits to power law creep (Eq 6) and temperature-compensated power law creep (Eq 7).

Experiment

Fig. 6 Steady-state creep rate ($\dot{\epsilon}_{ss}$) as a function of applied stress (σ) and temperature (T) for two heats of [100] oriented NASAIR 100 single crystals tested in tension at several temperatures in air

(a) Power law form (Eq 6). (b) Temperature-compensated power law form (Eq 7). Source: Ref 7

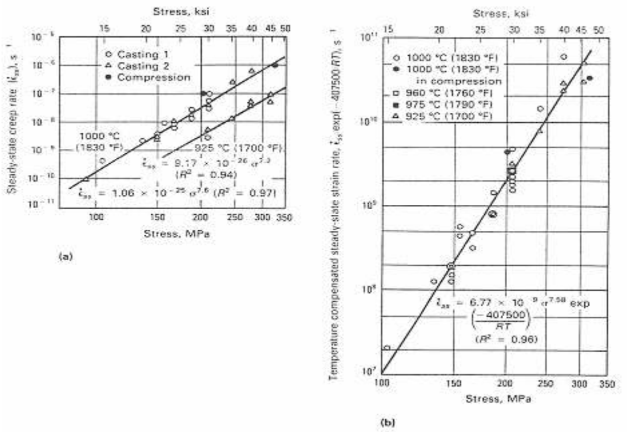

29

Experiment

- **Stress to Produce 1.0% Strain;** In many cases, the objective of testing is to determine the total amount of creep strain that can be expected during stress/tempera-ture exposures. Of particular interest are the stresses required to produce 0.5. 1.0, and 2.0% strain in a certain period of time as a function of temperature. A typical example of such a presentation is shown in Fig. 7 for several refractory alloys. Also illustrated is a case in which a metallurgical variable (grain size) was factored into the analysis to ac-count for the difference in behavior between the two lots of the tantalum-based alloy Astar 811C.

Fig. 7 Stress necessary for 1.0% strain in 10 000 h as a function of temperature for several tantalum alloys tested in vacuum

Materials include Ta-10W, T-222 (Ta-2.4Hf-9.6W-0.01C), and Astar 811C (Ta-1Hf-1Re-7.5W-0.02C) (all materials in wt%). Source: Ref 8

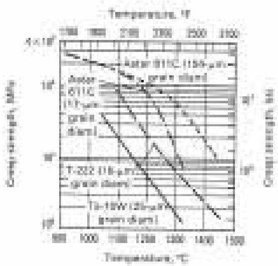

30

Experiment

- **Monkman-Grant Relationship.** For elevated-temperature tensile creep-rupture experiments, the product of the time-to-rupture and steady-state creep rate raised to the power *M* is approximately a constant for many materials (Ref 9):

$$t_r \dot{\varepsilon}_{ss}^{M} = K_8 \qquad \text{(Eq 8)}$$

- where *M* and K8 are constants with values roughly equal to 1. An example of this relationship is shown in Fig. 8 using a rearranged form of Eq 8:

$$\log t_r = \log K_8 - M(\log \dot{\varepsilon}_{ss}) \qquad \text{(Eq 9)}$$

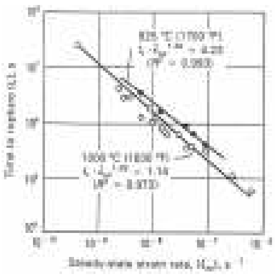

Fig. 8 Time-to-rupture (t_r) as a function of steady-state creep rate ($\dot{\varepsilon}_{ss}$) for [100] oriented NASAIR 100 single crystals tested in tension at several temperatures in air
Source: Ref 7

31

Experiment

- **Stress Relaxation** Traditional creep testing to develop descriptions of strain rate, stress, and temperature behavior can be time-intensive and expensive, involving many creep test stands, specimens, and thousands of hours of testing. Stress relaxation offers the potential to eliminate this difficulty by producing strain rate/stress data over a wide range of rates from a single specimen. This information is developed when the elastic strain of a specimen extended (or compressed) to a certain. constant length is converted to plastic strain. As the specimen slowly deforms. the load required to maintain the constant length is reduced, hence the term “stress relaxation" test. In addition, this type of experiment simulates the real engineering problem of the long-term loosening of tightened bolts and other fasteners.

32

رهایی (شل شدن) تنش Stress Relaxation

- در شکل دیگری از خزش که آن نیز تابع زمان میباشد **در کرنش ثابت، تنش کاهش می یابد**.
- یک مثال عمومی و رایج از این پدیده شل شدن (رها شدن) تنش محکم کردن پیچهای فلانچها در لوله های بخار و آب داغ است که باعث امکان نشست می شود. و یا در قطعاتی که با فشار جازده شده اند.

33

رهایی (شل شدن) تنش Stress Relaxation

- در نظر بگیرید یک نمونه که درمعرض یک کرنش کلی ε در درجه حرارت بالا قرارگرفته است (یعنی خزش می تواند اتفاق افتد)

$$\varepsilon = \varepsilon_e + \varepsilon_\rho = \frac{\sigma}{E} + \varepsilon_p$$

- همینکه ماده دچار خزش شود (افزایش طول یابد) کرنش کلی در حالتی می تواند ثابت بماند که کرنش الاستیک کاهش یابد.
- با دیفرانسیل گیری از معادله بالا نسبت به زمان و اینکه $d\epsilon/dt = 0$ است .

$$\frac{d\varepsilon_e}{dt} = -\frac{d\varepsilon_\rho}{dt}$$

34

Stress Relaxationتنش (شل شدن) رهایی

اما $\varepsilon_e = \sigma / E$ و اگر $d\varepsilon_p / dt = B\sigma^{n'}$ باشد

$$\frac{1}{\mathrm{E}}\frac{d\sigma}{dt} = -B\sigma^{n'} \qquad \int \frac{d\sigma}{\sigma^{n'}} = -B\mathrm{E}\int dt$$

$$-\frac{1}{(n'-1)\sigma^{n'-1}} = -BEt + c$$

در t=0 و $\sigma = \sigma_i$ در اینصورت

$$c = \frac{-1}{(n'-1)\sigma_i^{n'-1}}$$

بنابراین رابطه تنش و زمان در رها شدن تنش بقرار زیر است

$$\frac{1}{\sigma^{n'-1}} = \frac{1}{\sigma_i^{n'-1}} + BE(n'-1)t$$

35

Introduction

- **REFERENCES**
- Mechanical Metallurgy, G. E. Dieter, 3rd Ed., 1987, McGraw Hill
- ASM Handbook, Vol. 19, Fatigue and Fracture
- Foundations of Materials Science and Engineering, W.F. Smith, J. Hashemi, Fourth Edition, McGraw Hill, 2006

36

IOP Publishing   *Mater. Res. Express* **5** (2018) 026509   https://doi.org/10.1088/2053-1591/aaab04

Materials Research Express

CrossMark

RECEIVED
17 October 2017

REVISED
22 December 2017

ACCEPTED FOR PUBLICATION
29 January 2018

PUBLISHED
9 February 2018

PAPER

Characterization of creep damage and lifetime in Inconel-713C nickel-based superalloy by stress-based, strain/strain rate-based and continuum damage mechanics models

H Bahmanabadi[1], **S Rezanezhad**[1], **M Azadi**[1] **and M Azadi**[2]

[1] Faculty of Mechanical Engineering, Semnan University, Semnan, Iran
[2] Faculty of Materials and Metallurgical Engineering, Semnan University, Semnan, Iran

E-mail: m_azadi@semnan.ac.ir

Keywords: inconel-713C nickel-based superalloy, material characteristics, high-temperature creep loading, strain/strain rate-based model, stress-based model, continuum damage mechanics

Abstract

This article has presented suitable creep lifetime prediction models for Inconel-713C nickel-based superalloy. For such objective, the characterization of the creep damage and lifetime has been performed by considering stress-based model, strain/strain rate models and continuum damage mechanics models. For calibrating material models, creep tests at 850 °C have been performed on the Inconel-713C nickel-based superalloy under different stress levels. Obtained results indicated that reliable/valid models, according to a proper relative error and a low scatter-band, were the Monkman-Grant strain rate-based model and the continuum damage mechanics model. The scanning electron microcopy (SEM) analysis showed that the matrix pattern of crept specimens changed, when the applied stress changed under creep loading. In addition, the one-dimension form could be considered for the shape of carbides.

1. Introduction

The design of turbine blades is one of the important task for engineers in automotive and aero industries. According to the centrifugal force (due to the rotational speed of blades) under high-temperature working conditions, utilized materials in blades should have enough creep strength, such as superalloys. Todays, such materials have been widely used in manufacturing of turbine blades, weather in turbo-chargers of combustion engines or in gas turbines of aero engines [1–3]. Indeed, it is difficult and costly to perform multi-axial creep experiments for superalloys. However, the creep behavior of superalloys should be known for design engineers. Therefore, for designing such costly high-reliable parts, the development of materials models is in a special interest. Before using, they should be calibrated by experimental mechanical (monotonic), fatigue (cyclic) and creep data for finite element simulations, during a design process [1–4]. Several researchers have been studied material models for simulations of the creep damage and behavior in superalloys. Such models can be categorized in three types, including stress-based model, strain/strain rate models and continuum damage mechanics models. In the following literature, published researches about these models have been reviewed.

Hyde *et al* [5] represented the prediction of creep failures in the aero-engine material, under a multi-axial stress condition. From uniaxial creep testing results on a nickel-base superalloy, a creep continuum damage model was calibrated. Qi and Bertram [6] modeled the damage in a superalloy under creep testing. They derived a phenomenological creep damage model for superalloys, based on the theory of continuum damage mechanics. Sajjadi *et al* [7] evaluated the microstructure, deformation mechanisms and mechanical properties of the nickel-base superalloy. They also presented Larson-Miller and Monkman-Grant models for the creep lifetime prediction, comparing to creep test results. Hou *et al* [8] investigated the microstructure and mechanical properties of the cast nickel-base superalloy. They indicated that the modified Monkman-Grant relation with the time to onset of the tertiary creep and the Larson-Miller relation can describe exactly the creep lifetime of the

K44 superalloy. Yuan and Liu [9] studied the effect of the δ phase on the hot deformation behavior in the Inconel-718 superalloy. A hyperbolic-sine Arrhenius equation was utilized to characterize the dependence of the peak stress on the deformation temperature and the strain rate. Hyde *et al* [10] presented the failure estimation of welded Inconel-718 sheets. Then, the continuum damage approach was utilized for predicting the failure lifetime of welded sheets. Marahleh *et al* [11] suggested an exact method for estimating the service lifetime in turbine blades under creep loadings. They estimated the lifetime for an industrial gas turbine based on the Larson-Miller parameter. Kim *et al* [12] utilized the continuum damage mechanics for the creep-fatigue lifetime prediction of a nickel-based superalloy at high temperatures. Chen *et al* [13] combined the modified linear damage summation method and the modified strain range partitioning method for the lifetime prediction of turbine blades under creep-fatigue loading. Chateau and Remy [14] evaluated the creep damage in a wrought nickel-based superalloy. A constitutive model was proposed to take accounts for coarsening of precipitates and to use continuum damage mechanics to describe the creep damage. Chen [15] studied high-temperature mechanical behaviors of a superalloy in an aero engine, based on creep tests under 137–600 MPa and at 700 °C–900 °C. Obtained results showed that the minimum creep rate and the rupture time were well related by the Monkman-Grant relationship. Maharaj *et al* [16] investigated the creep behavior of the turbine disc, using the finite element model. They used the Norton-Bailey law for the creep relation. Shi *et al* [17] presented the creep and fatigue lifetime analysis of directionally solidified superalloy, based on continuum damage mechanics at elevated temperatures. They developed a model to predict the lifetime of specimens, based on continuum damage mechanics. Liu *et al* [18] predicted the creep rupture lifetime of a V-notched bar of the single-crystal superalloy. The creep rupture lifetime of smooth specimens was successfully predicted by the Kachanov-Rabotnov damage law. Martino *et al* [19] characterized creep properties of a superalloy under high-temperatures. Obtained experimental results were used as inputs for the validation of a micro-structurally-based continuum damage mechanics model. Sugui *et al* [20] studied creep properties of 4.5Re/3.0Ru superalloys at high temperatures. They found material constants of the Norton–Bailey law, as the relation between the strain rate of the superalloy, during the steady state creep regime. Wollgramm *et al* [21] investigated the role of Re in the stress/temperature dependence of the creep behavior in superalloys. They represented a power law type of the stress dependence and an exponential type of the temperature dependence. Liu *et al* [22] proposed a numerical approach of the lifetime assessment for the superalloy turbine blade, based on the Lemaitre-Chaboche creep damage model.

As mentioned in the literature review, different models have been utilized by researches for creep lifetime predicting of turbine blades. As a novelty for this article, researches about the Inconel-713C nickel-based superalloy are still rare, despite other superalloys. Then, comparing such these mentioned models, could be another novelty of this article to find a suitable creep lifetime prediction model. Besides, the characterization of the creep damage with material models has been presented in this article. For this objective, creep tests have been performed on the Inconel-713C nickel-based superalloy under different stress levels. Then, these experimental data have been utilized for finding material constants (as creep properties) and calibrating material models, including stress-based model, strain/strain rate models and continuum damage mechanics models. In addition, such characterization for the Inconel-713C nickel-based superalloy, which has been used in turbine blades of the engine turbo-charger, is still rare according to the literature review and it requires to be performed for designing the similar component.

2. Models

In this part, creep models, which have been presented by the literature [17, 23–33] until now, are discussed in details. As mentioned before, material models for predicting the creep damage and lifetime can be categorized in three types, as follows,

- material models based on the stress: includes the stress-lifetime relation (and sometimes, the stress-lifetime-temperature relation),
- material models based on the strain or the strain rate: includes the stress-strain relation or the stress-minimum strain rate relation (and sometimes, the stress-strain-temperature relation or the stress-minimum strain rate-temperature relation),
- and material models based on continuum damage mechanics, or the Rabotnov-Kachanov model [17].

For better understanding of different formulations in various models, table 1 is represented. More details of each model can be found in the appendix of the article, which were described in the literature [17, 23–34].

Table 1. Formulations of different models for the creep lifetime prediction.

Model type	Model Name	Abbreviations	Formulations
Type 1: stress-based models for predicting the creep lifetime	Monson-Brown	MB	$t_{cr} = 10^{[P_{MB}(T-C_2)^n + \log(C_1)]}$
	Monson-Haferd	MH	$t_{cr} = 10^{[P_{MH}(T-C_2) + \log(C_1)]}$
	Sherby-Dorn	SD	$t_{cr} = \frac{P_{SD}}{\exp\left(-\frac{Q}{RT}\right)}$
	Orr-Sherby-Dorn	OSD	$t_{cr} = 10^{\left[P_{OSD}+\frac{C}{T}\right]}$
	Larson-Miller	LM	$t_{cr} = 10^{\left[\frac{P_{LM}}{T}-C\right]}$
	Simple Model	SM	$t_{cr} = (P_{SM})\frac{1}{m}$
Type 2: strain rate-based models for predicting the creep lifetime	Monkman-Grant	MG	$t_{cr} = \frac{C}{(\dot{\varepsilon}_{\min})^n}$
	Dobes-Milicka	DM	$t_{cr} = \frac{C\varepsilon_R}{(\dot{\varepsilon}_{\min})^n}$
	Temperature-dependent Power Law	TD-PL	$t_{cr} = \left[\frac{\dot{\varepsilon}_{\min}}{C\,\sigma^n \exp\left(\frac{-Q}{RT}\right)}\right]^{\frac{1}{m}}$
	Temperature-independent Power Law	TI-PL	$t_{cr} = \left(\frac{\dot{\varepsilon}_{\min}}{C\,\sigma^n}\right)^{\frac{1}{m}}$
Type 3: damage-based models for predicting the creep lifetime and the damage	Continuum Damage Mechanics	CDM	$t_{cr} = \frac{1}{k+1}\left[\frac{\sigma}{A}\right]^{-r}$ $D_{CDM} = 1 - \left\{1 - \frac{t}{t_{cr}}\right\}^{\frac{1}{k+1}}$ $D_{\dot{\varepsilon}} = D_{\min} + 1 - \left(\frac{\dot{\varepsilon}}{\dot{\varepsilon}_{\min}}\right)^{N_1}$ $D_{\varepsilon} = \left[1 - \left(\frac{\varepsilon_0}{\varepsilon}\right)^{N_2}\right]^M$
Type 4: strain rate-based models for predicting the minimum strain rate	Arrhenius Law	AL	$\dot{\varepsilon}_{\min} = C\exp\left(\frac{-Q}{RT}\right)$
	Simple Power Law	SPL	$\dot{\varepsilon}_{\min} = C\,\sigma^n$
	Norton Power Law	NPL	$\dot{\varepsilon}_{\min} = C\,\sigma^n \exp\left(\frac{-Q}{RT}\right)$
	hyperbolic-sine Law	HSL	$\dot{\varepsilon}_{\min} = C\sinh(\overline{C}\sigma)\exp\left(\frac{-Q}{RT}\right)$
Type 5: strain-based models for predicting the creep strain during the time	Bailey-Norton	BN	$\varepsilon_c = C\sigma^n(t)^m$
	Findley Law modified by Hadid *et al* [32]	FH	$\varepsilon_c = \varepsilon_0 + A\sigma^B(t)^m$
	Du *et al* [30]	DU	$\varepsilon_c = \frac{\sigma}{C_1} + \frac{\sigma}{C_2}\left[1 - \exp\left(-\frac{C_2}{\overline{C_2}}t\right)\right] + \frac{\sigma}{\overline{C_1}}t$
Type 6: strain-based models for predicting the strain rate	ABAQUS Software [29]	AS	$\dot{\varepsilon} = (C\,\sigma^n[(m+1)\varepsilon_c]^m)^{\frac{1}{m+1}}$

To find material constants, the Levenberg-Marquardt method [17, 35] has been employed in the present article, as a nonlinear least squares data fitting approach. In this method, the squared value of errors between experimental and predicted data has been minimized. For this objective, a solver (mathworks) in the MATLAB software was utilized. These relative errors is to evaluate the accuracy of each material model, based on experimental data ($t_{cr,\exp}$, $\dot{\varepsilon}_{\min,\exp}$, $\varepsilon_{c,\exp}$ and $\dot{\varepsilon}_{\exp}$) and calculated data ($t_{cr,\mathrm{cal}}$, $\dot{\varepsilon}_{\min,\mathrm{cal}}$, $\varepsilon_{c,\mathrm{cal}}$ and $\dot{\varepsilon}_{cal}$). Relative errors (E_1 to E_4) are considered as follows,

$$E_1(\%) = \left|\frac{t_{cr,\exp} - t_{cr,\mathrm{cal}}}{t_{cr,\exp}}\right| \times 100 \tag{1}$$

$$E_2(\%) = \left|\frac{\dot{\varepsilon}_{\min,\exp} - \dot{\varepsilon}_{\min,cal}}{\dot{\varepsilon}_{\min,\exp}}\right| \times 100 \tag{2}$$

$$E_3(\%) = \left|\frac{\varepsilon_{c,\exp} - \varepsilon_{c,cal}}{\varepsilon_{c,\exp}}\right| \times 100 \tag{3}$$

$$E_4(\%) = \left|\frac{\dot{\varepsilon}_{\exp} - \dot{\varepsilon}_{cal}}{\dot{\varepsilon}_{\exp}}\right| \times 100 \tag{4}$$

Above relative errors including E_1 to E_4 are used for mentioned models in table 1 (including models: type 1 to 6). The other evaluation (for models: type 1 to 4 in table 1) can be the scatter-band value in the curve of experimental data versus calculated data. Such curves have been shown in the part, results and discussions.

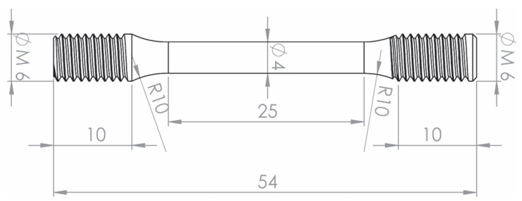

Figure 1. The geometry of high-temperature creep specimens (in millimeter).

3. Materials and experiments

The Inconel-713C nickel-based superalloy is the case study of this article, which has been utilized in turbine blades, in the engine turbo-charger. The chemical composition of the mentioned material is measured as 5.50% Al, 0.97% Ti, 1.91% Ta+Nb, 0.04% Mn, 14.00% Cr, 4.50% Mo, 0.12% C, 0.13% Fe, 0.01% B, 0.06% Zr, 0.04% Si, 0.01% Cu and Ni is the remainder.

Creep tests on cylindrical specimens (shown in figure 1) were carried out based on the standard: ASTM-E139-11 [36], at the temperature of 850 °C and under different stress levels, including 507.7, 546.7 and 585.8 MPa. It should be noted that standard specimens were machined from a casted Inconel-713C nickel-based superalloy cylinder. Creep test equipments included a creep testing machine (the SCT-300 model, SANTAM Company). In this machine, values of the load and the displacement were measured by the load cell and the extensometer, respectively. In addition, the temperature was measured by K-type thermo-couples. In this article, the engineering stress ($\sigma_e = F/A_0$) and the engineering strain ($\varepsilon_e = \Delta l/l_0$) are reported, where F is the measured load, A_0 is the initial area of specimens, l is the specimen length during testing, l_0 is the initial length of specimens and Δl is the difference between the length and the initial length ($\Delta l = l - l_0$). More details about the material and creep testing can be found in the literature [3, 4].

In addition, for characterizing the creep damage of the material, the scanning electron microscopy has been performed on all specimens, before and after testing.

4. Results and discussions

As the first result, curves of the engineering strain versus the time and the engineering strain rate versus the time, for the Inconel-713C nickel-based superalloy are shown in figure 2. As it can be seen in this figure, one creep test under 585.8 MPa was repeated for checking the repeatability of testing. For such specimens, although their minimum strain rates were approximately different; however, their creep lifetimes were so similar. More details for the repeatability of creep testing can be found in the previous research [3, 4]. Another analysis from obtained results is that by increasing the stress value, from 507.7 to 546.7 MPa, the creep lifetime decreased significantly. Higher stress level (585.8 MPa) decreased the creep lifetime again, but not as the sharp as other stress level. It should be noted that the temperature was constant (as 850 °C) in these reported creep tests. For better understanding, other results obtained from figure 2 are presented in table 2, including the temperature, the applied stress, the creep lifetime, the initial strain, the rupture strain, and the minimum strain rate.

As known, there are three regions in the creep phenomenon. In the first region, the creep rate decreases by the time, which is called as the transient stage. The second region is related to the minimum strain rate as the steady state condition. In this stage, the strain rate is approximately constant. In the third region, the strain rate increases by the time, which is call as the acceleration stage [4]. As it can be seen in figure 2, by increasing the stress level, the steady state region shortened and consequently, the creep lifetime decreased.

Obtained results including maximum and average relative errors for stress-based (Type 1 in table 2), strain rate-based (Type 2 in table 2) and damage-based (Type 3 in table 2) models can be found in table 3. In addition, the scatter-band for experimental and predicted data for such models can be seen in figure 3. As it can be observed from obtained results, the superior stress-based model was the Monson-Haferd one (by linear fitting), with the maximum relative error and the average relative error of 77.6% and 24.9%, respectively. Lower relative errors could be reported for the Monkman-Grant strain rate-based model. For the mentioned model, the maximum relative error and the average relative error were 28.1% and 16.5%, respectively. Besides, using continuum damage mechanics for predicting the creep lifetime of the Inconel-713C nickel-based superalloy resulted in obtaining 39.7% for the maximum relative error and 26.8% for the average relative error. According to figure 3, the scatter-band was obtained as 1.4X and 1.7X for the Monkman-Grant strain rate-based model and the continuum damage mechanics model, respectively. Other prediction models had higher values (more than

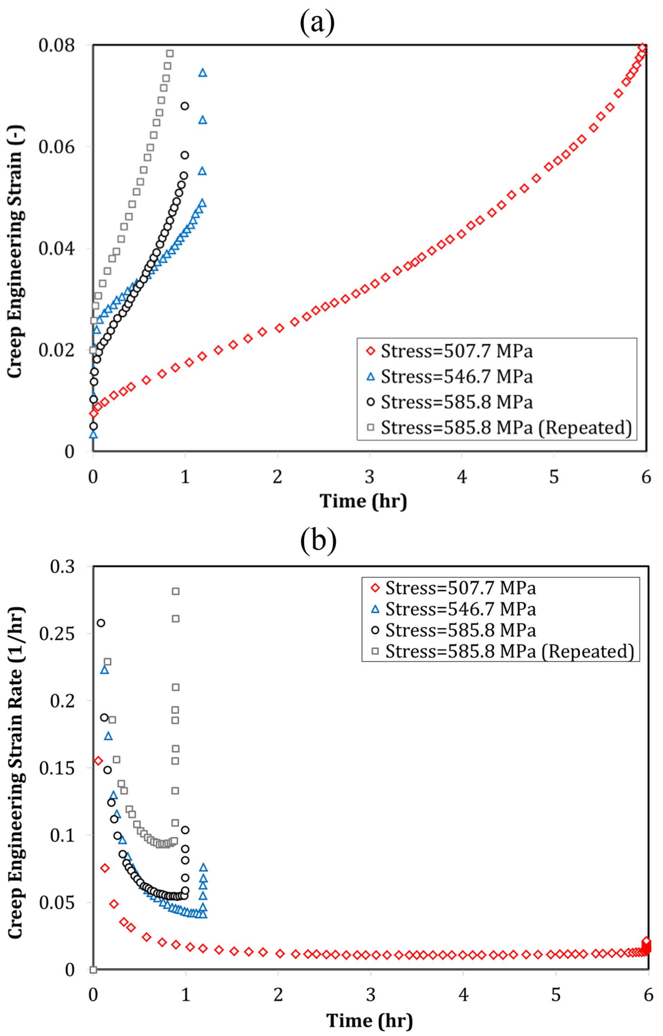

Figure 2. Curves of creep testing for the Inconel-713C nickel-based superalloy, including (a) the creep engineering strain versus the time and (b) the creep engineering strain rate versus the time.

Table 2. Obtained results from creep testing for the Inconel-713C nickel-based superalloy.

Specimen No.	1	2	3	4 (Repeated)
Temperature (°C)	850	850	850	850
Applied stress (MPa)	507.7	546.7	585.8	585.8
Creep lifetime (hr)	5.974	1.190	0.993	0.889
Initial strain (−)	0.008	0.003	0.005	0.020
Rupture strain (−)	0.127	0.091	0.103	0.250
Minimum strain rate (1/hr)	0.011	0.041	0.054	0.093

3.0X) for the scatter-band and their predictions were in an un-safe region (lower predicted lifetime data in comparison to higher experimental lifetime data).

The physical reason is that in the Monkman-Grant strain rate-based model is only based on one parameter including the minimum strain rate and the continuum damage mechanics model is only based on the stress level. In other stress-based and strain rate-based models, two or three parameters were considered together for predicting the creep lifetime, such as the temperature, the stress level and the minimum strain rate. In this research, the temperature, as this first parameter, was constant at each testing condition. Therefore, it could not be a proper parameter for the prediction. Then also, the interaction between stress level and minimum strain rate parameters was complicated, which would be more described in next section, based on microstructural and morphological investigations. The relation between the stress level and the minimum strain rate is not linear and their related experimental data could be fitted by a power-law. It means that by increasing the stress level, the minimum strain rate increased sharply.

Table 3. Obtained results for predicting the creep lifetime of the Inconel-713C nickel-based superalloy.

Model type	Model Name	Abbreviations	Best fit	$(E_1)maximum$	$(E_1)average$
Type 1: stress-based models	Monson-Brown	MB	$A_1 + A_2\sigma$	83.4	27.9
	Monson-Haferd	MH	$A_1 + A_2\sigma$	**77.6**	**24.9**
	Sherby-Dorn	SD	$A_1 + A_2\sigma$	82.6	29.3
	Orr-Sherby-Dorn	OSD	$A_1 + A_2\sigma$	83.3	28.1
	Larson-Miller	LM	$A_1 + A_2\log(\sigma)$	83.3	28.1
	Simple Model	SM	$A_1\sigma^{A_2}$	83.2	28.3
Type 2: strain rate-based models	Monkman-Grant	MG	—	**28.1**	**16.5**
	Dobes-Milicka	DM	—	94.3	67.6
	Temperature-dependent Power Law	TD-PL	—	82.7	29.4
	Temperature-independent Power Law	TI-PL	—	82.7	29.4
Type 3: damage-based models	Continuum Damage Mechanics	CDM	—	**39.7**	**26.8**

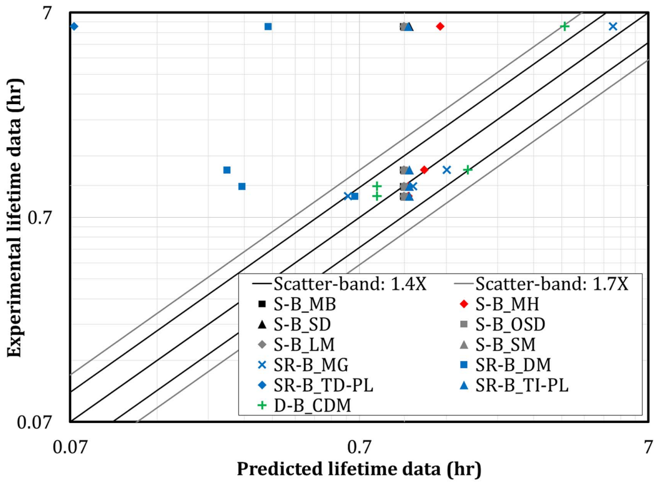

Figure 3. The scatter-band of experimental and predicted data for the creep lifetime of the Inconel-713C nickel-based superalloy (S-B: stress-based, SR-B: strain rate-based, and D-B: damage-based models).

As a conclusion, for the objective of predicting the creep lifetime in the Inconel-713C nickel-based superalloy, only two reliable/valid models could be utilized with a proper error and a low scatter-band, including the Monkman-Grant strain rate-based model and the continuum damage mechanics model. As an advantage of the Monkman-Grant strain rate-based model, a creep test can be performed on a material, only in the first creep stage. By finding the minimum strain rate, the creep lifetime can be estimated without performing a complete creep test to reduce costs and the time of testing. As an advantage of the continuum damage mechanics model, the creep damage can be predicted during the time. Knowing the damage behavior of materials helps engineers for an appropriate design of mechanical structures under creep loading.

As a verification, average errors for stress-based models in the present work are 27.9%, 24.9%, 28.1% and 28.1% for MB, MH, OSD and LM models, respectively. Such values in the literature [23] are 365.7%, 67.7%, 125.8% and 35.9%, for MB, MH, OSD and LM models, respectively.

Comparing obtained results (material constants in the continuum damage mechanics model) in the present work to other results of other researches can be seen in table 4. Such table could verify obtained material constants in this work. As another verification, the average error for predicting the creep lifetime based on continuum damage mechanics in the present work had an appropriate value (as 26.8%), comparing to literatures [12] (as 88.3%) and [17] (as 14.6%).

The damage parameter for the Inconel-713C nickel-based superalloy during creep testing, based on the continuum damage mechanics method, can be seen in figure 4, under different stress levels. As it can be seen, the creep damage parameter started from zero and ended to unity, during testing. As a first result, there is no proper prediction by the damage model based on the strain rate, before the minimum strain rate occurred. However, the final damage value and the changing behavior of the damage can be appropriately predicted by the

Table 4. Obtained results including material constants in the continuum damage mechanics model for the Inconel-713C nickel-based superalloy.

Reference	Material	Temperature (°C)	Material Constants		
			k	A	r
[12]	Waspaloy	650	20.0	2.1	15.8
[17]	DZ125	980	5.6	725.2	5.4
[17]	NHT-BJ	980	2.2	423.8	6.4
[17]	HT-BJ	980	3.3	498.8	6.2
Present Work	713C	850	7.0	700.0	10.5

mentioned model. Obtained results by the damage model based on the strain showed that the estimation of the damage (including the trend) can be acceptable and not exactly correct; however, the final damage value was not predicted truly.

Obtained results for predicting of the minimum strain rate based on the strain rate-based models (Type 4 in table 1) is presented in table 5. Besides, the scatter-band for experimental and predicted data for strain rate-based models can be seen in figure 5. From obtained results, it can be noted that the superior model was the hyperbolic-sine law based on the relative error. If the objective is the scatter-band; then again, the hyperbolic-sine law had a reliable response (with the scatter-band of 1.5X) in comparison to other strain rate-based models for predicting the minimum strain rate of the Inconel-713C nickel-based superalloy. Other strain rate-based models had higher scatter-band of 3.2X in predicting the minimum strain rate of the Inconel-713C nickel-based superalloy.

To predict the strain or the strain rate during the time (or creep testing), four models (Types 5 and 6 in table 2) were used, including Bailey-Norton (BN), Findley law modified by Hadid *et al* [32] (FH), Du *et al* [30] (DU) and ABAQUS software [29] (AS). Relative errors for these modeling can be seen in table 6. It should be noted that the DU model was not able to predict the strain during creep testing of the Inconel-713C nickel-based superalloy. Experimental and predicted data for BN, FH and AS models can be observed in figures 6–8, respectively.

Figure 9 shows SEM images from specimens, before and after creep testing. According to figure 9(a), the microstructure of the specimen before creep testing was consisted the γ matrix and γ' phase participates, plus MC carbides, which was observed in the white-colored region. The energy disperse spectroscopy (EDS) result of such image was found in the previous research [3]. When the specimen crept under the stress of 507.7 MPa (specimen No. 1) for about 6 h, the size of γ' phase participates seemed to be changed, as shown in figure 9(b). The phase size changed to the smaller value in some participates. Such behavior could be attributed to the interaction of dislocations and γ' phase participates. This interaction led to decrease the creep strain rate, with respect to other specimens.

By increasing the stress value, from 507.7 to 546.7 MPa (specimen No. 2), the matrix that consisted of γ phase and γ' participate changed homogenously, as indicated in figure 9(c). In some regions, the γ matrix was similar to the image matrix of the specimen before creep testing, as illustrated in figure 9(a). It seems that the specimen was not crept homogenously and this event caused to decrease the creep lifetime, drastically. When the applied stress increased to 585.8 MPa (specimen No. 3), the size of γ' phase participates did not change comparing with specimen before the creep as shown in figure 9(d). Besides, MC carbides changed to $M_{23}C_6$ carbides, which was observed in the black-colored region, in figure 9(d). This behavior was the result of the high applied stress under creep testing. The high magnitude of the applied stress provided the energy to cause the carbide conversion, as this change could be done when the temperature was higher than 930 °C [37]. In addition, the thickness of MC carbides decreased and their shape was observed in the one-dimensional form.

To describe the reason for appreciate modeling of Monkman-Grant strain rate-based and continuum damage mechanics models, microstructural and morphological investigations could be used. When the stress level was 507.7 MPa, the amount of the strain rate was low and based on Monkman-Grant strain rate-based and continuum damage mechanics models, the creep lifetime increased. In this situation, dislocations interacted with γ' phase participates and led to cutting them, as described before. When the stress level increased to 546.7 MPa, the strain rate increased and therefor, dislocations had no enough time to move in the material and interact to γ' phase participates. This caused to shorten the second region of the creep phenomenon and the specimen was not crept homogenously. When the stress level increased to 585.8 MPa, the interaction between dislocations and γ' phase participates was limited to a small amount and only the carbides length was changed. Therefore, based on Monkman-Grant strain rate-based and continuum damage mechanics models, the creep lifetime was at the minimum value.

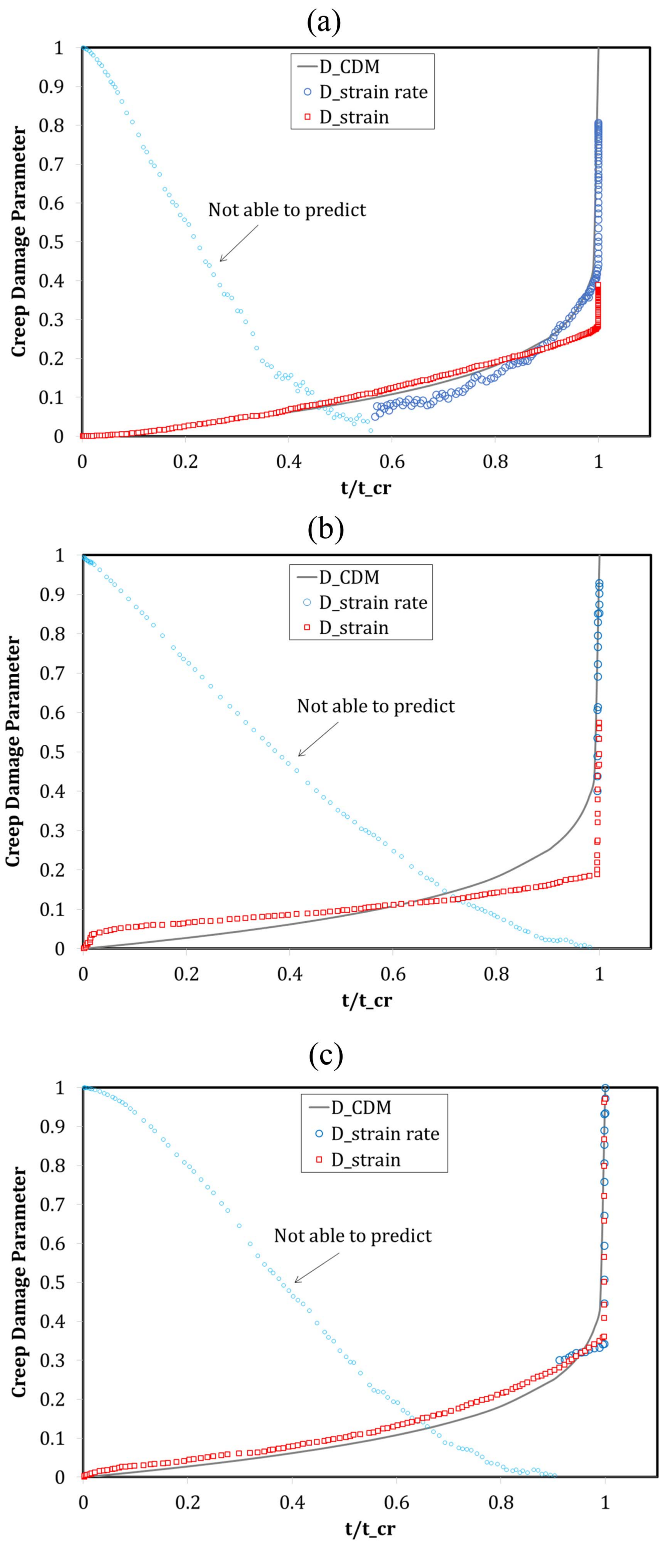

Figure 4. The damage parameter for the Inconel-713C nickel-based superalloy during creep testing under the stress of (a) 507.7 MPa, (b) 546.7 MPa and (c) 585.8 MPa (Note: D_strain rate means $D_{\dot{\varepsilon}}$ and D_strain means D_{ε}).

Table 5. Obtained results for predicting the minimum strain rate of the Inconel-713C nickel-based superalloy.

Model type	Model Name	Abbreviations	(E_2)*maximum*	(E_2)*average*
Type 4: strain rate-based models	Arrhenius Law	AL	84.1	65.3
	Simple Power Law	SPL	80.2	63.4
	Norton Power Law	NPL	69.3	51.0
	hyperbolic-sine Law	HSL	**31.9**	**23.6**

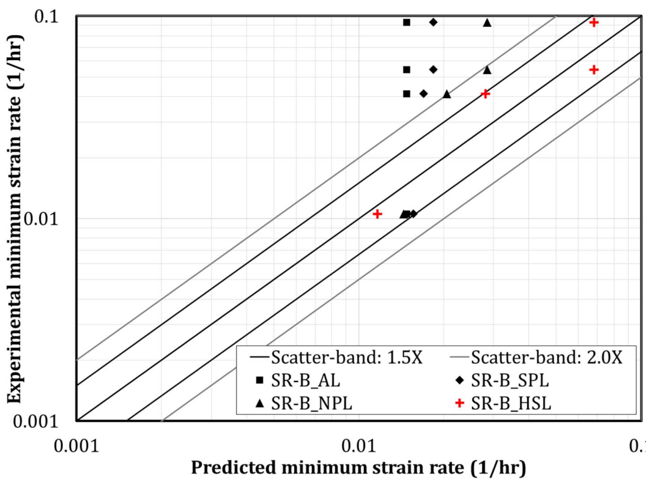

Figure 5. The scatter-band of experimental and predicted data for the minimum strain rate of the Inconel-713C nickel-based superalloy (SR-B: strain rate-based models).

5. Conclusions

In the present article, the characterization of creep damage at 850 °C in Inconel-713C nickel-based superalloy has been performed by stress-based, strain/strain rate-based and continuum damage mechanics models. Obtained results can be presented as follows,

- Increasing the stress value (from 507.7 to 546.7 MPa) caused to a significant decrease in the creep lifetime. Such reduction in the creep lifetime was not so significant under higher stress level.
- The Monson-Haferd model was calibrated by experimental data as a superior stress-based mode, according to linear fitting. Between strain rate-based models, the Monkman-Grant model had appropriate results. Based on continuum damage mechanics, the relative error was in a proper range.
- The scatter-band (the creep lifetime based on experimental data and results of models) was calculated less than 2X for the Monkman-Grant strain rate-based model and continuum damage mechanics model.
- The strain-based damage parameter indicated that predicting of the damage value (including the trend) was acceptable and not exactly correct; however, the final damage value was not predicted truly.
- Based on SEM images of crept specimens, the matrix pattern changed, when the applied stress under the creep testing was various. Besides, the carbide shape changed to the one-dimension form.

Acknowledgments

This study was not funded and authors have received no research grants from any companies or institutes. Besides, authors have declared that there is no conflict of interests.

Appendix

In the first section of this part, stress-based material models are described by different formulations. It should be mentioned that in these models, t_{cr} and T are the creep lifetime (hr) and the temperature (°K), respectively.

The equation based on the Monson-Brown parameter (P_{MB}) is given by the following formulation [23].

$$P_{MB} = \frac{\log(t_{cr}) - \log(C_1)}{(T - C_2)^n} \tag{A1}$$

Where C_1, C_2 and n are material constants.

The equation of the Monson-Haferd parameter (P_{MH}) can be mentioned as follows [23],

$$P_{MH} = \frac{\log(t_{cr}) - \log(C_1)}{T - C_2} \tag{A2}$$

Table 6. Obtained results for predicting the strain and the strain rate of the Inconel-713C nickel-based superalloy.

Model type	Model Name	Abbreviations	(E_3)*maximum*	(E_3)*average*	(E_4)*maximum*	(E_4)*average*
Type 5: strain-based models	Bailey-Norton	BN	**78.8**	28.4	—	—
	Findley Law modified by Hadid *et al* [32]	FH	442.1	**23.5**	—	—
	Du *et al* [30]	DU	Not able to predict	Not able to predict	—	—
Type 6: strain-based models	ABAQUS Software [29]	AS	—	—	45.2	33.3

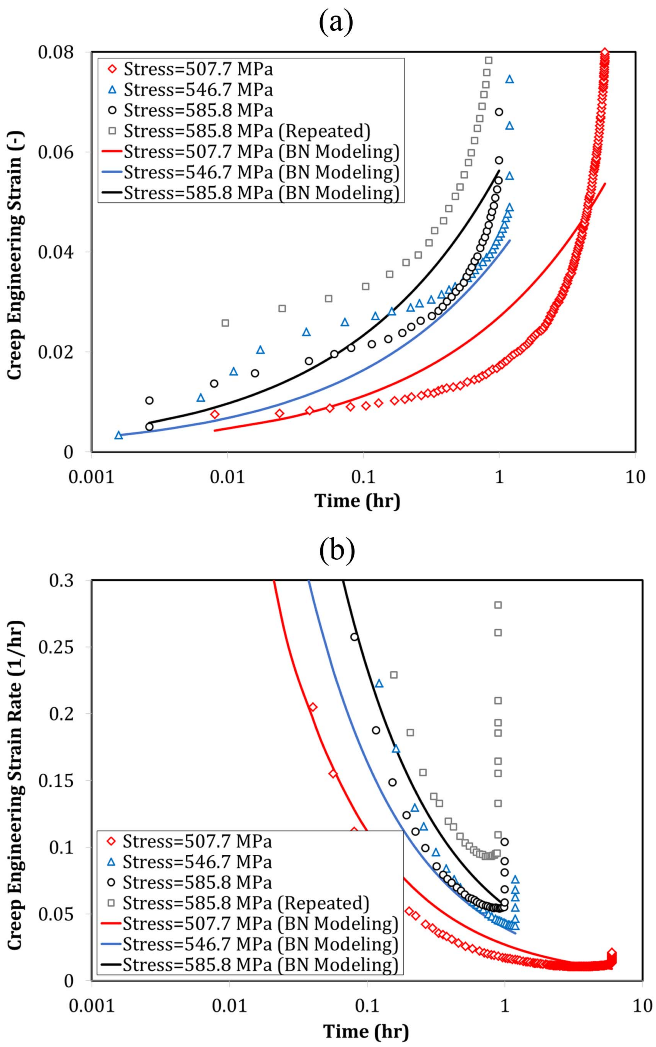

Figure 6. Experimental and predicted data by the BN model for (a) the strain-time curve and (b) the strain rate-time curve of the Inconel-713C nickel-based superalloy.

In which, C_1 and C_2 are material constants. This material model is similar to the Monson-Brown parameter, when n is unit.

The Sherby-Dorn parameter (P_{SD}) is given by the following equation [24].

$$P_{SD} = t_{cr} \exp\left(\frac{-Q}{RT}\right) \tag{A3}$$

In which, Q is the creep activation energy and R is the universal gas constant.

The Orr-Sherby-Dorn parameter (P_{OSD}) is described as follows [23],

$$P_{OSD} = \log(t_{cr}) - \frac{C}{T} \tag{A4}$$

Where C is a material constant.

The equation of the Larson-Miller parameter (P_{LM}) is written as follows [25],

$$P_{LM} = T[\log(t_{cr}) + C] \tag{A5}$$

In this model, C is a material constant, which value is generally assumed to be 20, approximately [25].

Another simple model, which is a relation between the stress and the creep lifetime, is given by the following equation [33].

$$\sigma^n (t_{cr})^m = C \tag{A6}$$

In which, C, m and n are temperature-dependent material constants. Considering P_{SM} as the simple model parameter, such formulation can be rewritten as follows,

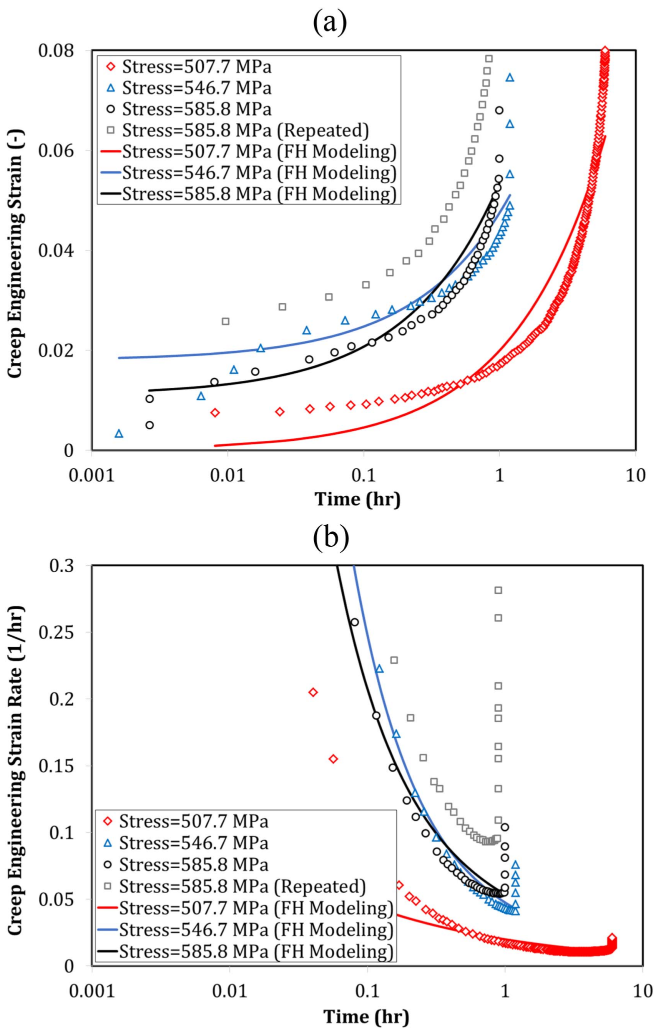

Figure 7. Experimental and predicted data by the FH model for (a) the strain-time curve and (b) the strain rate-time curve of the Inconel-713C nickel-based superalloy.

$$P_{SM} = (t_{cr})^m \tag{A7}$$

Where P_{SM} has been defined in following equations.

It should be noted that above material constants in stress-based material models are generally temperature-independent. In addition, all mentioned models include a damage parameter (P_i, i: the model name), which is dependent on the temperature and the creep lifetime of materials, in one hand. On the other hand, these parameters are usually based on the stress (σ), according to power, linear, logarithmic and etc curve fitting. Such functions can be written as follows,

$$P_i(t_{cr}, T) = f(\sigma) = A_1\sigma^{A_2} \tag{A8}$$

$$P_i(t_{cr}, T) = f(\sigma) = A_1 + A_2\sigma \tag{A9}$$

$$P_i(t_{cr}, T) = f(\sigma) = A_1 + A_2 \log(\sigma) \tag{A10}$$

$$P_i(t_{cr}, T) = f(\sigma) = A_1 \exp(A_2\sigma) \tag{A11}$$

$$P_i(t_{cr}, T) = f(\sigma) = A_1 + A_2\sigma + A_3\sigma^2 \tag{A12}$$

$$P_i(t_{cr}, T) = f(\sigma) = A_1 + A_2 \log(\sigma) + A_3 \log(\sigma)^2 \tag{A13}$$

Where A_i are temperature-independent material constants.

In the second section of this part, strain/strain rate-based material models are described in details. In these material models, σ is the applied stress (MPa), ε_c is the creep strain (−) and $\dot{\varepsilon}_{\min}$ is the minimum creep strain rate (1/hr).

The equation of the Monkman-Grant model is given as follows [26, 27],

$$(\dot{\varepsilon}_{\min})^n (t_{cr}) = C \tag{A14}$$

In which, n and C are material constants.

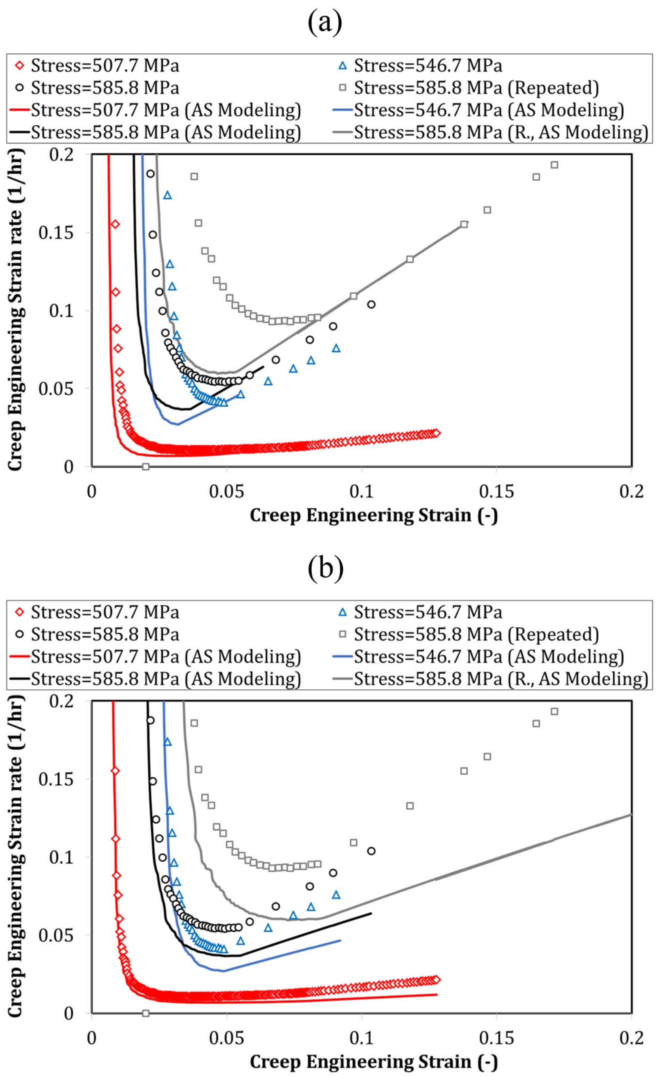

Figure 8. Experimental and predicted data by the AS model for the strain rate-strain curve of the Inconel-713C nickel-based superalloy, including (a) the predicated strain rate versus the predicted strain and (b) the predicted strain rate versus the experimental strain.

The equation of the Dobes-Milicka model is written as the following formulation [26, 28].

$$(\dot{\varepsilon}_{\min})^n \left(\frac{t_{cr}}{\varepsilon_R}\right) = C \tag{A15}$$

Where ε_R is the strain at the rupture. In addition, n and C are material constants. Since the temperature and the stress are not considered in two above material models, all material constants depend to the stress and the temperature. In other words, these material constants vary at different temperatures and under different stresses.

A general form for the temperature-dependent power law is offered in the following formulation.

$$\dot{\varepsilon}_{\min} = C\ \sigma^n (t_{cr})^m \exp\left(\frac{-Q}{RT}\right) \tag{A16}$$

In the proposed model, C, n and m are material constants, which are stress-independent and temperature-independent.

According to the suggested general form of the power law, the following equation regardless to the temperature effect (entitled as the temperature-independent power law), can be mentioned [29].

$$\dot{\varepsilon}_{\min} = C\ \sigma^n (t_{cr})^m \tag{A17}$$

In which, C, n and m are temperature-dependent material constants.

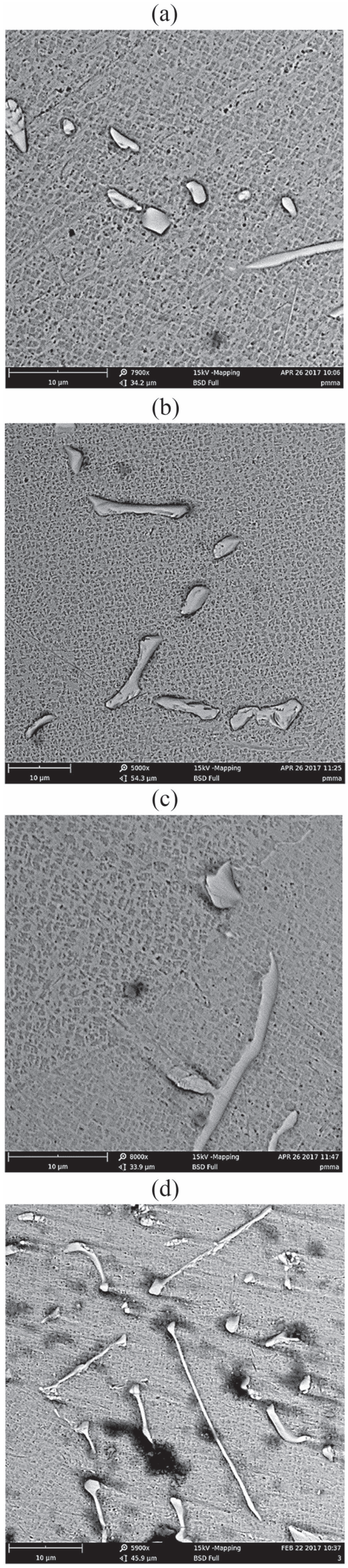

Figure 9. SEM images of specimens including (a) before creep testing and (b), (c), (d) after creep testing; (b) specimen No. 1, (c) specimen No. 2 and (d) specimen No. 3.

The Norton power law is defined as follows [25],

$$\dot{\varepsilon}_{\min} = C\,\sigma^{n}\exp\left(\frac{-Q}{RT}\right) \tag{A18}$$

In which, Q is the creep activation energy and R is the universal gas constant. In addition, C and n are material constants, which are stress-independent and temperature-independent.

The Arrhenius law is written as follows [25],

$$\dot{\varepsilon}_{\min} = C\exp\left(\frac{-Q}{RT}\right) \tag{A19}$$

This model is similar to the Norton power law, when n is zero. Therefore, C (the material constant) is only stress-dependent.

Another type of the power law (entitled as the simple power law) is given by the following equation [25].

$$\dot{\varepsilon}_{\min} = C\,\sigma^{n} \tag{A20}$$

Where C and n are material constants, which are only temperature-dependent.The hyperbolic-sine law is available in the form of the following formulation [29].

$$\dot{\varepsilon}_{\min} = C\,\sinh(\overline{C}\sigma)\exp\left(\frac{-Q}{RT}\right) \tag{A21}$$

Where $\overline{C}$ is a material constant.

To estimate the curve of the creep strain (ε_c) during the testing time (t), the equation of the Bailey-Norton model is mentioned as follows [30],

$$\varepsilon_c = C\,\sigma^{n}(t)^{m} \tag{A22}$$

Where C, n and m are temperature-dependent material constants.

As another estimation for the creep strain, the equation of the Findley power law is given by the following formulation [26, 31].

$$\varepsilon_c = \varepsilon_0 + C(t)^{m} \tag{A23}$$

In which, C and m are stress-dependent and temperature-dependent material constants. In addition, ε_0 is the instantaneous strain during creep testing. In some cases, values of ε_0 could be estimated using the Remberge-Osgood relation [26]. In order to find the variation of C with the stress, the following equation suggested by Hadid *et al* [32] can be utilized.

$$C = A\sigma^{B} \tag{A24}$$

Where A and B are temperature-dependent material constants.

Another strain-based model presented by Du *et al* [30] for estimating the creep strain can be given by the following formulation.

$$\varepsilon_c = \frac{\sigma}{C_1} + \frac{\sigma}{C_2}\left[1 - \exp\left(-\frac{C_2}{\overline{C_2}}t\right)\right] + \frac{\sigma}{\overline{C_1}}t \tag{A25}$$

Where C_1, C_2, $\overline{C_1}$ and $\overline{C_2}$ are temperature-dependent material constants.

Another strain rate-based model that shows the relation between the stress, the creep strain and the strain rate ($\dot{\varepsilon}$) can be written as the following equation [29].

$$\dot{\varepsilon} = (C\,\sigma^{n}[(m+1)\varepsilon_c]^{m})^{\frac{1}{m+1}} \tag{A26}$$

In which, C, m and n are temperature-dependent material constants.

In the third section of this part, a material model based on continuum damage mechanics is described. This method is also named as the Rabotnov-Kachanov model [17]. The evaluation of the creep damage can be expressed by a damage variable (D_{CDM}) during creep testing for the lifetime estimation. The damage rate parameter depends on the damage value, the stress, the creep lifetime. The following formulation is the uniaxial form of the damage growth, caused by the creep phenomenon [17].

$$dD_{CDM} = \left(\frac{\sigma}{A}\right)^{r}(1 - D_{CDM})^{-k}dt \tag{A27}$$

In which, r, k and A are temperature-dependent material constants.

The creep lifetime to failure under a constant load can be obtained by integrating the above equation, from $t = 0$ to and $t = t_{cr}$ also from $D_{CDM} = D_0$ (the initial damage) to $D_{CDM} = D_{cr}$ (the damage value, when the material fails) [17].

$$t_{cr} = \frac{1}{k+1}[(1+D_0)^{k+1} - (1-D_{cr})^{k+1}]\left[\frac{\sigma}{A}\right]^{-r} \tag{A28}$$

And therefore, the creep damage can be represented by the following form [17].

$$D_{CDM} = 1 - \left\{(1-D_0)^{k+1} - [(1-D_0)^{k+1} - (1-D_{cr})^{k+1}]\frac{t}{t_{cr}}\right\}^{\frac{1}{k+1}} \tag{A29}$$

Considering $D_0 = 0$ (no initial damage in the material) and $D_{cr} = 1$ (for the failure), above formulations change to the following state.

$$t_{cr} = \frac{1}{k+1}\left[\frac{\sigma}{A}\right]^{-r} \tag{A30}$$

$$D_{CDM} = 1 - \left\{1 - \frac{t}{t_{cr}}\right\}^{\frac{1}{k+1}} \tag{A31}$$

To compare values of D_{CDM} to experimental data, another formulation presented by Chaboche [34] for the damage parameter based on the strain rate can be considered as follows,

$$D_{\dot{\varepsilon},i} = 1 - \left(\frac{\dot{\varepsilon}}{\dot{\varepsilon}_{\min}}\right)^{N_1} \tag{A32}$$

Where N_1 is a material constant. The above damage parameter should be modified, since there are three stages for the curve of the creep strain rate and the mentioned formulation cannot be fitted to experimental data. The first stage of the creep is eliminated for such fitting and at the second stage of the creep, where the minimum strain rate occurs, $D_{\min}$ is defined and added to equation (28). Therefore, the modified damage parameter based on strain rate can be modified as follows,

$$D_{\dot{\varepsilon}} = D_{\min} + D_{\dot{\varepsilon},i} = D_{\min} + 1 - \left(\frac{\dot{\varepsilon}}{\dot{\varepsilon}_{\min}}\right)^{N_1} \tag{A33}$$

In which, $D_{\min}$ can be found by equation (27). It should be mentioned, this model can be used for the time after the minimum strain rate occurred. Since the behavior of the strain rate-time curve is descending firstly and then becomes ascending. However, the damage curve is always ascending. In other words, the damage parameter based on the strain rate ($D_{\dot{\varepsilon}}$) cannot predict the damage value in first times of creep testing.

By benchmarking from the above model, another formulation for the damage parameter based on the strain can be mentioned as follows,

$$D_{\varepsilon,i} = 1 - \left(\frac{\varepsilon_0}{\varepsilon}\right)^{N_2} \tag{A34}$$

Where ε_0 is the initial strain. Again for better fitting, the mentioned model can be modified as follows,

$$D_{\varepsilon} = (D_{\varepsilon,i})^M = \left[1 - \left(\frac{\varepsilon_0}{\varepsilon}\right)^{N_2}\right]^M \tag{A35}$$

Where N_2 and M and are material constants.

ORCID iDs

M Azadi https://orcid.org/0000-0001-8686-8705

References

[1] Hollander D, Kulawinski D, Thiele M, Damm C, Henkel S, Biermann H and Gampe U 2016 Investigation of isothermal and thermo-mechanical fatigue behavior of the nickel-base superalloy IN738LC using standardized and advanced test methods *Materials Science and Engineering* A **670** 314–24
[2] Lee K O, Bae K H and Lee S B 2009 Comparison of prediction methods for low-cycle fatigue life of HIP superalloys at elevated temperatures for turbopump reliability *Materials Science and Engineering* A **519** 112–20
[3] Azadi M and Azadi M 2017 High-temperature creep behavior of Inconel-713C nickel-based superalloy considering effects of stress levels *Materials Science and Engineering* A **689** 298–305
[4] Azadi M, Marbout A, Safarloo S, Azadi M, Shariat M and Rizi M H 2018 Effects of solutioning and ageing treatments on properties of Inconel-713C nickel-based superalloy under creep loading *Materials Science and Engineering* A **711** 195–204
[5] Hyde T H, Xia L and Becker A A 1996 Prediction of creep failure in aero engine materials under multi-axial stress state *Mechanical Sciences* **38** 385–403
[6] Qi W and Bertram A 1998 Damage modeling of the single crystal superalloy SRR99 under monotonous creep *Comput. Mater. Sci.* **13** 132–41

[7] Sajjadi S A, Nategh S and Guthrie R I L 2002 Study of microstructure and mechanical properties of high performance Ni-base superalloy GTD-111 *Materials Science and Engineering* A **325** 484–9
[8] Houa J S, Guoa J T, Zhoua L Z, Yuana C and Ye H Q 2004 Microstructure and mechanical properties of cast Ni-base superalloy K44 *Materials Science and Engineering* A **374** 327–34
[9] Yuan H and Liu W C 2005 Effect of the gama phase on the hot deformation behavior of Inconel 718 *Materials Science and Engineering* A **408** 281–9
[10] Hyde T H, Becker A A, Song Y and Sun W 2006 Failure estimation of TIG butt-welded Inco718 sheets at 620 °C under creep and plasticity conditions *Comput. Mater. Sci.* **35** 35–41
[11] Marahleh G, Kheder A R I and Hamad H F 2006 Creep life prediction of service-exposed turbine blades *Materials Science and Engineering* A **433** 305–9
[12] Kim T W, Kang D H, Yeom J T and Park N K 2007 Continuum damage mechanics-based creep-fatigue-interacted life prediction of nickel-based Superalloy at high temperature *Scr. Mater.* **57** 1149–52
[13] Chen L, Liu Y and Xie L 2007 Power-exponent function model for low-cycle fatigue life prediction and its applications-Part II: life prediction of turbine blades under creep–fatigue interaction *Int. J. Fatigue* **29** 10–9
[14] Chateau E and Remy L 2010 Oxidation-assisted creep damage in a wrought nickel-based superalloy *Materials Science and Engineering* A **527** 1655–64
[15] Chen L 2010 Tensile creep behavior and strain-rate sensitivity of superalloy GH4049 at elevated temperatures *Materials Science and Engineering* A **527** 1120–5
[16] Maharaj C, Morris A and Dear J P 2012 Modeling of creep in Inconel 706 turbine disc fir-tree *Materials Science and Engineering* A **558** 412–21
[17] Shi D, Dong C, Yang X, Sun Y, Wang J and Liu J 2013 Creep and fatigue lifetime analysis of directionally solidified superalloy and its brazed joints based on continuum damage mechanics at elevated temperature *Materials and Design* **45** 643–52
[18] Liu D S, Zhang D X, Liang J W, Wen Z X and Yue Z F 2014 Prediction of creep rupture life of a V-notched bar in DD6 Ni-based single crystal superalloy *Materials Science and Engineering* A **615** 14–21
[19] Martino S F D, Faulkner R G, Hogg S C, Vujic S and Tassa O 2014 Characterization of microstructure and creep properties of alloy 617 for high-temperature applications *Materials Science and Engineering* A **619** 77–86
[20] Sugui T, Baoshuai Z, Delong S, Jing W, Qiuyang L and Chongliang J 2015 Creep properties and deformation mechanism of the containing 4.5Re/3.0Ru single crystal nickel-based superalloy at high temperatures *Materials Science and Engineering* A **643** 119–26
[21] Wollgramm P, Buck H, Neuking K, Parsa A B, Schuwalow S, Rogal J, Drautz R and Eggeler G 2015 On the role of Re in the class and temperature dependence of creep of Ni-bas single crystal superalloys *Materials Science and Engineering* A **628** 382–95
[22] Liu D, Li H and Liu Y 2015 Numerical simulation of creep damage and life prediction of superalloy turbine blade *Mathematical Problems in Engineering* **2015** 1–10
[23] Seruga D, Fajdiga M and Nagode M 2011 Creep damage calculation for thermo-mechanical fatigue *Journal of Mechanical Engineering* **57** 371–8
[24] Donchie M J and Donchie S J 2002 *Superalloys: A Technical Guide* (Materials Park, OH: ASM International)
[25] Dieter G E 1998 *Mechanical Metallurgy* (New York: McGraw Hill)
[26] Eftekhari M and Fatemi A 2016 Creep behavior and modeling of neat, talc-filled, and short glass fiber reinforced thermoplastics *Composites Part* B **97** 68–83
[27] Monkman C F C F and Grant N J 1956 An empirical relationship between rupture life and minimum creep rate in creep-rupture tests *ASTM Proceeding* **56** 593–620
[28] Dobes F and Milicka K 1976 The relation between minimum creep rate and time to fracture *Met. Sci.* **10** 382–4
[29] Creep and Swelling, Help of ABAQUS Software
[30] Du Y, Yan N and Kortschot M T 2013 An experimental study of creep behavior of lightweight natural fiber-reinforced polymer composite/honeycomb core sandwich panels *Compos. Struct.* **106** 160–116
[31] Findley W N 1960 Mechanism and mechanics of creep of plastics *Division of Engineering* (Brown University)
[32] Hadid M, Rechak S and Tati A 2004 Long-term bending creep behavior prediction of injection molded composite using stress-time correspondence principle *Materials Science Engineering* A **385** 8–54
[33] Zhao Y, Gong J, Yong J, Wang X, Shen L and Li Q 2016 Creep behaviors of Cr25Ni35Nb and Cr35Ni45N alloys predicted by modified theta method *Materials Science and Engineering* A **649** 1–8
[34] Chaboche J L 1988 Continuum damage mechanics: II. General concepts *Journal of Applied Mechanics* **55** 59–64
[35] Griva I, Nash S G and Sofer A 2009 Linear and nonlinear optimization, edn 1, appendix D: nonlinear least squares for data fitting *Society for Industrial and Applied Mathematics*
[36] Standard test methods for conducting creep, creep-rupture and stress-rupture tests of metallic materials, ASTM-E139-11, ASTM International 2012
[37] Bhambri A, Kattamis T Z and Morral J E 1975 Cast microstructure of Inconel 713C and its dependence on solidification variable *Metall. Trans.* B **6** 523–38

Mechanical Failure

Chapter 9

Overview

- Failure Modes
  - Fracture, Fatigue, Creep
- Fracture Modes
  - Ductile, Brittle, Intergranular, Transgranular
- Fracture Toughness
- Stress Concentrators (Flaws)
- Crack Propagation

Fracture Modes

- Simple fracture is the separation of a body into 2 or more pieces in response to an applied stress that is static (constant) and at temperatures that are low relative to the T_m of the material.
- Classification is based on the ability of a material to experience plastic deformation.
- Ductile fracture
  - Accompanied by significant plastic deformation
- Brittle fracture
  - Little or no plastic deformation
  - Sudden, catastrophic

Fracture Mechanism

Imposed stress → Crack Formation → Propagation

- Ductile failure has extensive plastic deformation in the vicinity of the advancing crack. The process proceeds relatively slow (stable). The crack resists any further extension unless there is an increase in the applied stress.
- In brittle failure, cracks may spread very rapidly, with little deformation. These cracks are more unstable and crack propagation will continue without an increase in the applied stress.

Crack Propagation

Cracks propagate due to sharpness of crack tip

- **A plastic material deforms at the tip, "blunting" the crack.**

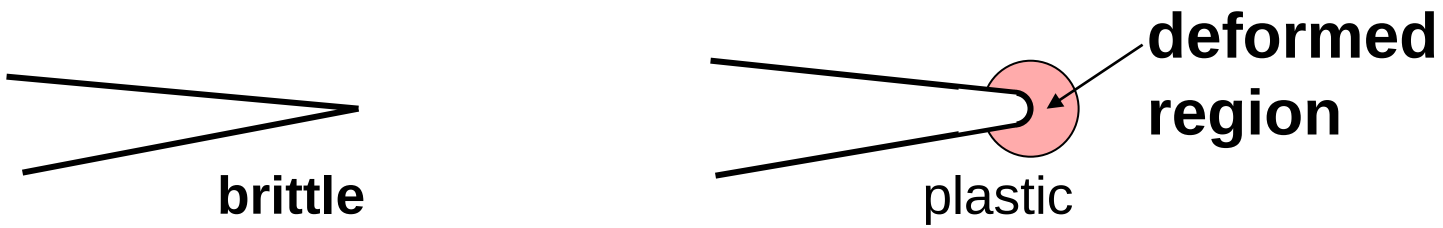

Energy balance on the crack

- **Elastic strain energy-**
    - **energy stored in material as it is elastically deformed**
    - **this energy is released when the crack propagates**
    - **creation of new surfaces requires energy**

Ductile vs Brittle Failure

Fracture behavior:	Very Ductile	Moderately Ductile	Brittle

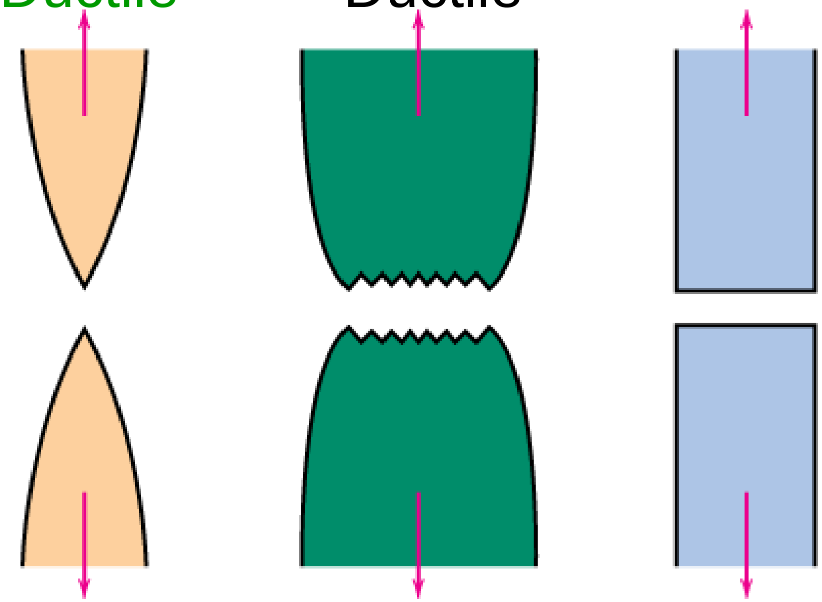

%*AR* or %*EL*	Large	Moderate	Small

- Ductile fracture is usually more desirable than brittle fracture.

Ductile: Warning before fracture

Brittle: No warning

Moderately Ductile Failure

- Evolution to failure:

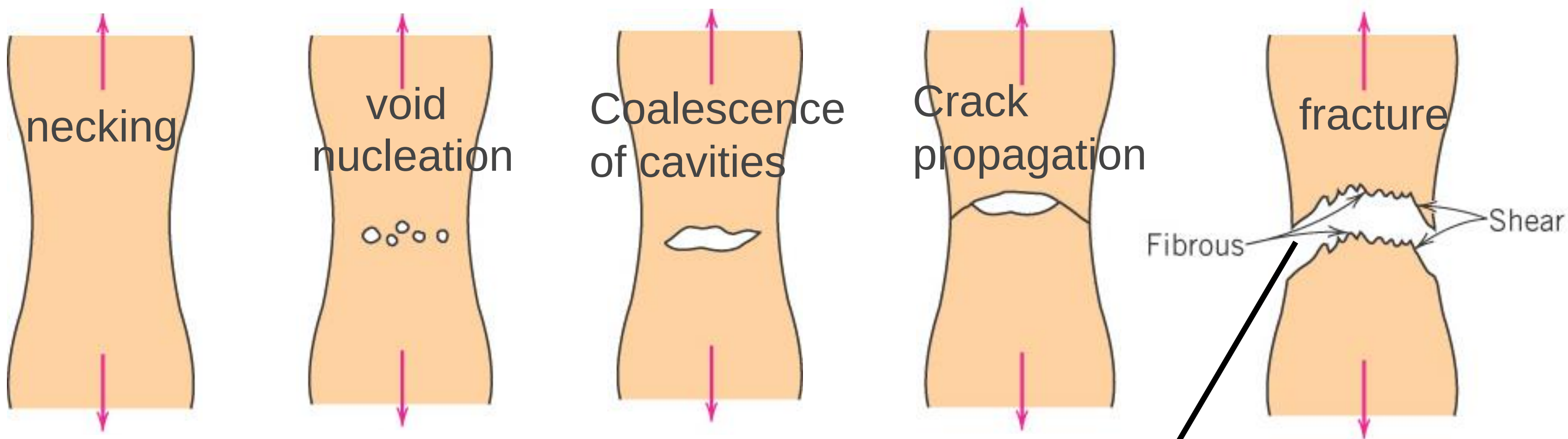

- Resulting fracture surfaces (steel)

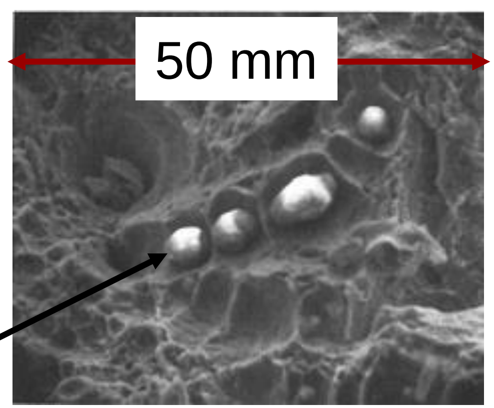

From V.J. Colangelo and F.A. Heiser, *Analysis of Metallurgical Failures* (2nd ed.), Fig. 11.28, p. 294, John Wiley and Sons, Inc., 1987. (Orig. source: P. Thornton, *J. Mater. Sci.*, Vol. 6, 1971, pp. 347-56.)

particles serve as void nucleation sites.

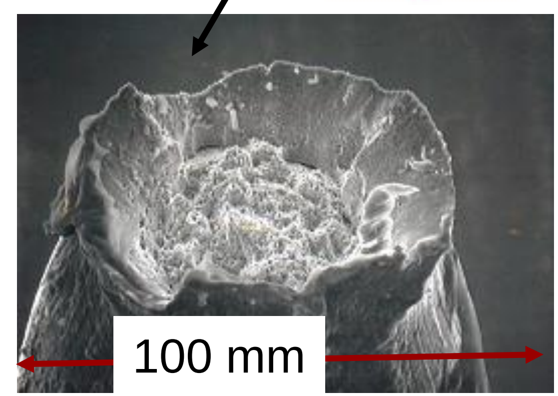

Fracture surface of tire cord wire loaded in tension. Courtesy of F. Roehrig, CC Technologies, Dublin, OH. Used with permission.

Example: Pipe Failures

- **Ductile failure:**
  -- one piece
  -- large deformation

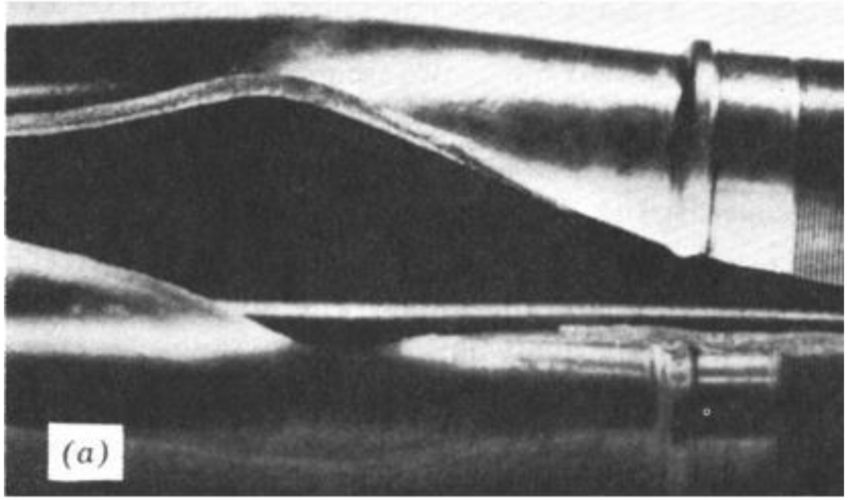

- **Brittle failure:**
  -- many pieces
  -- small deformations

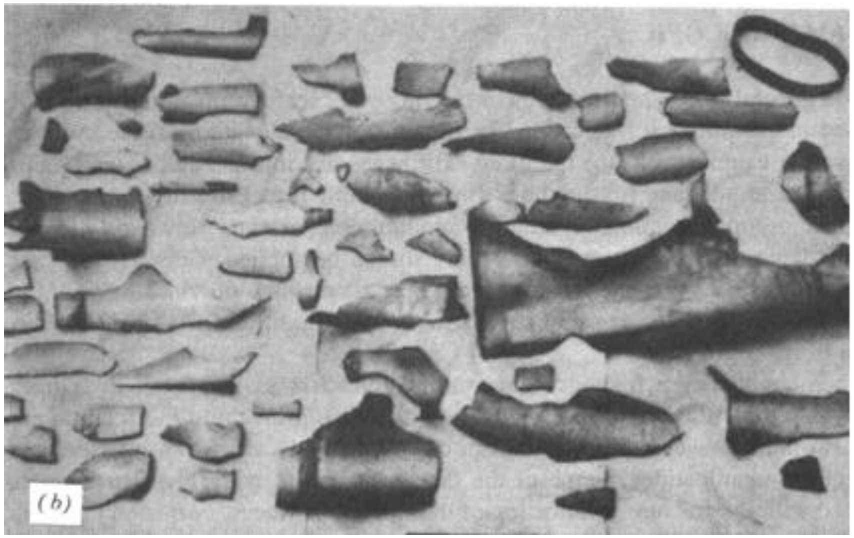

Figures from V.J. Colangelo and F.A. Heiser, *Analysis of Metallurgical Failures* (2nd ed.), Fig. 4.1(a) and (b), p. 66 John Wiley and Sons, Inc., 1987. Used with permission.

Ductile vs. Brittle Failure

(a)

cup-and-cone fracture

(b)

brittle fracture

Ductile Failure

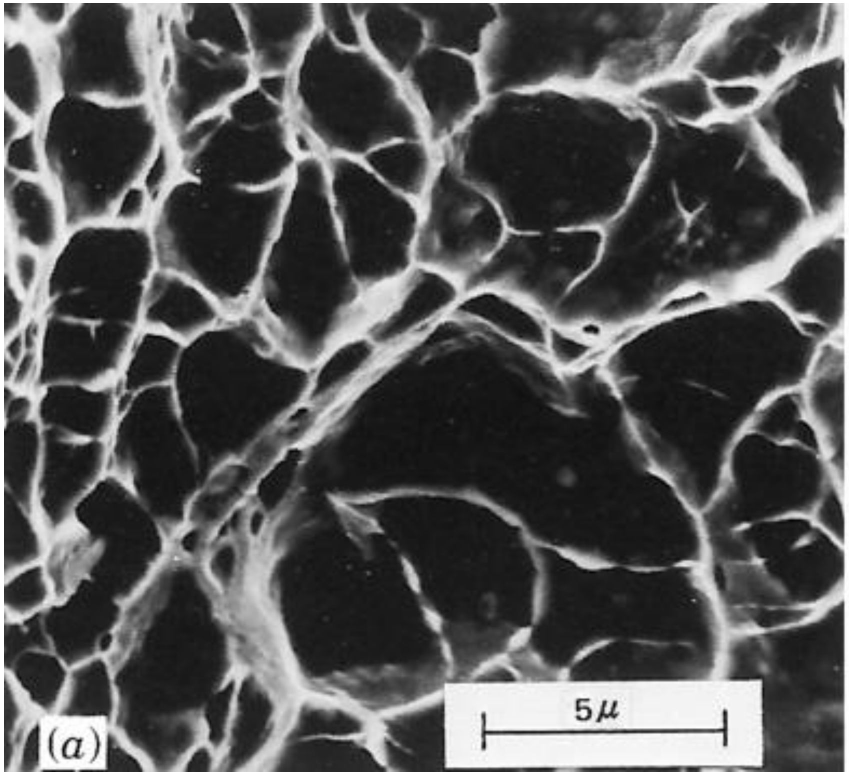

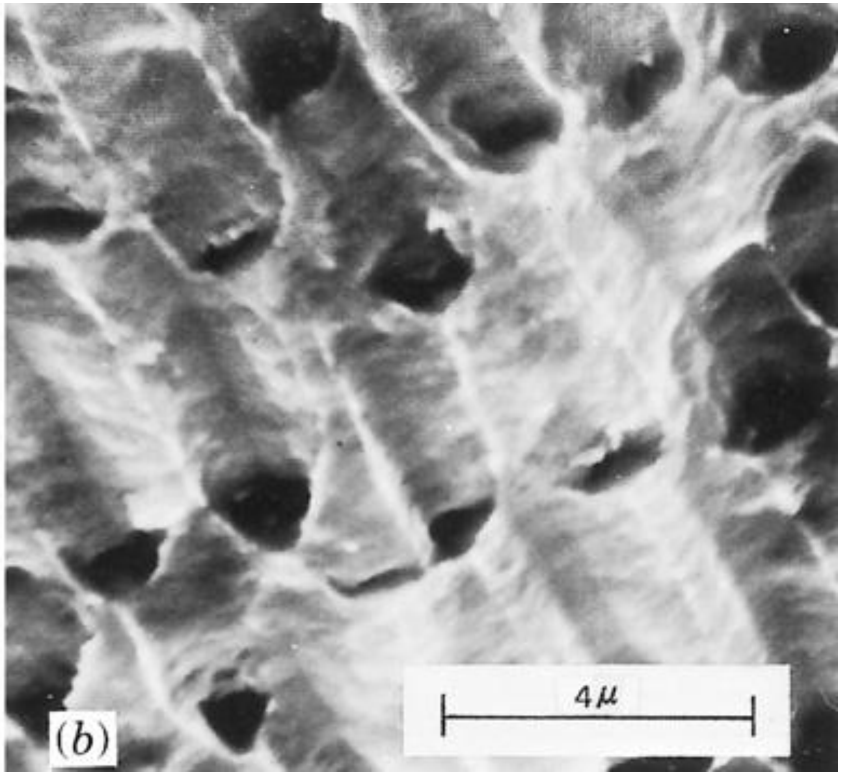

(a) SEM image showing spherical dimples resulting from a uniaxial tensile load. (b) SEM image of parabolic dimples from shear loading.

Brittle Fracture

Arrows indicate point at failure origination

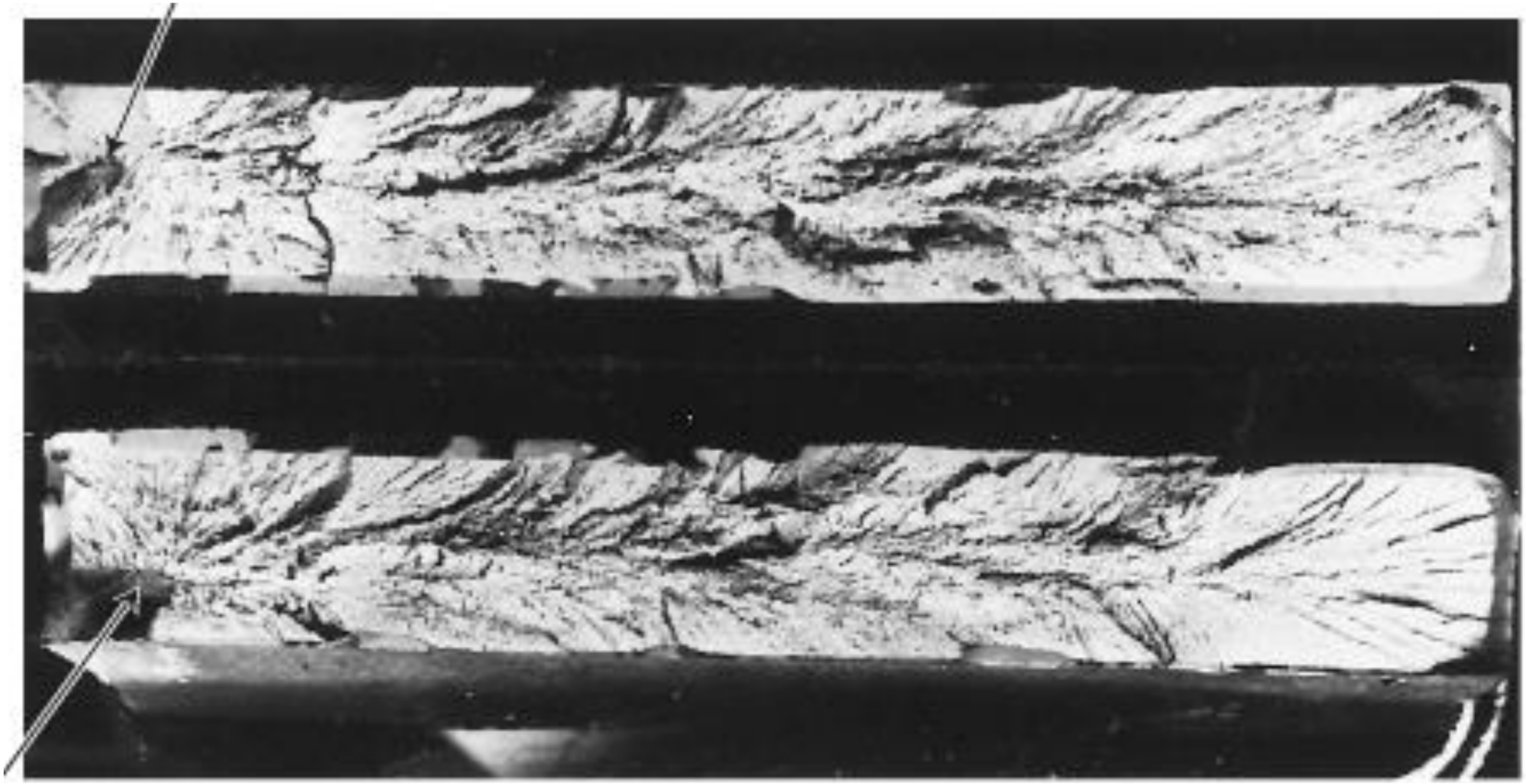

Distinctive pattern on the fracture surface: V-shaped “chevron” markings point to the failure origin.

Transgranular Fracture

- Cleavage - in most brittle crystalline materials, crack propagation that results from the repeated breaking of atomic bonds along specific planes.
- This leads to transgranular fracture where the crack splits (cleaves) through the grains.

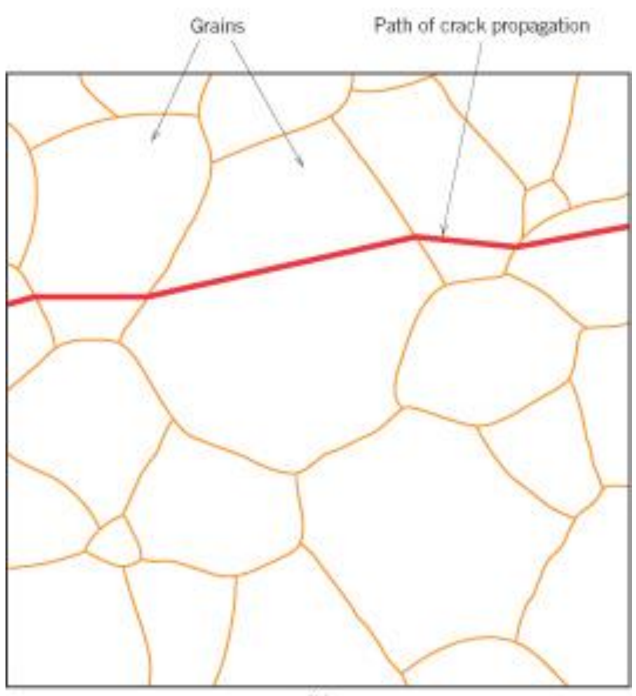

(a)

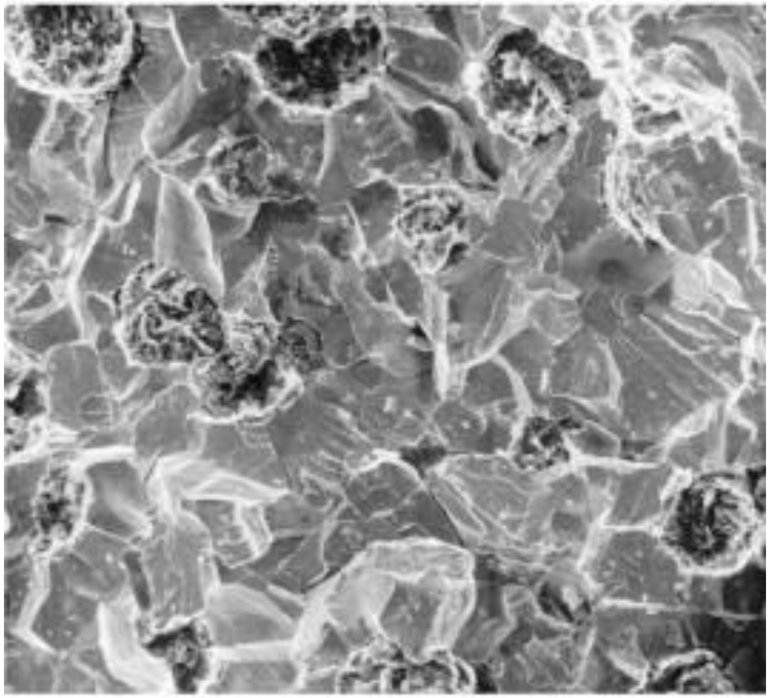
(b)

Intergranular Fracture

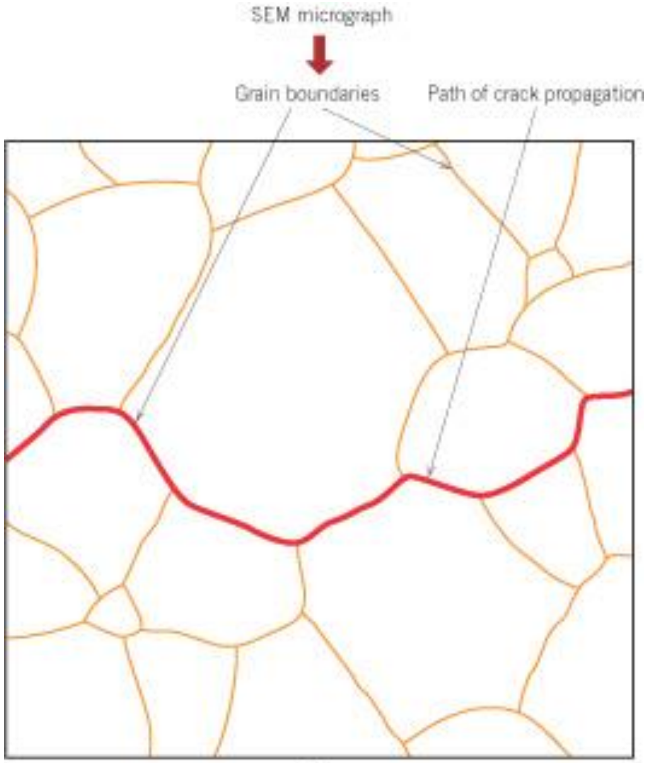

(a)


(b)

- Intergranular failure is typically due to elemental depletion (chromium) at the grain boundaries or some type of weakening of the grain boundary due to chemical attack, oxidation, embrittlement.

Fracture Mechanics

Studies the relationships between:

- material properties
- stress level
- crack producing flaws
- crack propagation mechanisms

Stress Concentration

- The measured fracture strengths for most brittle materials are significantly lower than those predicted by theoretical calculations based on atomic bond energies.
- This discrepancy is explained by the presence of very small, microscopic flaws or cracks that are inherent to the material.
- The flaws act as stress concentrators or stress raisers, amplifying the stress at a given point.
- This localized stress diminishes with distance away from the crack tip.

Fracture Toughness

- Fracture toughness measures a material's resistance to brittle fracture when a crack is present.
- It is an indication of the amount of stress required to propagate a preexisting flaw.
- Flaws may appear as cracks, voids, metallurgical inclusions, weld defects, design discontinuities, or some combination thereof.
- It is common practice to assume that flaws are present and use the linear elastic fracture mechanics (LEFM) approach to design critical components.
- This approach uses the flaw size and features, component geometry, loading conditions and the fracture toughness to evaluate the ability of a component containing a flaw to resist fracture.

Ductile vs Brittle

- The effect of a stress raiser is more significant in brittle than in ductile materials.
- For a ductile material, plastic deformation results when the maximum stress exceeds the yield strength.
- This leads to a more uniform distribution of stress in the vicinity of the stress raiser; the maximum stress concentration factor will be less than the theoretical value.
- In brittle materials, there is no redistribution or yielding.

Fracture Toughness

Table 9.1 Room-Temperature Yield Strength and Plane Strain Fracture Toughness Data for Selected Engineering Materials

Material	*Yield Strength* *MPa*	*Yield Strength* *ksi*	K_{Ic} $MPa\sqrt{m}$	K_{Ic} $ksi\sqrt{in.}$
Metals				
Aluminum alloy[a] (7075-T651)	495	72	24	22
Aluminum alloy[a] (2024-T3)	345	50	44	40
Titanium alloy[a] (Ti-6Al-4V)	910	132	55	50
Alloy steel[a] (4340 tempered @ 260°C)	1640	238	50.0	45.8
Alloy steel[a] (4340 tempered @ 425°C)	1420	206	87.4	80.0
Ceramics				
Concrete	—	—	0.2–1.4	0.18–1.27
Soda-lime glass	—	—	0.7–0.8	0.64–0.73
Aluminum oxide	—	—	2.7–5.0	2.5–4.6
Polymers				
Polystyrene (PS)	25.0–69.0	3.63–10.0	0.7–1.1	0.64–1.0
Poly(methyl methacrylate) (PMMA)	53.8–73.1	7.8–10.6	0.7–1.6	0.64–1.5
Polycarbonate (PC)	62.1	9.0	2.2	2.0

[a] **Source:** Reprinted with permission, *Advanced Materials and Processes,* ASM International, © 1990.

stress-intensity factor (K)

- The stress-intensity factor (K) is used to determine the fracture toughness of most materials.
- A Roman numeral subscript indicates the mode of fracture and the three modes of fracture are illustrated in the image to the right.
- Mode I fracture is the condition where the crack plane is normal to the direction of largest tensile loading. This is the most commonly encountered mode.
- The stress intensity factor is a function of loading, crack size, and structural geometry. The stress intensity factor may be represented by the following equation: $K_I = \sigma\sqrt{\pi a \beta}$

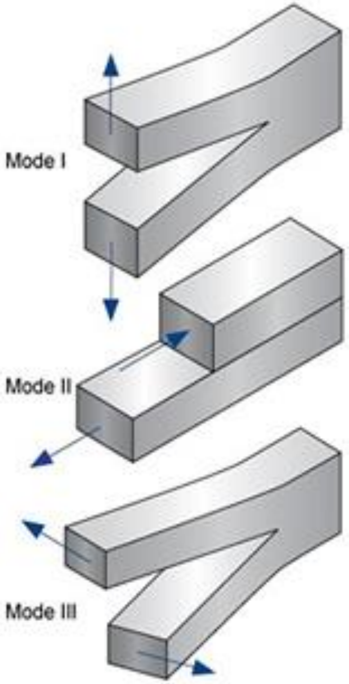

K_I is the fracture toughness in $MPa\sqrt{m}$ $(psi\sqrt{in})$

σ is the applied stress in MPa or psi

a is the crack length in meters or inches

β is a crack length and component geometry factor that is different for each specimen, dimensionless.

Critical Stress

- All brittle materials contain a population of small cracks and flaws that have a variety of sizes, geometries and orientations.
- When the magnitude of a tensile stress at the tip of one of these flaws exceeds the value of this critical stress, a crack forms and then propagates, leading to failure.
- Condition for crack propagation:

$$K \geq K_c$$

Stress Intensity Factor:
--Depends on load & geometry.

Fracture Toughness:
--Depends on the material, temperature, environment & rate of loading.

Fracture toughness - good diagrams
http://www.ndt-ed.org/EducationResources/CommunityCollege/Materials/Mechanical/FractureToughness.htm

Compact tension (CT) specimen

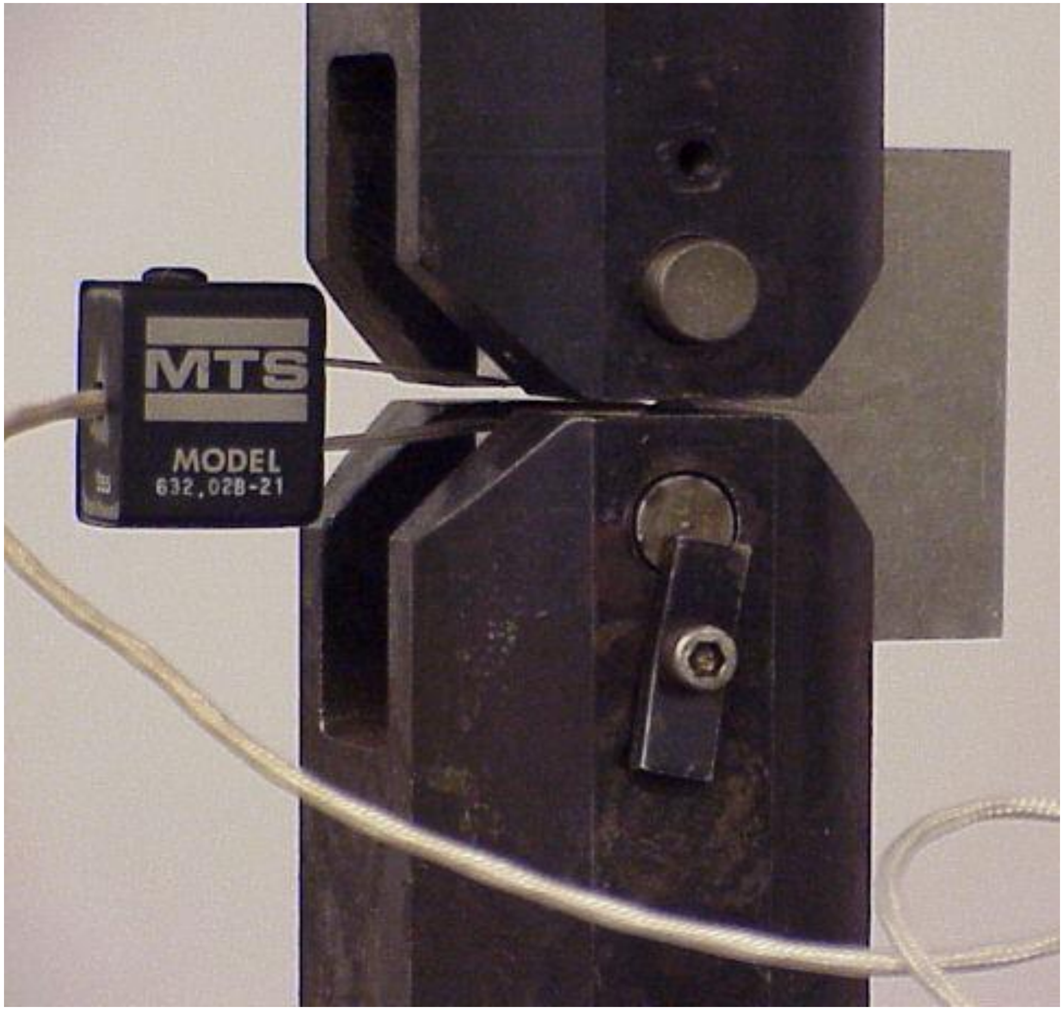

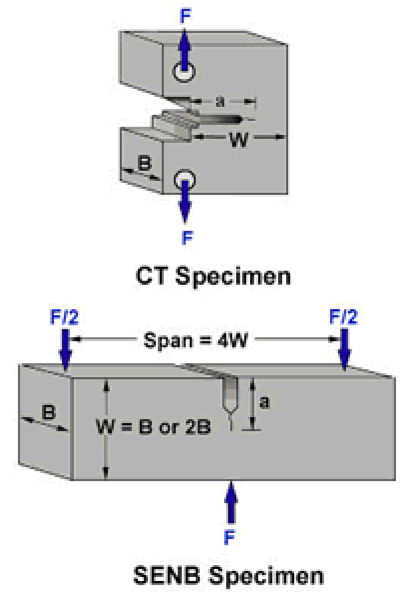

single edge notch bend (SENB or three-point bend)

Flaws are Stress Concentrators

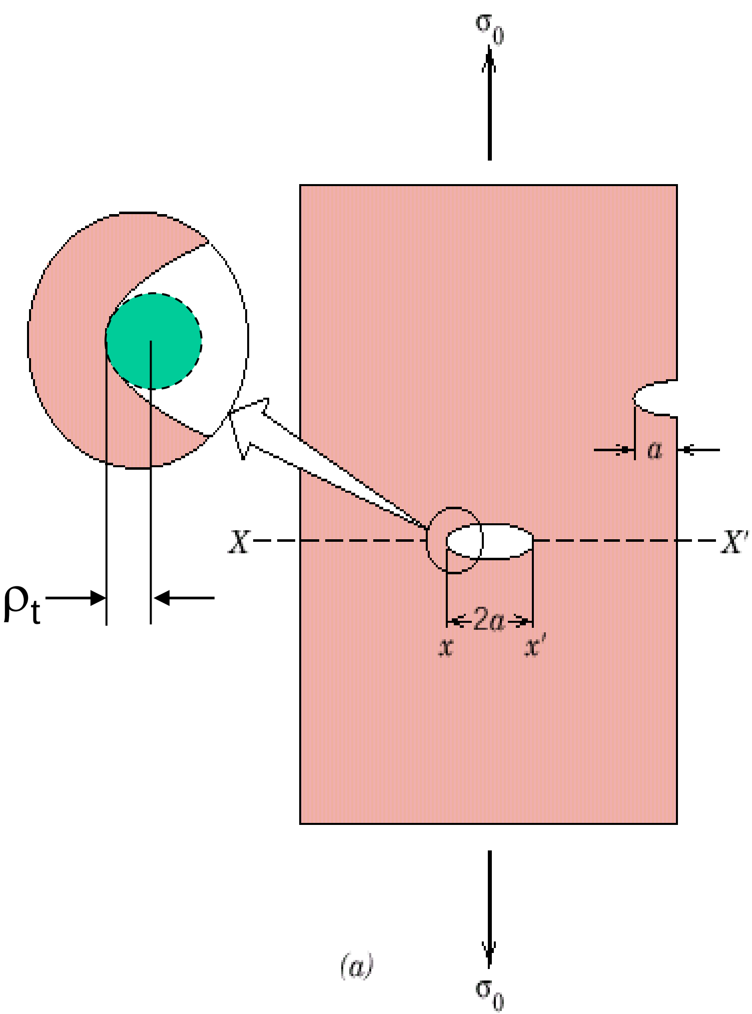

If the crack is similar to an elliptical hole through plate, and is oriented perpendicular to applied stress, the maximum stress σ_m=

$$\sigma_m = 2\sigma_o \left(\frac{a}{\rho_t} \right)^{1/2} = K_t \sigma_o$$

where

ρ_t = radius of curvature

σ_o = applied stress

σ_m = stress at crack tip

a = length of surface crack or ½ length of internal crack

$\sigma_m / \sigma_o = K_t$ the stress concentration factor

DESIGN AGAINST CRACK GROWTH

- **Crack growth condition:** $K \geq K_c$

  $K = Y\sigma\sqrt{\pi a}$

- **Largest, most stressed cracks grow first.**

--Result 1: Max flaw size dictates design stress.

$$\sigma_{design} < \frac{K_c}{Y\sqrt{\pi a_{max}}}$$

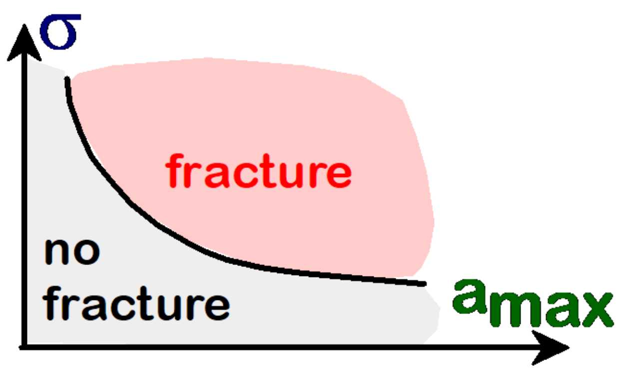

--Result 2: Design stress dictates max. flaw size.

$$a_{max} < \frac{1}{\pi}\left(\frac{K_c}{Y\sigma_{design}}\right)^2$$

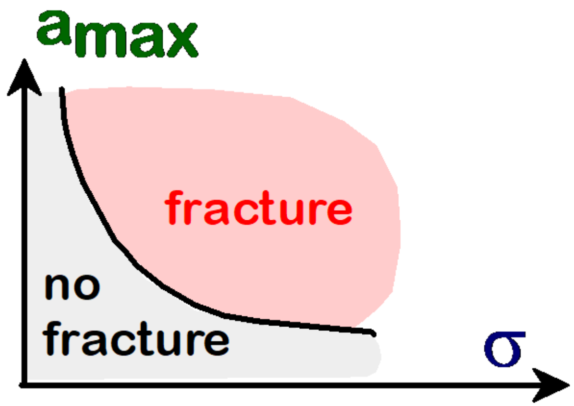

Design Example: Aircraft Wing

- Material has K_c = 26 MPa-m$^{0.5}$
- Two designs to consider...

Design A

-- largest flaw is 9 mm

-- failure stress = 112 MPa

Design B

-- use same material

-- largest flaw is 4 mm

-- failure stress = ?

- Use...

$$\sigma_c = \frac{K_c}{Y\sqrt{\pi a_{max}}}$$

- Key point: Y and K_c are the same in both designs. Y is a dimensionless parameter; see Callister page 298.

-- Result:

$$\left(\sigma_c \sqrt{a_{max}}\right)_A = \left(\sigma_c \sqrt{a_{max}}\right)_B$$

112 MPa 9 mm 4 mm

Answer: $(\sigma_c)_B = 168\,\text{MPa}$

- Reducing flaw size pays off.

Sensors made to mesh with plane

- Structural engineers have long imagined the day when materials used in an aircraft, a wind turbine blade or a bridge could sense if they had been strained to the point of damage, reducing their load-carrying capacity, and report that information in real time before the structure's safety is compromised.
- For many years, such a scenario was more the stuff of science fiction than fact, but today, structural health monitoring (SHM) systems that can perform these tasks are closer to reality.
- Scientists have created a fiber mesh embedded with sensors designed to monitor an airplane’s structural integrity and outside temperature.
- When wrapped around an aircraft, the sensors could help prevent microscopic cracks from developing into catastrophic failures.
- Made from a plastic polymer, the mesh is designed so it doesn’t add significant weight or drag to an aircraft.
- The technology also could be used in autos, packaging and medical devices.

Structural health monitoring (SHM) systems can be arrayed in similar fashion to the human nervous system, with sensors concentrated in key areas where loads are highest.

A piezoelectric-based sensor system from Acellent Technologies, called SMART Layer, identifies damage with small ceramic actuators

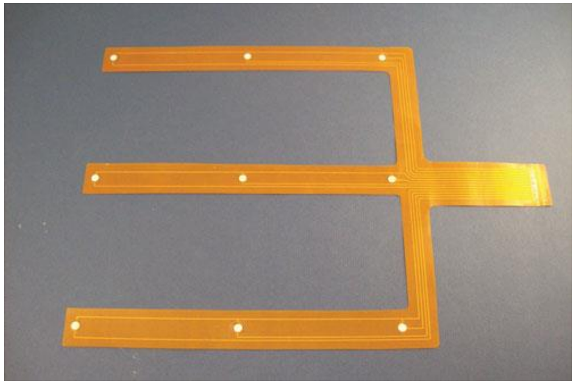

A comparative vacuum-monitoring (CVM) sensor, is a thin, self-adhesive rubber patch that detects cracks in the underlying material. The rubber is laser-etched with rows of tiny, interconnected channels or galleries, to which an air pressure is applied. Any propagating crack under the sensor breaches the galleries and the resulting change in pressure is monitored.

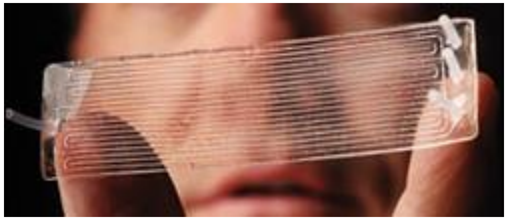

An FAA-sponsored study on curved honeycomb-cored panels showed that acoustic emission (AE) monitoring is a reliable method for locating damage initiation sites and for tracking crack progression. Source: Physical Acoustics Corp

http://www.compositesworld.com/articles/structural-health-monitoring-composites-get-smart
http://www.photonics.com/Article.aspx?AID=30528

Table 9.2 A List of Several Common Nondestructive Testing (NDT) Techniques

Technique	*Defect Location*	*Defect Size Sensitivity (mm)*	*Testing Location*
Scanning electron microscopy (SEM)	Surface	>0.001	Laboratory
Dye penetrant	Surface	0.025–0.25	Laboratory/in-field
Ultrasonics	Subsurface	>0.050	Laboratory/in-field
Optical microscopy	Surface	0.1–0.5	Laboratory
Visual inspection	Surface	>0.1	Laboratory/in-field
Acoustic emission	Surface/subsurface	>0.1	Laboratory/in-field
Radiography (X-ray/gamma ray)	Subsurface	>2% of specimen thickness	Laboratory/in-field

Brittle Fracture of Ceramics

- Most ceramics (at room temperature) fracture before any plastic deformation can occur.
- Typical crack configurations for 4 common loading methods.

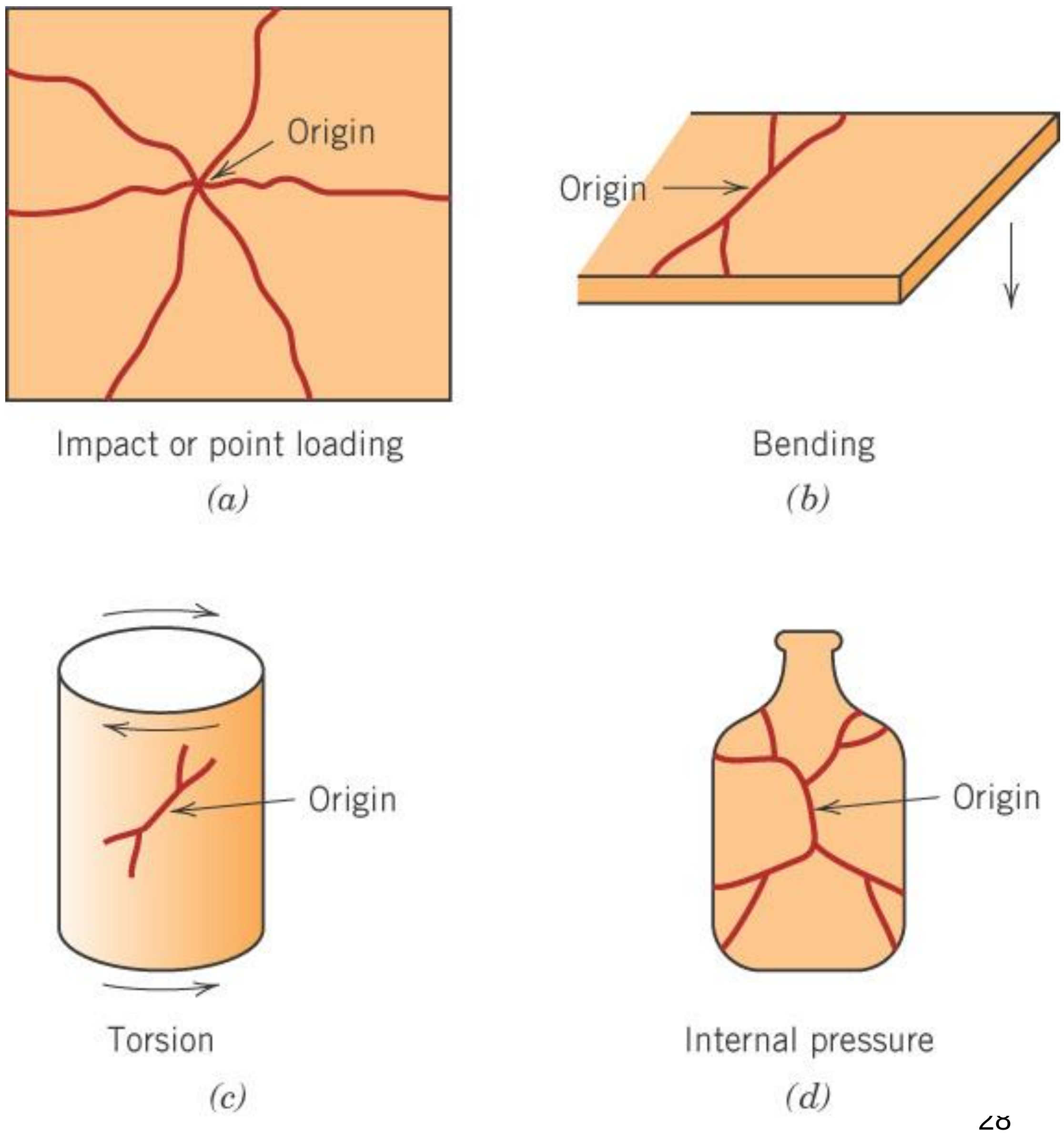

Brittle Fracture of Ceramics

- Surface of a 6-mm diameter fused silica rod.
- Characteristic fracture behavior in ceramics
  - Origin point
  - Initial region (mirror) is flat and smooth
  - After reaches critical velocity crack branches
    - mist
    - hackle

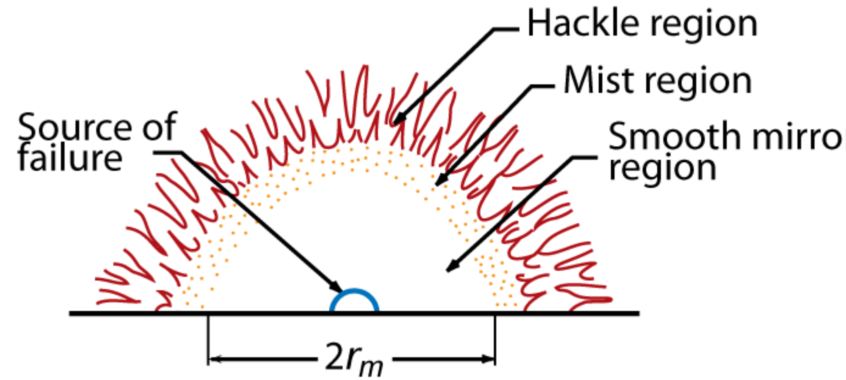

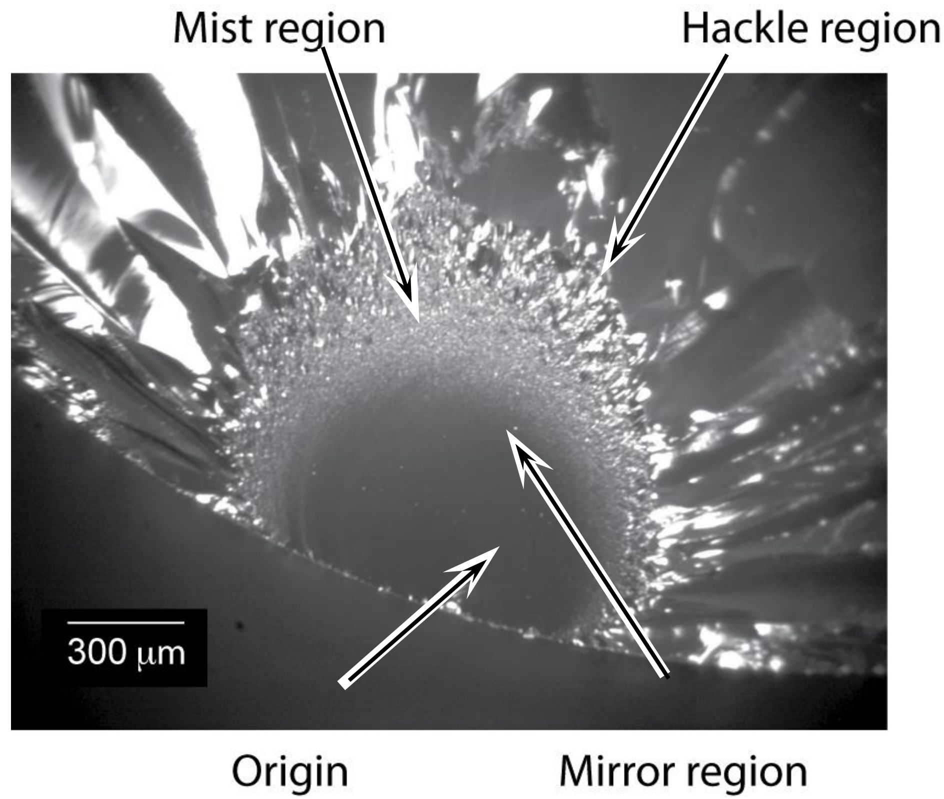

Fracture of Polymers

- The fracture strengths of polymers are low relative to ceramics and metals.
- The fracture mode in thermosetting polymers (heavily crosslinked networks) is typically brittle.
- For thermoplastic polymers, both ductile and brittle modes are possible. Reduced temperature, increased strain rate, sharp notches, increased specimen thickness are some factors that can influence a brittle fracture.
- One phenomenon that occurs in thermoplastics is crazing, very localized plastic deformation and formation of microvoids and fibrillar bridges

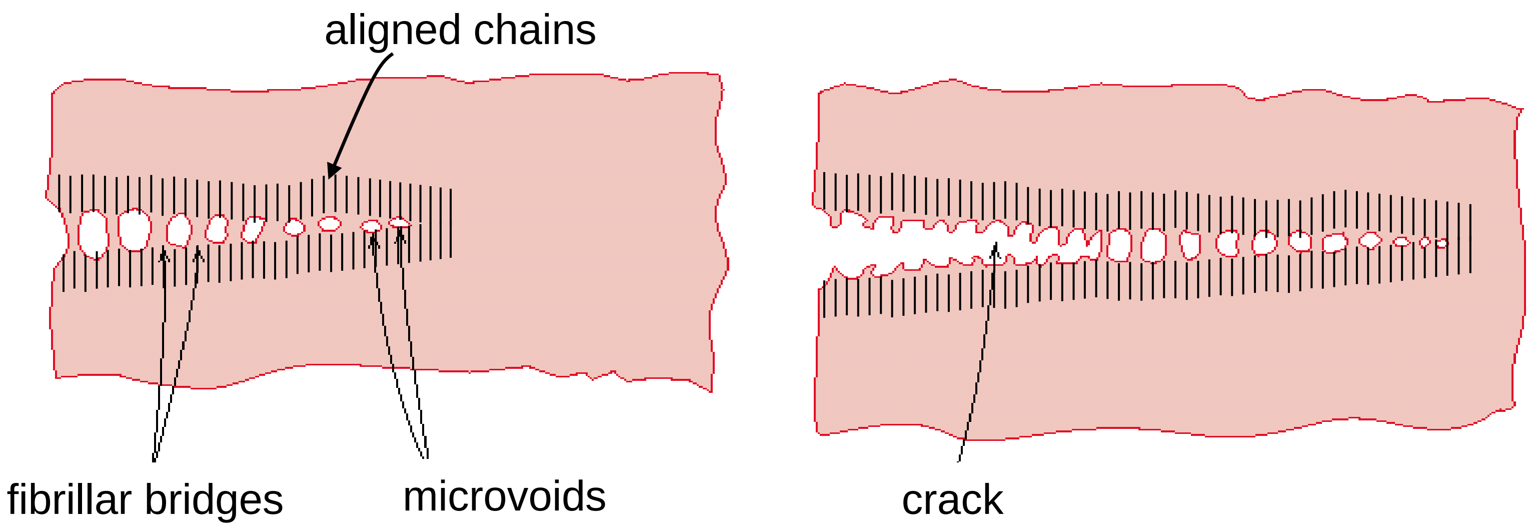

Impact Testing

- Impact loading:
  - -- severe testing case
  - -- makes material more brittle
  - -- decreases toughness

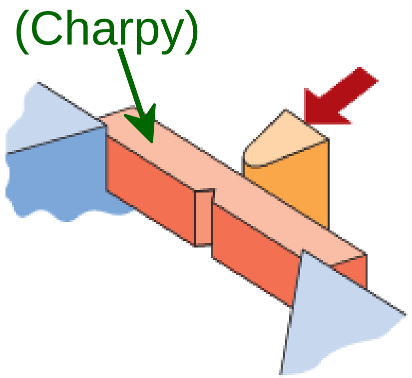

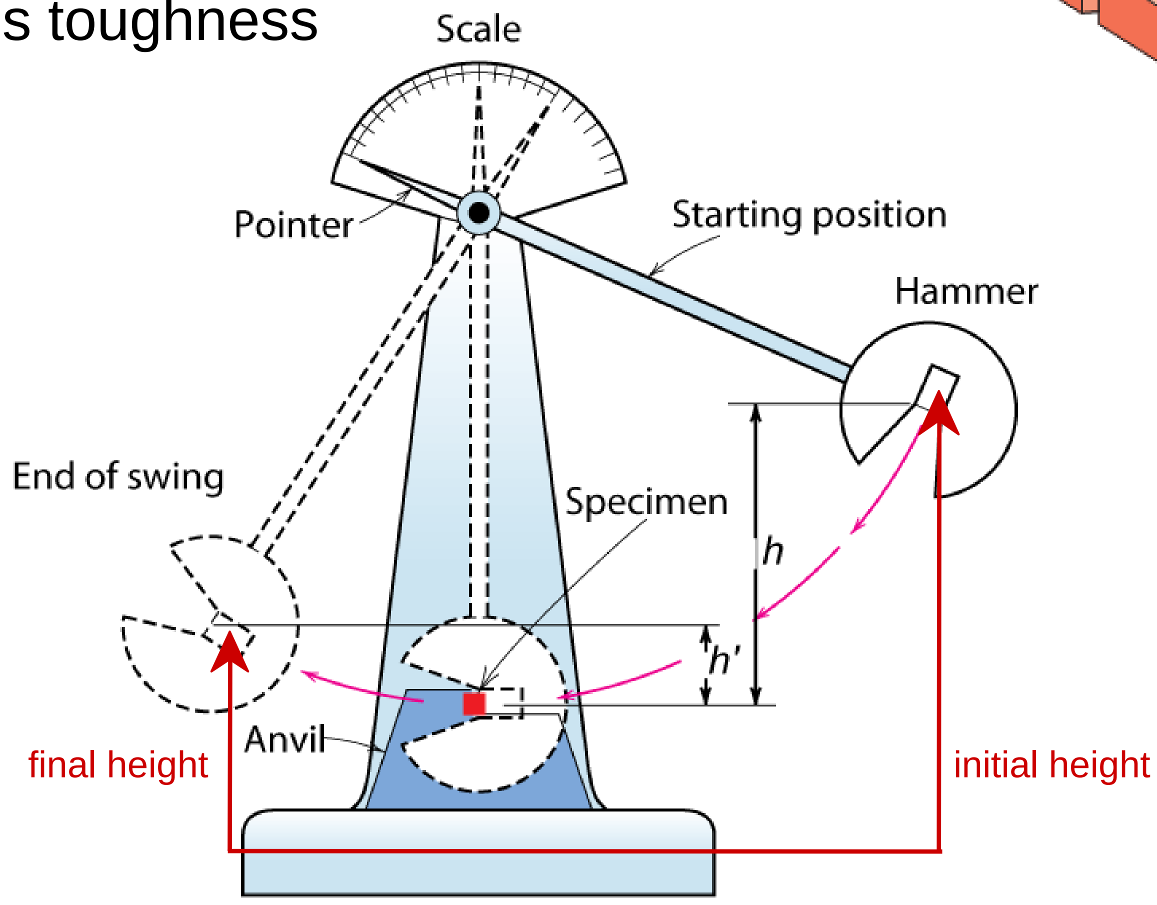

Ductile to Brittle Transition Temperature (DBTT)

- **Pre-WWII: The Titanic**

- **WWII: Liberty ships**

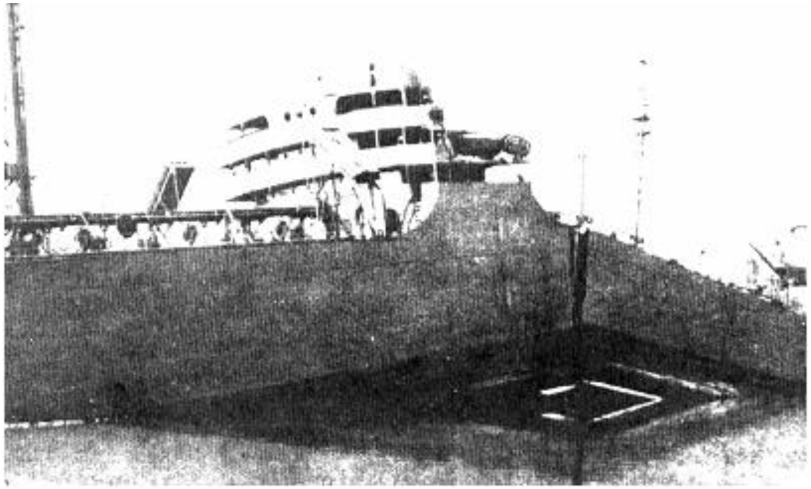

Disastrous consequences for a welded transport ship, suddenly split across the entire girth of the ship (40˚F). The vessels were constructed from steel alloys that exhibit a DBTT ≈ room temp

Reprinted w/ permission from R.W. Hertzberg, "Deformation and Fracture Mechanics of Engineering Materials", (4th ed.) Fig. 7.1(a), p. 262, John Wiley and Sons, Inc., 1996. (Orig. source: Dr. Robert D. Ballard, *The Discovery of the Titanic*.)

Charpy Impact Energy (A) and Shear Fracture % (B) Correlated with Temperature

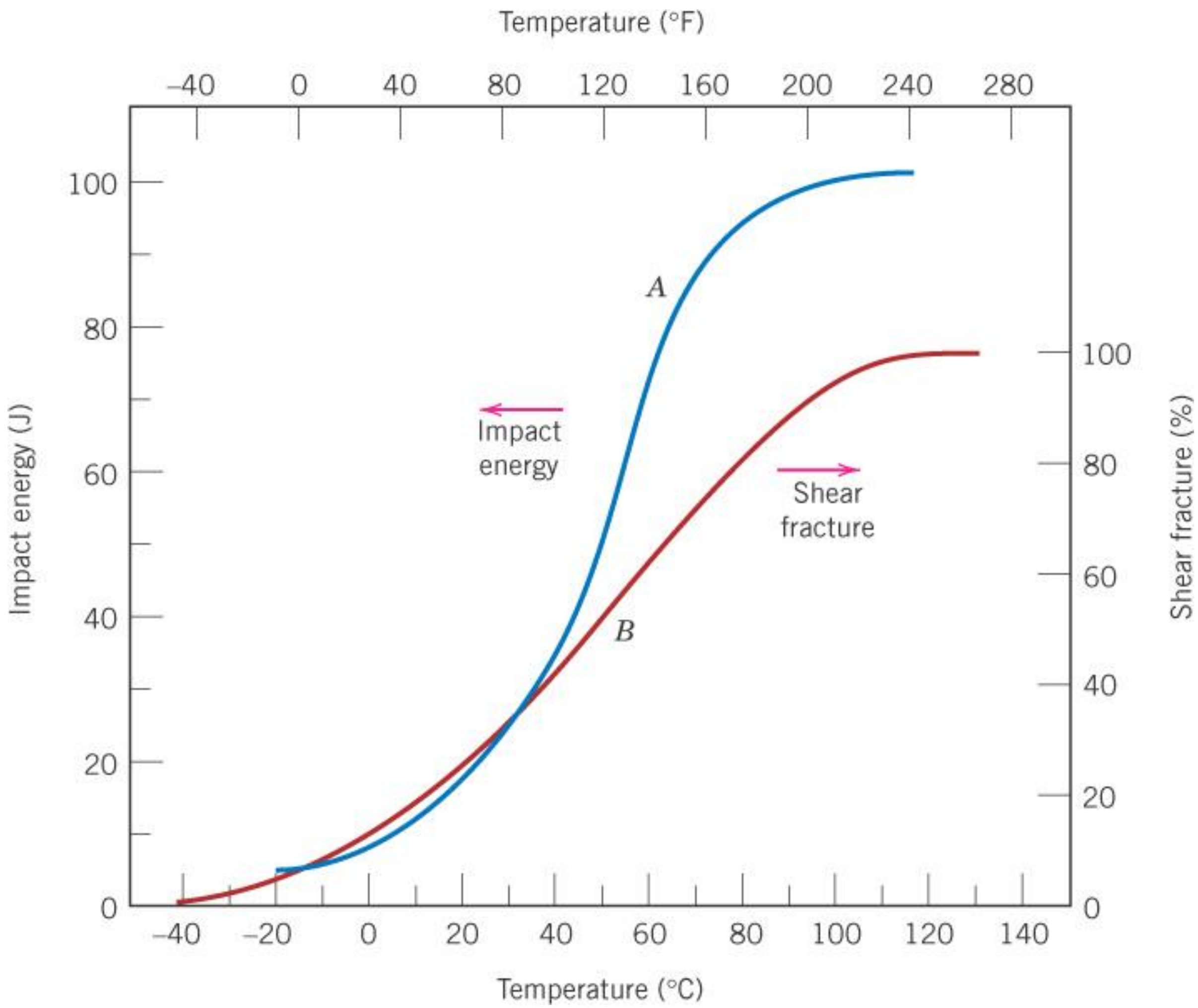

Steel Charpy Samples

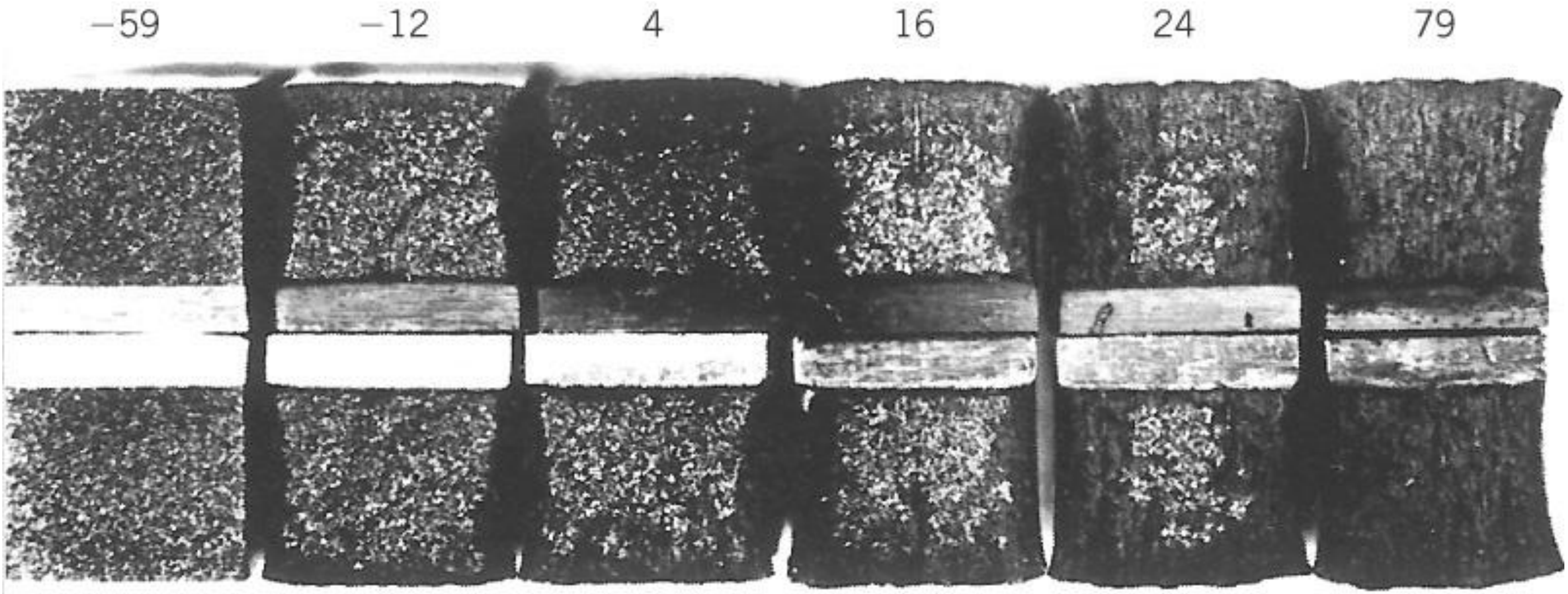

Fracture surfaces after impact showing the variation in ductility with testing temperature (˚C).

Temperature

- **Increasing temperature...**
  -- increases %EL and K_c
- **Ductile-to-Brittle Transition Temperature (DBTT)...**

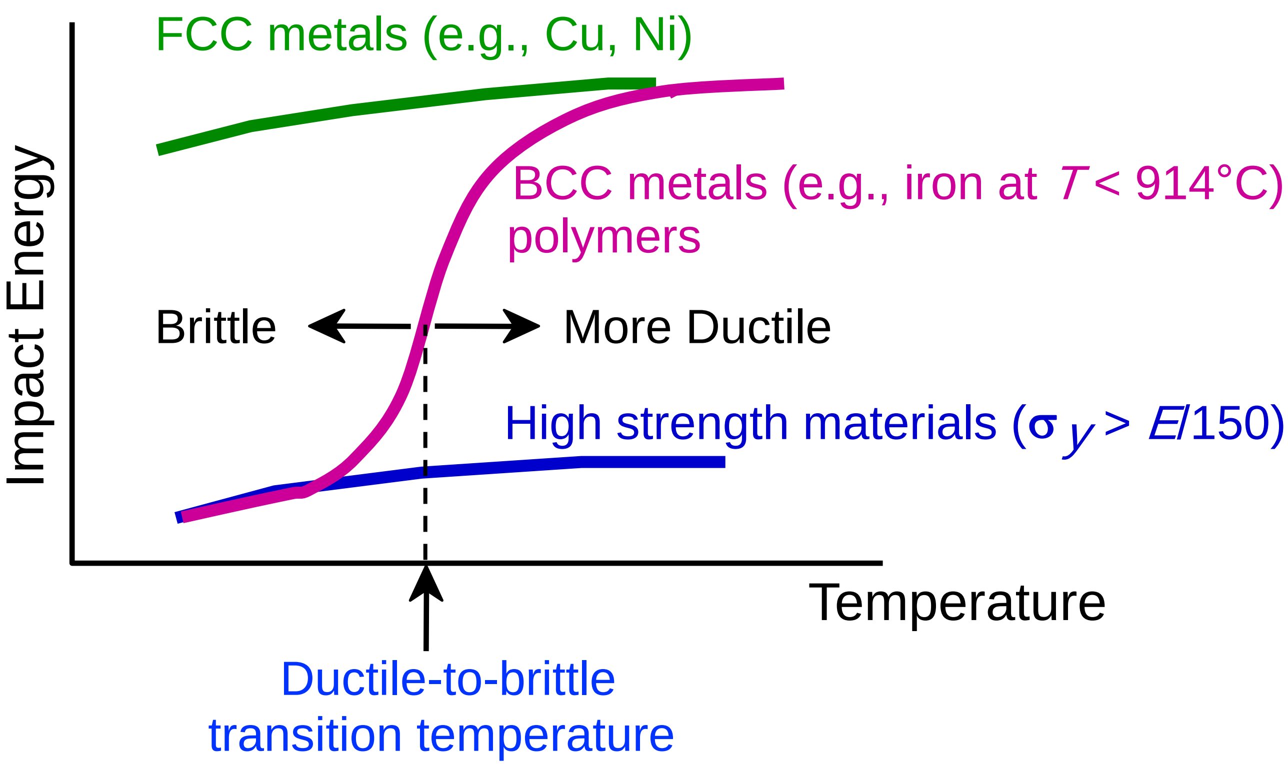

Fatigue

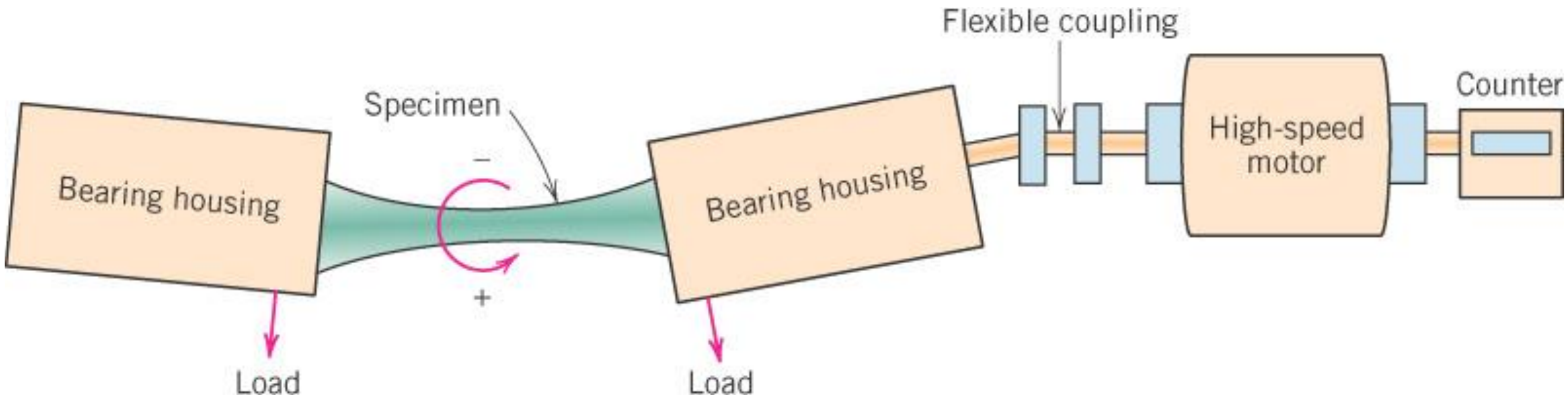

Fatigue testing apparatus for rotating bending test

- Fatigue is a form of failure that occurs in structures subjected to dynamic stresses over an extended period.
- Under these conditions it is possible to fail at stress levels considerably lower than tensile or yield strength for a static load.
- Single largest cause of failure in metals; also affects polymers and ceramics.
- Common failure in bridges, aircraft and machine components.

Cyclic Stress - Fatigue

- Variation of stress with time that accounts for fatigue failures.
- The stress may be axial (tension-compression), flexural (bending) or torsional (twisting) in nature.
- There are 3 fluctuating stress-time modes seen in the figure: (a) reversed stress cycle - symmetrical amplitude about a mean zero stress level; (b) repeated stress cycle - asymmetrical maxima and minima relative to the zero stress level; (c) variable (random) stress level

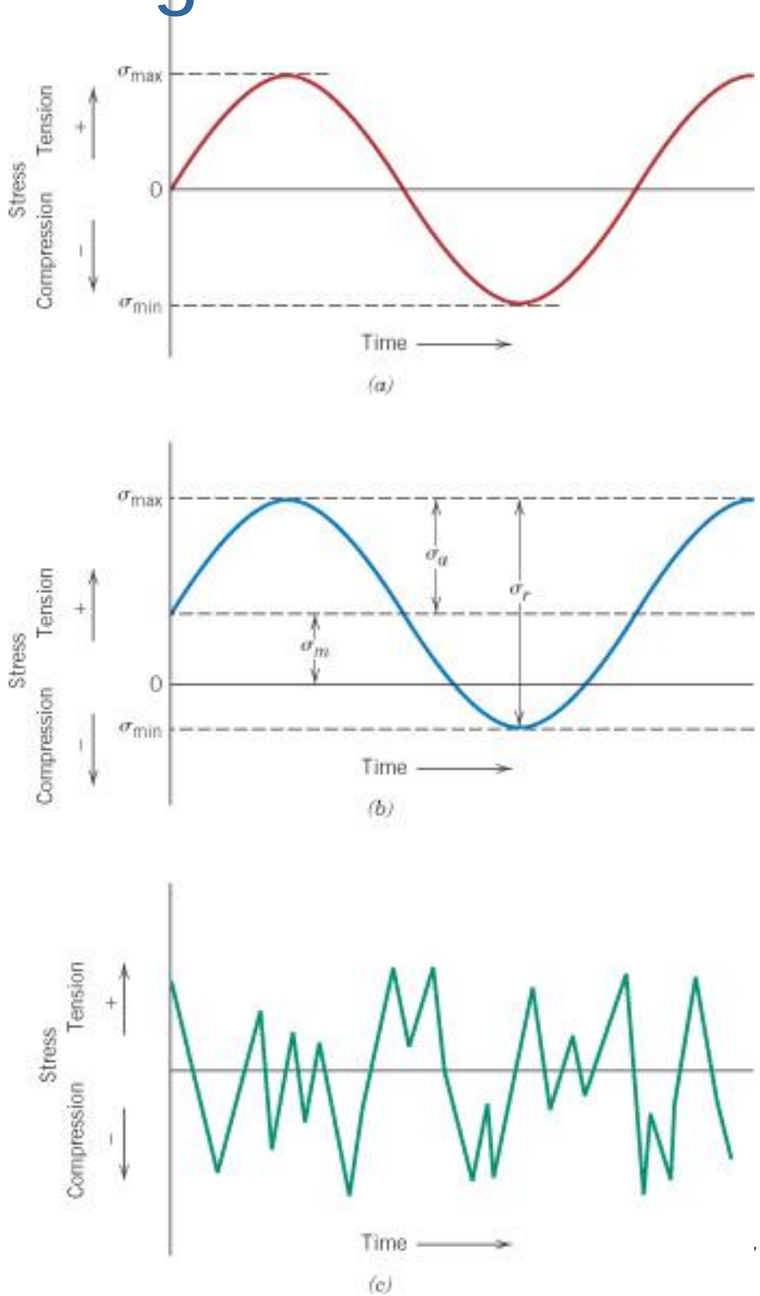

Fatigue

- Fracture surface with crack initiation at top. Surface shows predominantly dull fibrous texture where rapid failure occurred after crack achieved critical size.

- Fatigue failure
  1. Crack initiation
  2. Crack propagation
  3. Final failure

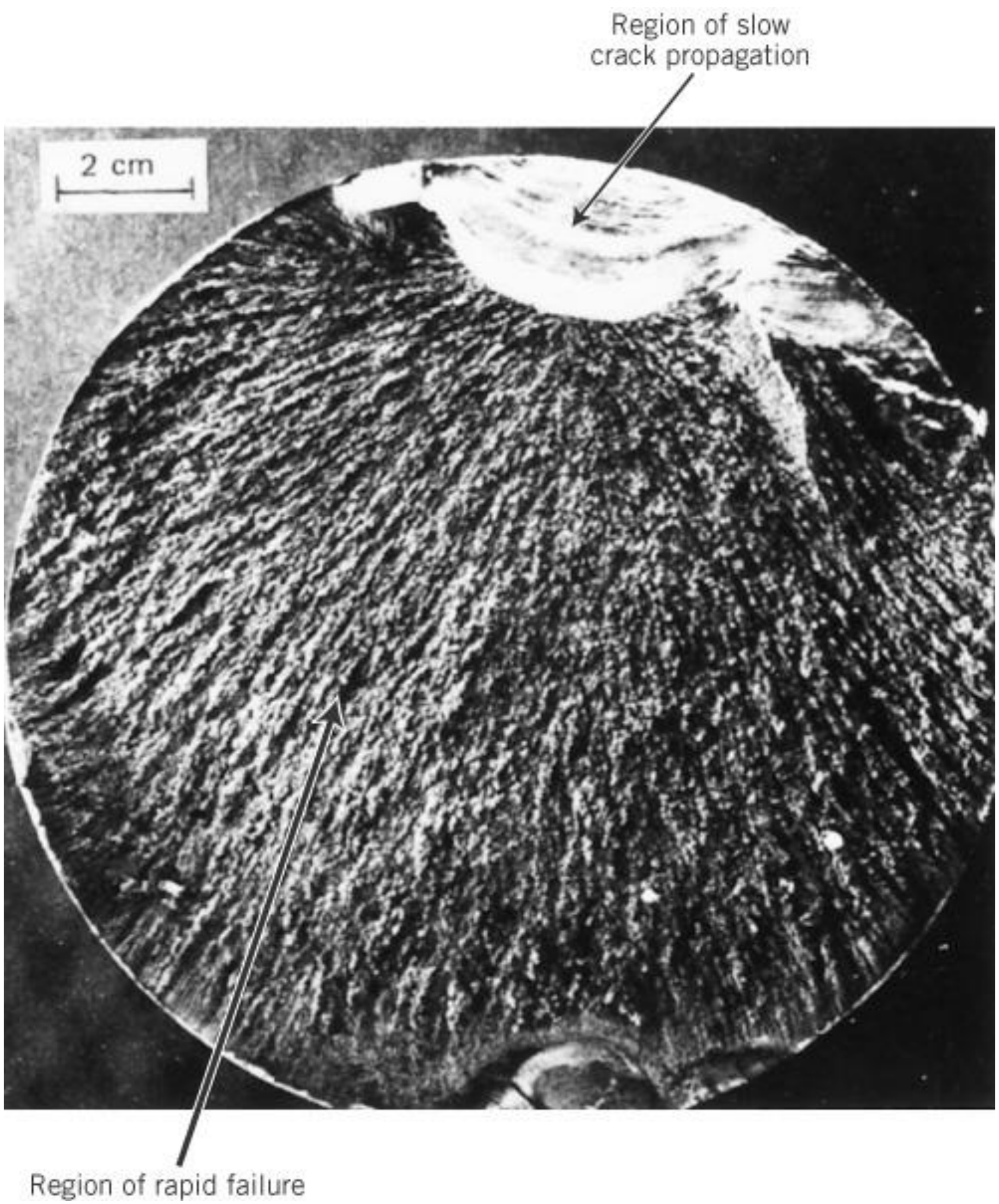

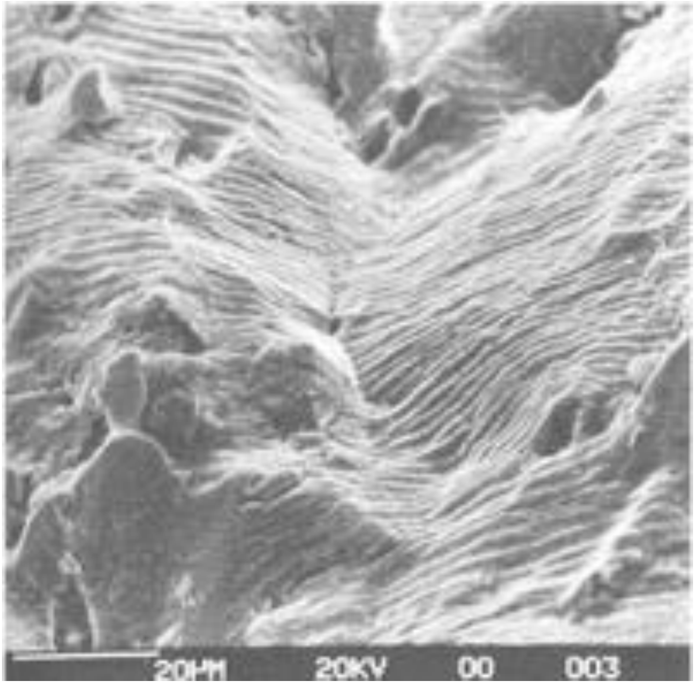

- Striations are close together indicating low stress, many cycles.
- Widely spaced striations mean high stress few cycles.

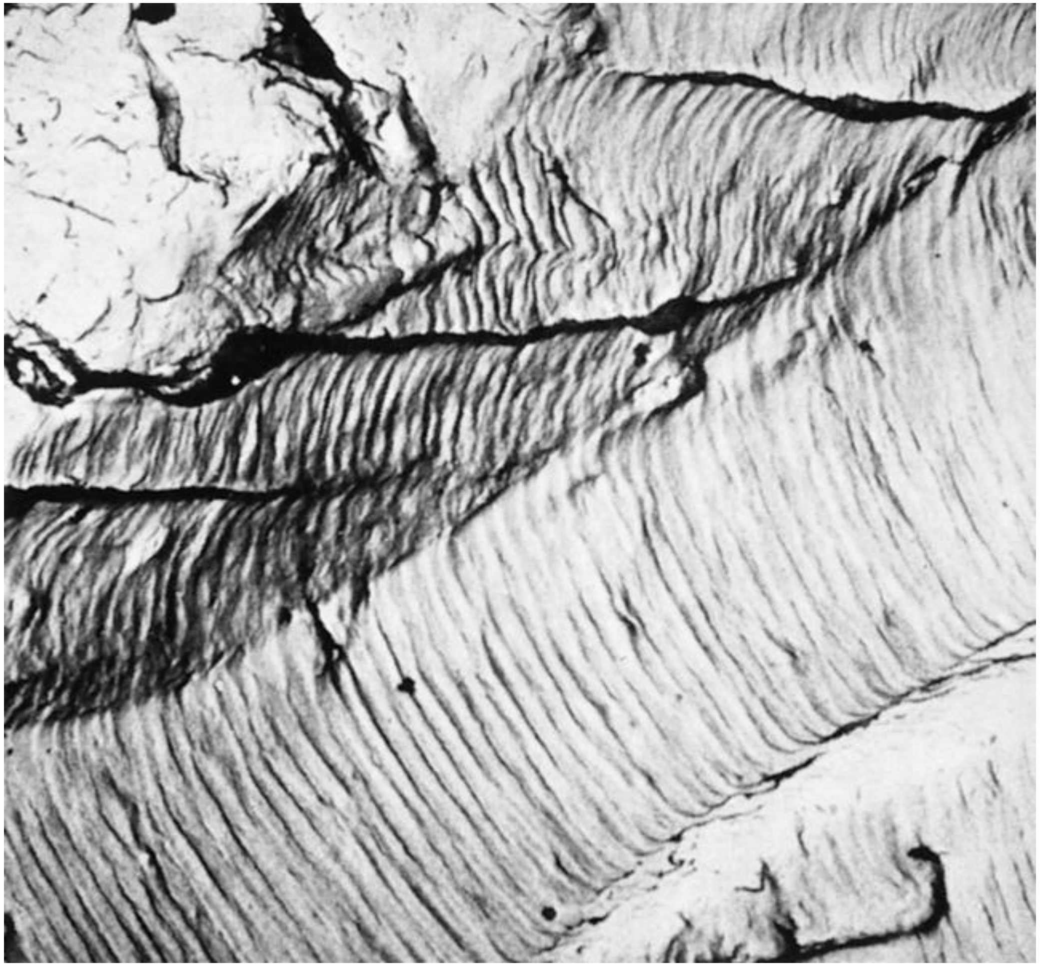

- Fatigue failure is brittle in nature, even in normally ductile materials; there is very little plastic deformation associated with the failure.
- The image shows fatigue striations (microscopic).


- Federal investigators say metal fatigue caused a hole to rip open in the roof of a Southwest Airlines jet as it cruised at 35,000 feet last year (2009). The National Transportation Safety Board says the 14-inch crack developed in a spot where two sheets of aluminum skin were bonded together on the Boeing 737 jet.
- The pilot made an emergency landing in Charleston, W.Va. There were no injuries among the 126 passengers and five crew members. Two months after the scare, Boeing told all airlines with 737s to conduct repeated inspections of the top of the fuselage near the vertical tail fin. The Federal Aviation Administration has since made those inspections mandatory.
- Southwest got the plane in 1994 — it's much older than the average Southwest jet — and had flown it for 50,500 hours and made 42,500 takeoffs and landings before it sprang a hole in the roof, according to the safety board report. The safety board said it found signs of metal fatigue by magnifying the area in front of the tail fin. In a 3-inch stretch, the crack penetrated completely through the aluminum skin.
- FAA records showed that eight cracks had been found and repaired in the fuselage during the plane's 14-year checkup.

Fatigue Mechanism

- Crack grows *incrementally*

$$\frac{da}{dN} = \left(\Delta K\right)^m$$

typ. 1 to 6

$$\sim (\Delta\sigma)\sqrt{a}$$

increase in crack length per loading cycle

- Failed rotating shaft
  -- crack grew even though

  $K_{max} < K_c$

  -- crack grows faster as
  - $\Delta\sigma$ increases
  - crack gets longer
  - loading freq. increases.

crack origin

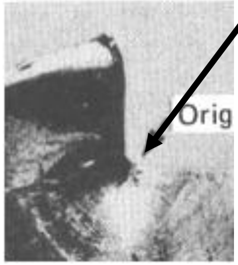

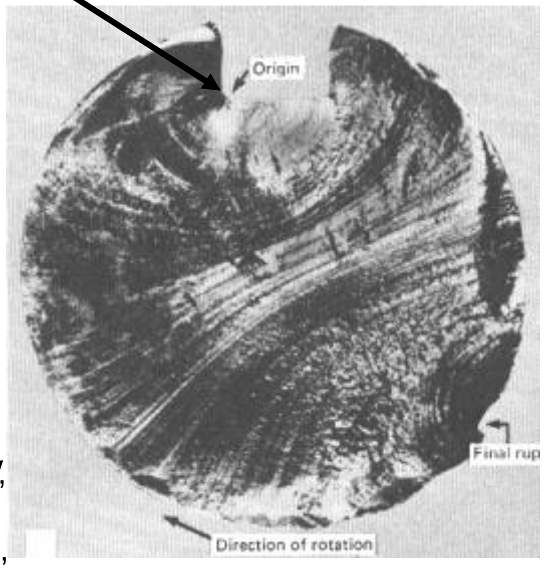

Adapted from Fig. 9.28, *Callister & Rethwisch 3e.* (Fig. 9.28 is from D.J. Wulpi, *Understanding How Components Fail*, American Society for Metals, Materials Park, OH, 1985.)

Crack growth rate

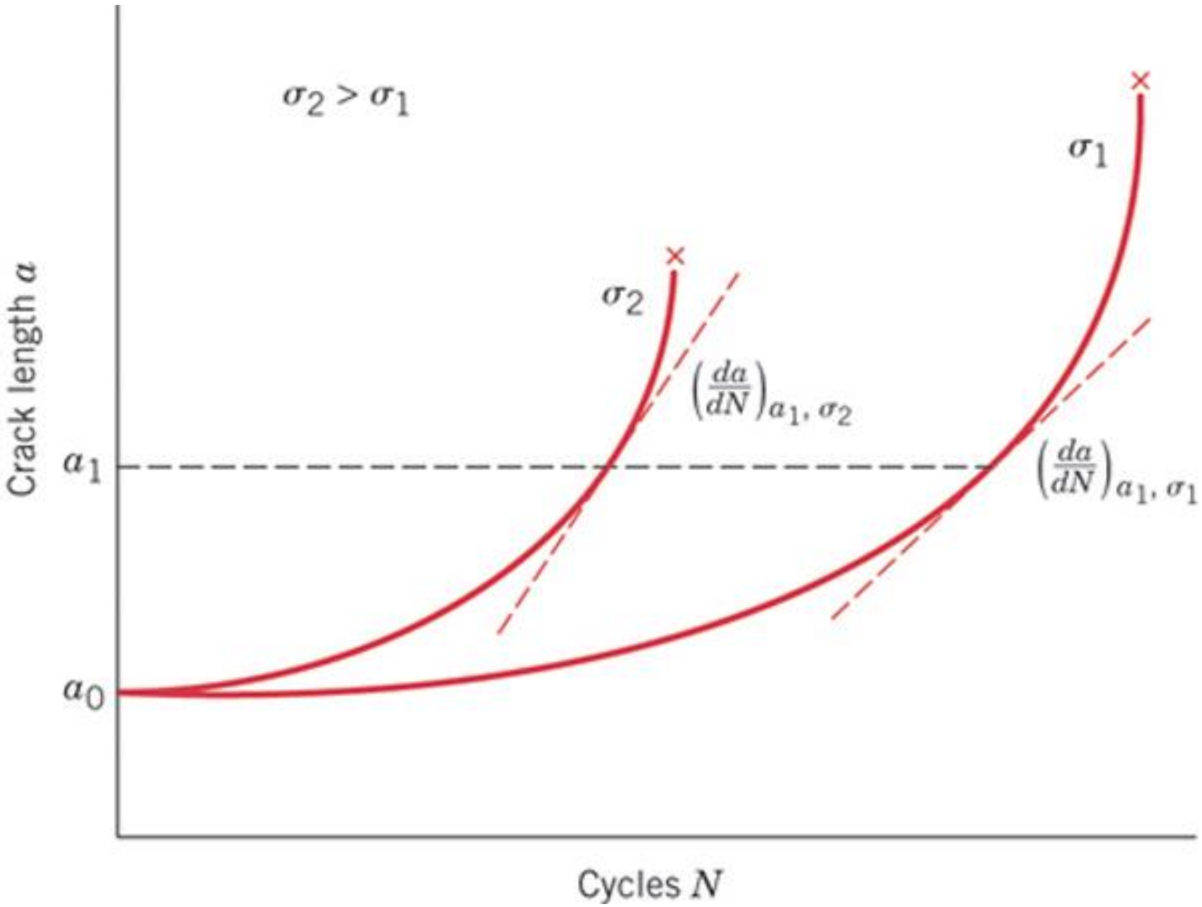

1. Initially, growth rate is small, but increases with increasing crack length.
2. Growth rate increases with applied stress level for a given crack length (a_1).

S-N Curves

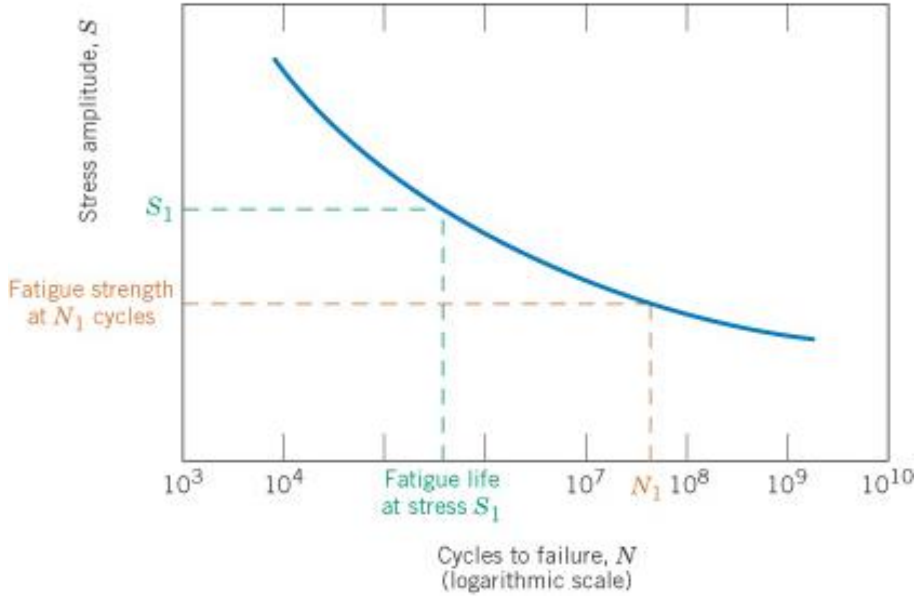

- A specimen is subjected to stress cycling at a maximum stress amplitude; the number of cycles to failure is determined.
- This procedure is repeated on other specimens at progressively decreasing stress amplitudes.
- Data are plotted as stress S versus number N of cycles to failure for all the specimen.
- Typical S-N behavior: the higher the stress level, the fewer the number of cycles.

Fatigue Limit

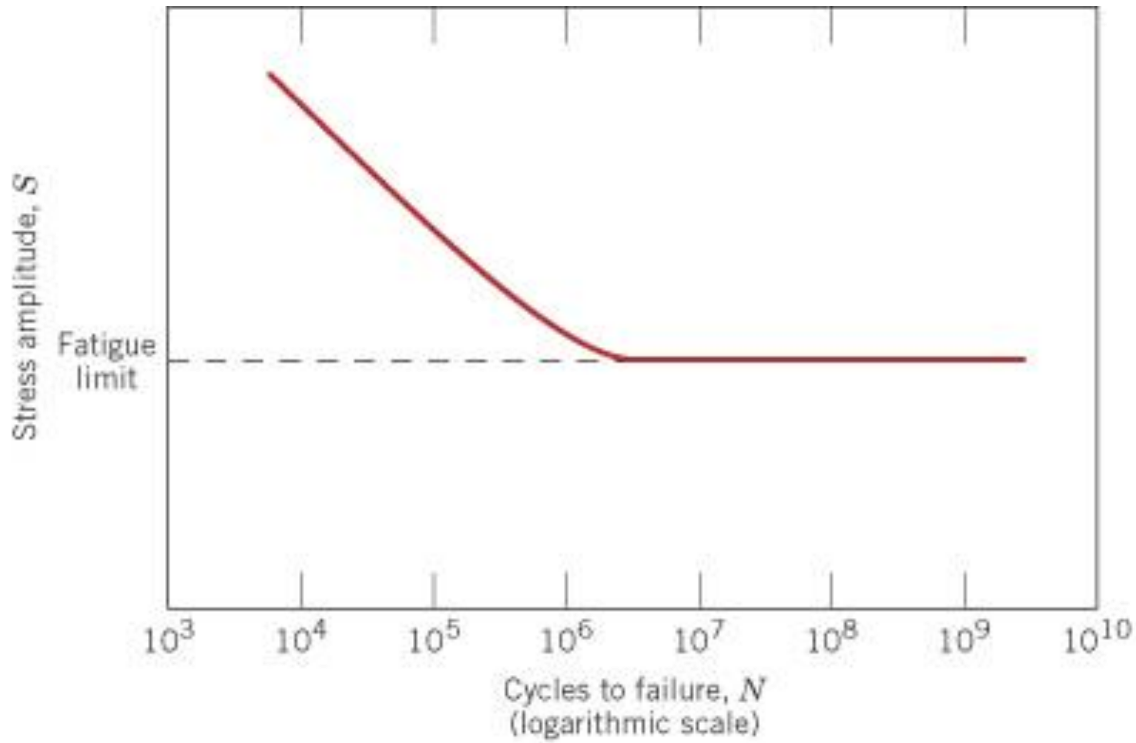

- For some iron and titanium alloys, the S-N curve becomes horizontal at higher number of cycles N.
- Essentially it has reached a fatigue limit, and below this stress level the material will not fatigue.
- The fatigue limit represents the largest value of fluctuating stress that will not cause failure for an infinite number of cycles.

Fatigue Curves for Polymers

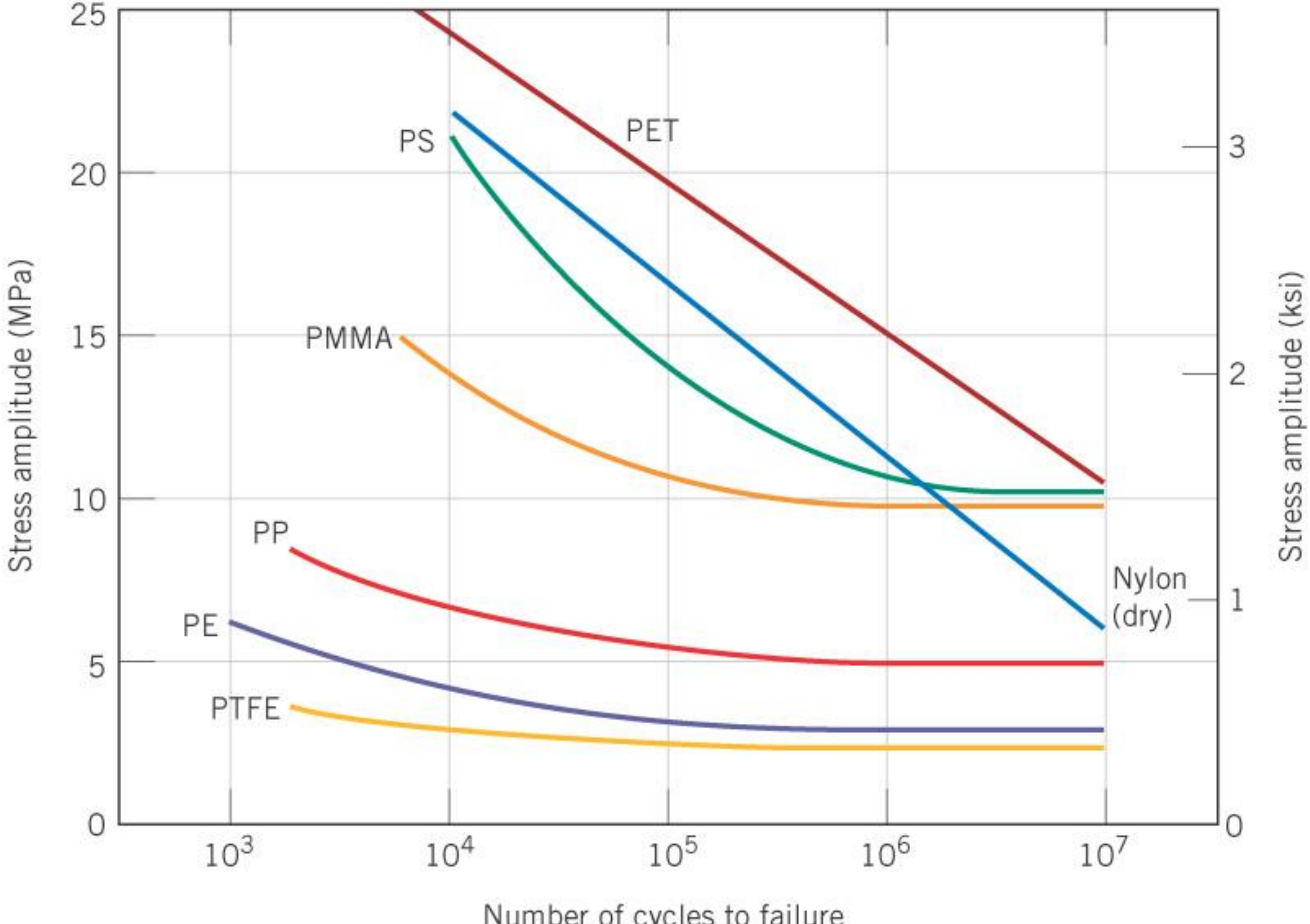

Surface Treatments

- During machining operations, small scratches and grooves can be introduced; these can limit the fatigue life.
- Improving the surface finish by polishing will enhance fatigue life significantly.
- One of the most effective methods of increasing fatigue performance is by imposing residual compressive stresses within a thin outer surface layer. A surface tensile stress will be offset by the compressive stress.
- Shot peening (localized plastic deformation) with small (diameters ranging from 0.1 to 1.0 mm), hard particles (shot) are projected at high velocities on to the surface. The resulting deformation induces compressive stresses to a depth of roughly ¼ to ½ of the shot diameter.
- The influence of shot peening is compared in the graph.

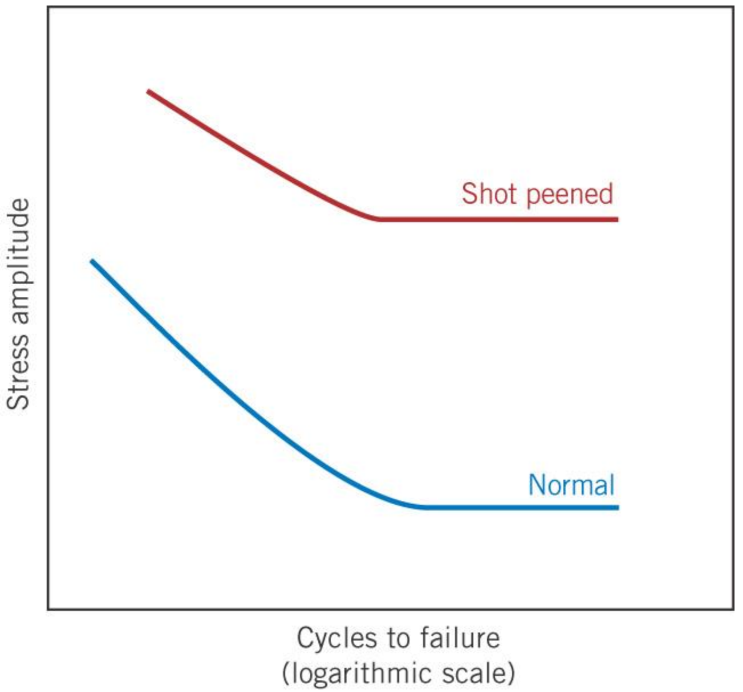

Improving Fatigue Life

1. Impose a compressive surface stress
   (to suppress surface cracks from growing)

--Method 1: shot peening

--Method 2: carburizing

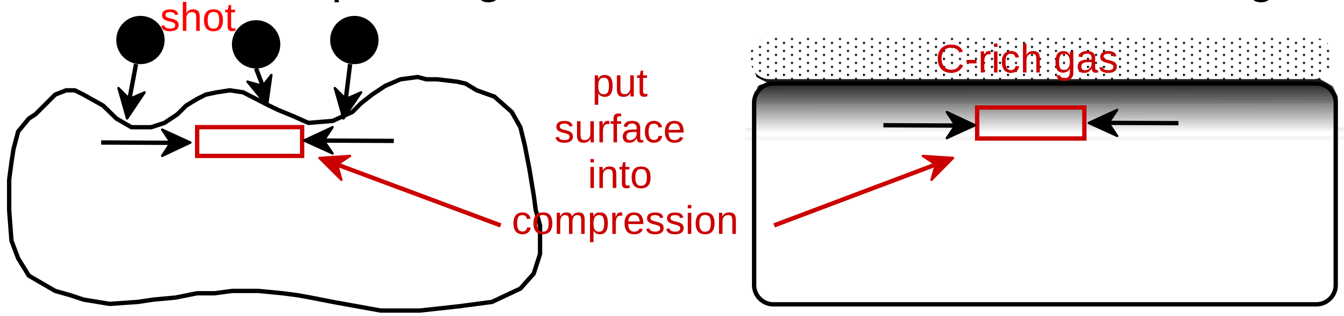

2. Remove stress
   concentrators.

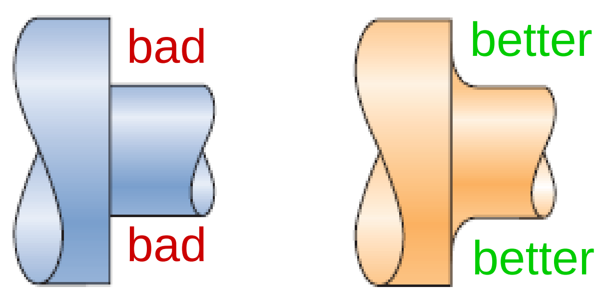

Case Hardening

- Case hardening is a technique where both surface hardness and fatigue life are improved for steel alloys.
- Both core region and carburized outer case region are seen in image. Knoop microhardness shows case has higher hardness (smaller indent).
- A carbon or nitrogen rich outer surface layer (case) is introduced by atomic diffusion from the gaseous phase. The case is typically 1mm deep and is harder than the inner core material.

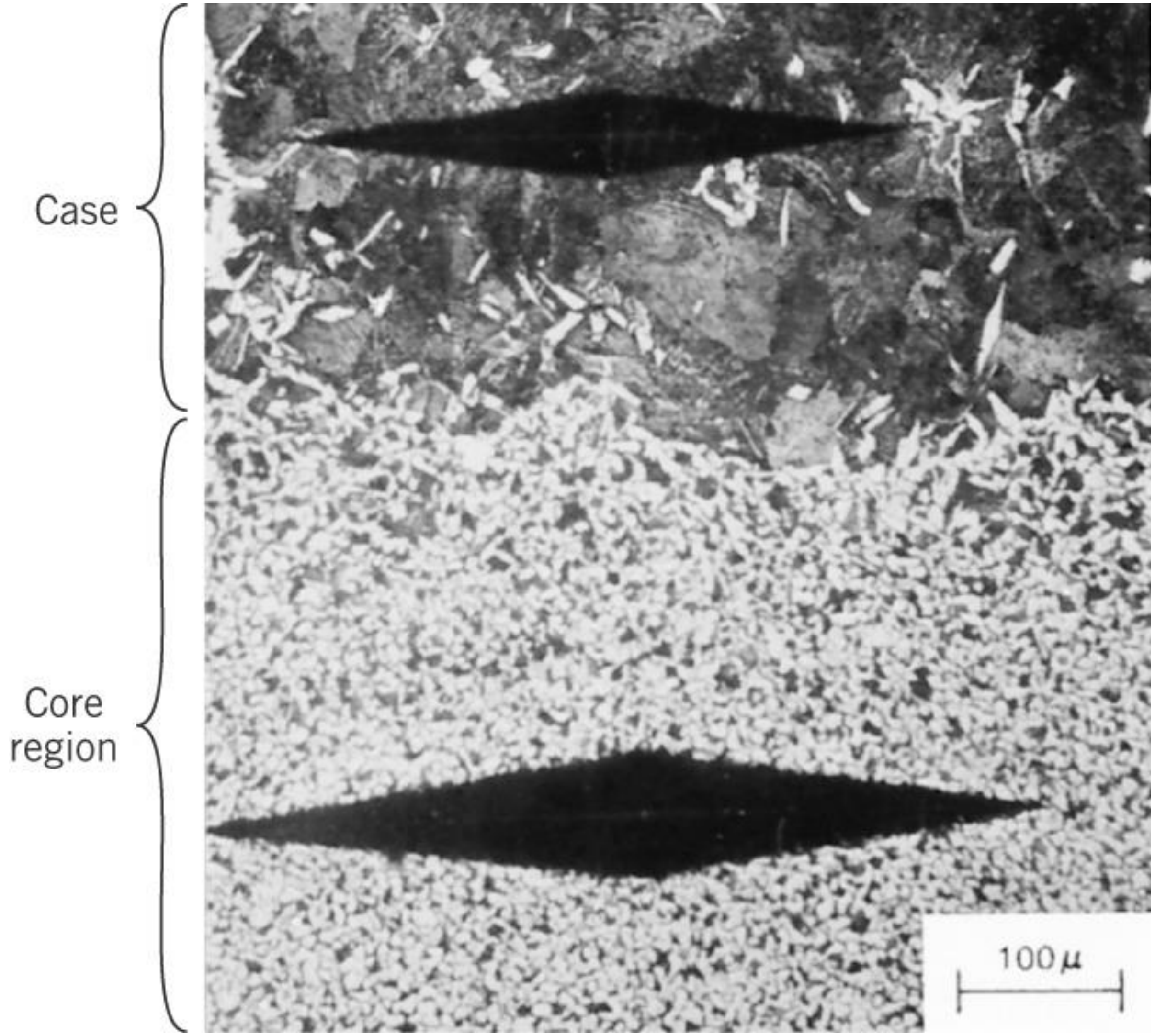

High Temperature - Creep

Temp ↑

- Atoms move faster → ***diffusion-controlled process***. This affects mechanical properties of materials.
- Greater mobility of dislocations (climb).
- Increased amount of vacancies.
- Deformation at grain boundaries.
- Metallurgical changes, i.e., phase transformation, precipitation, oxidation, recrystallisation.

High temperature materials/alloys

- Improved high temperature strength.
- Good oxidation resistance.

Creep

- Materials are often placed in service at elevated temperatures (>0.4 T_m) and exposed to static mechanical stresses.
- Examples are turbine rotors in jet engines and steam generators that experience centrifugal stresses and high pressure steam lines.
- Creep is time dependent, permanent deformation of the material when subjected to a constant load or stress.


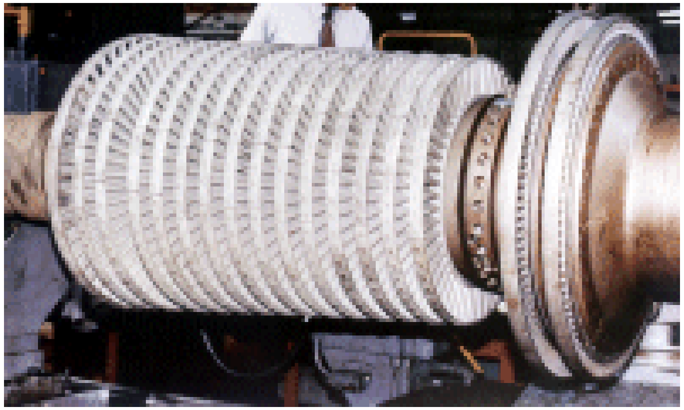

Creep

- A typical creep test consists of subjecting a specimen to a constant load or stress while maintaining constant temperature.
- Upon loading, there is instant elastic deformation. The resulting creep curve consists of 3 regions: primary or transient creep adjusts to the creep level (creep rate may decrease); secondary creep-steady state-constant creep rate, fairly linear region (strain hardening and recovery stage); tertiary creep, there is accelerated rate of strain until rupture (grain boundary separation, internal crack formation, cavities and voids).

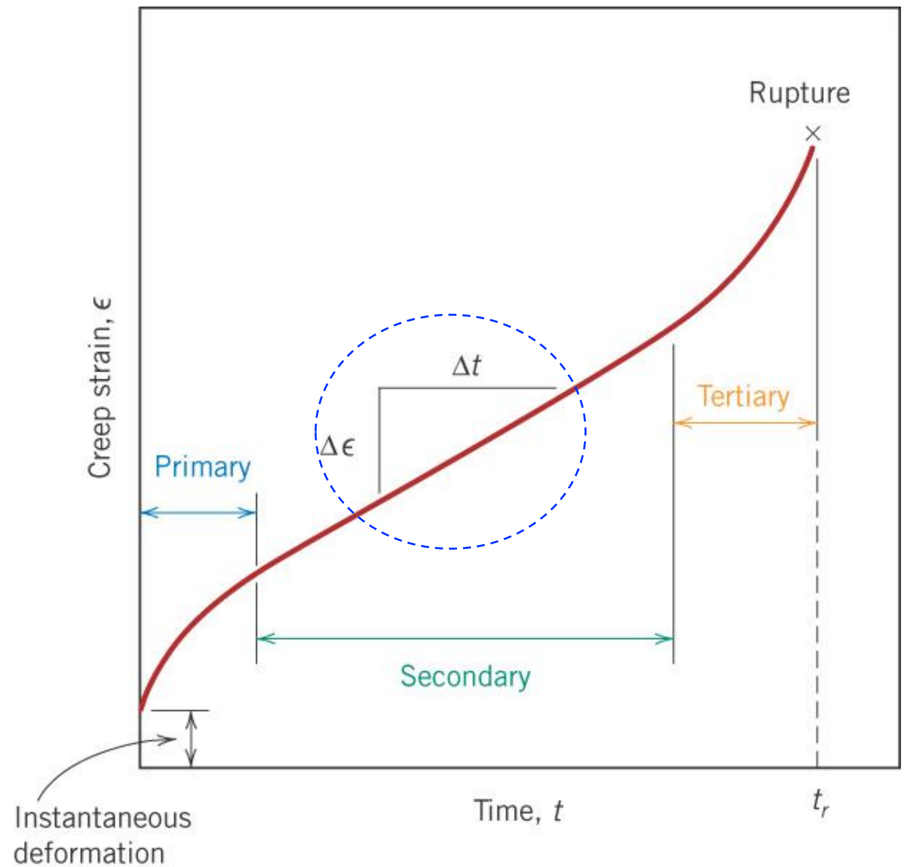

Creep strain vs time at constant load and constant elevated temperature. Minimum creep rate (steady-state creep rate), is the slope of the linear segment in the secondary region. Rupture lifetime t_r is the total time to rupture.

Creep

Sample deformation at a constant stress (σ) vs. time

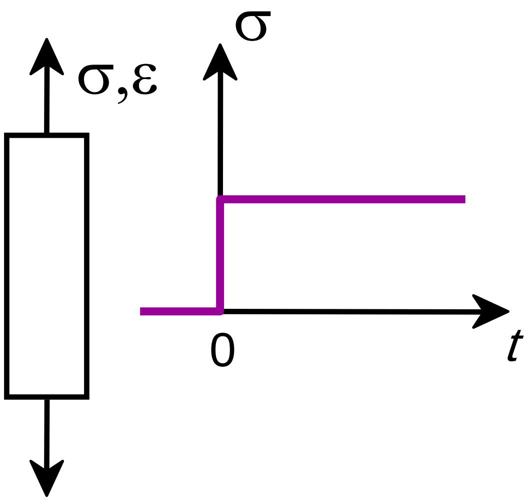

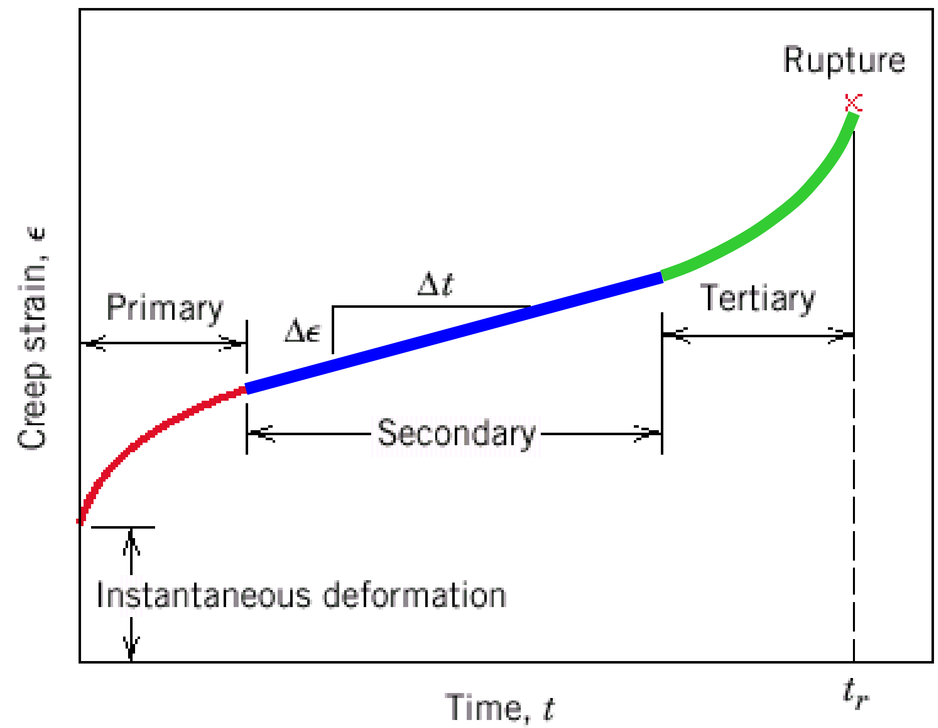

Primary Creep: slope (creep rate) decreases with time.

Secondary Creep: steady-state i.e., constant slope.

Tertiary Creep: slope (creep rate) increases with time, i.e. acceleration of rate.

Creep Failure

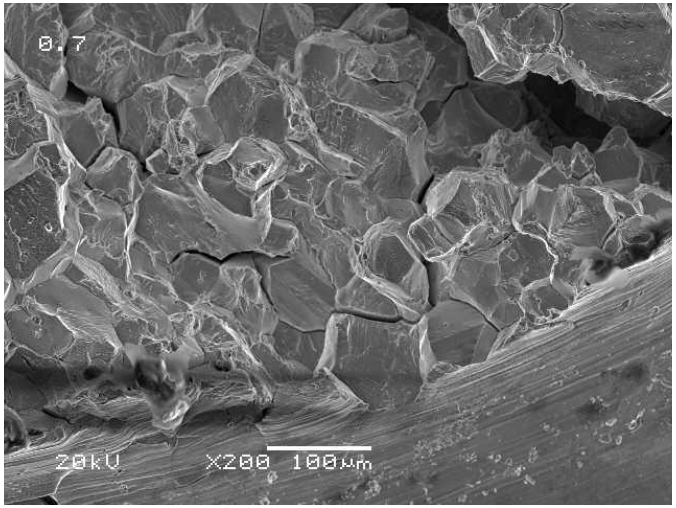

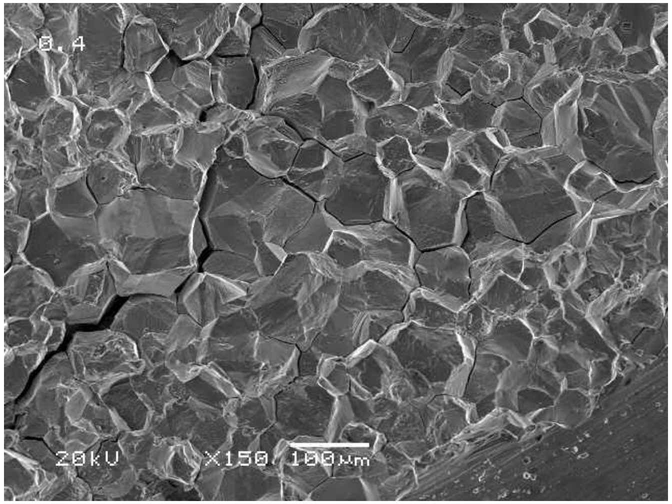

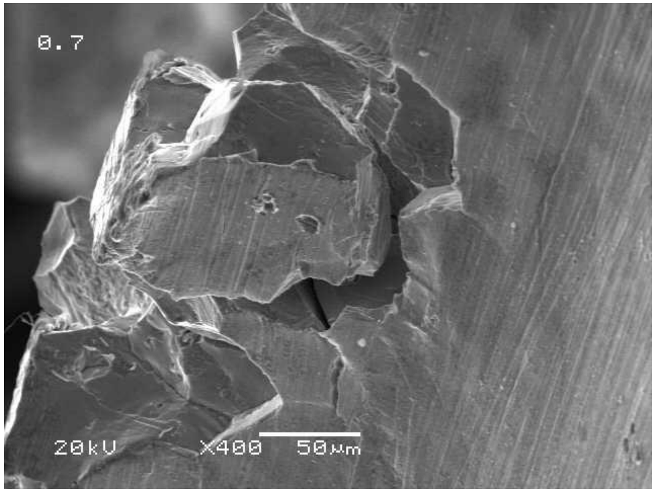

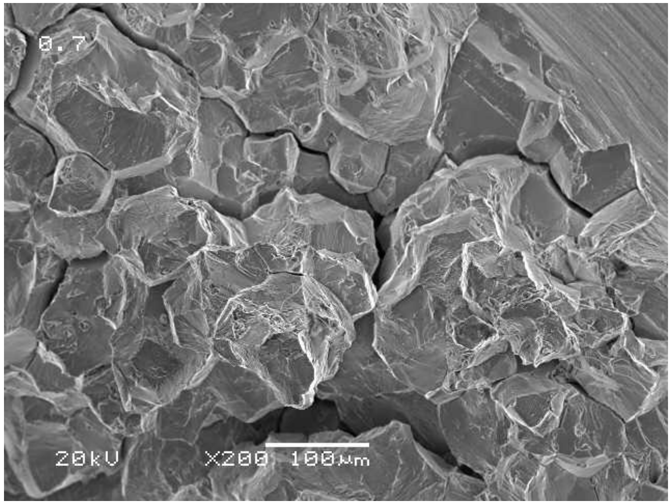

Creep

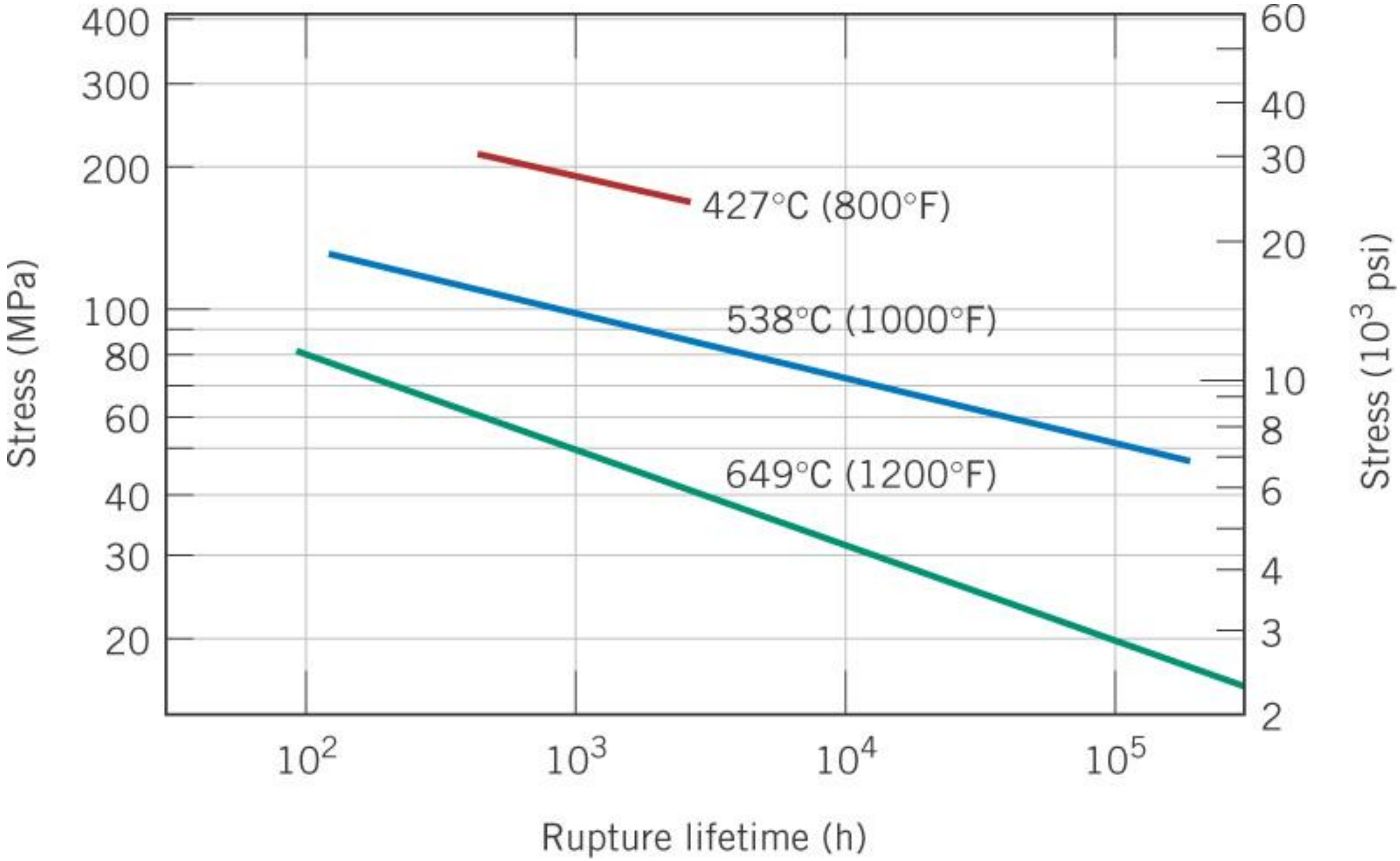

Dependence of creep strain rate on stress; stress versus rupture lifetime for a low carbon-nickel alloy at 3 temperatures.

Secondary Creep

- Strain rate is constant at a given T, σ
  -- strain hardening is balanced by recovery

stress exponent (material parameter)

$$\dot{\varepsilon}_s = K_2 \sigma^n \exp\left(-\frac{Q_c}{RT}\right)$$

strain rate

material const.

applied stress

activation energy for creep (material parameter)

- Strain rate increases for higher T, σ

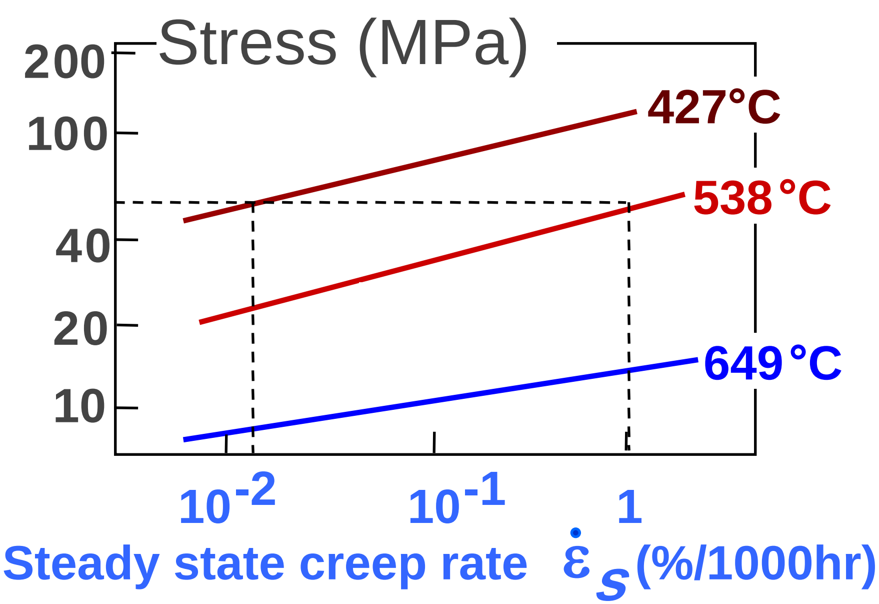

SUMMARY

- Engineering materials don't reach theoretical strength.
- Flaws produce stress concentrations that cause premature failure.
- Sharp corners produce large stress concentrations and premature failure.
- Failure type depends on T and stress:
  - for noncyclic σ and $T < 0.4\,T_m$, failure stress decreases with:
    - increased maximum flaw size,
    - decreased T,
    - increased rate of loading.
  - for cyclic σ:
    - cycles to fail decreases as $\Delta\sigma$ increases.
  - for higher T ($T > 0.4\,T_m$):
    - time to fail decreases as σ or T increases.